Journal of
Materials Chemistry A

Materials for energy and sustainability

rsc.li/materials-a

Volume 6
Number 12
28 March 2018
Pages 4883-5230

ISSN 2050-7488

**ROYAL SOCIETY
OF CHEMISTRY**

COMMUNICATION
Zhema Wen et al
An electrochemically neutralized energy-assisted low-cost
acid-alkaline electrolyzer for energy-saving electrolysis
hydrogen generation

**ROYAL SOCIETY
OF CHEMISTRY**

rsc.li/materials-a

Advanced metal-organic frameworks for superior carbon capture, high-performance energy storage and environmental photocatalysis – A critical review

Farooq Sher[1],*, Anna Hayward[2], Abdelqader El Guerraf[3,4], Bohong Wang[5], Imane Ziani[4,6],

Harun Hrnjić[4,7], Emina Boškailo[4,7], Alexander Chupin[8], Monica R. Nemțanu[9]

[1]*Department of Engineering, School of Science and Technology, Nottingham Trent University, Nottingham NG11 8NS, United Kingdom*

[2]*School of Mechanical, Aerospace and Automotive Engineering, Coventry University, Coventry CV1 5FB, United Kingdom*

[3]*Laboratory of Applied Chemistry and Environment, Faculty of Sciences and Technologies, Hassan First University, Settat 26002, Morocco*

[4]*International Society of Engineering Science and Technology, Nottingham, United Kingdom*

[5]*National and Local Joint Engineering Research Center of Harbor Oil and Gas Storage and Transportation Technology, Zhejiang Key Laboratory of Petrochemical Environmental Pollution Control, Zhejiang Ocean University, No. 1 Haida South Road, 316022, Zhoushan, P.R. China*

[6]*Physical Chemistry of Natural Substances and Process Research Team, Laboratory of Applied Chemistry and Environment (LCAE-CPSUNAP), Faculty of Sciences, Mohammed 1st University, Oujda 60000, Morocco*

[7]*Department of Chemistry, Faculty of Science, University of Sarajevo, Sarajevo 71000, Bosnia and Herzegovina*

[8]*Peoples' Friendship University of Russia (RUDN University), Moscow 117198, Russia*

[9]*Electron Accelerators Laboratory, National Institute for Laser, Plasma and Radiation Physics, 409 Atomiștilor Street, Bucharest-Măgurele, Romania*

*Corresponding author:

Dr. F. Sher
Assistant Professor
Department of Engineering, School of Science and Technology
Nottingham Trent University
Nottingham
NG11 8NS
UK
E-mail address: Farooq.Sher@ntu.ac.uk
Tel.: +44 (0) 115 84 86679

Journal of Materials Chemistry A Accepted Manuscript

Contents

Abstract

Metal-organic frameworks (MOFs) have emerged as a transformative class of materials, offering unprecedented versatility in applications ranging from energy storage to environmental remediation and photocatalysis. This groundbreaking review navigates the recent advancements in MOFs, positioning them against traditional materials to underscore their unique strength and potential drawbacks. In the context of energy storage, particularly within the realm of supercapacitors (SCs), MOF-based electrodes are evaluated for their superior specific capacitance (exceeding 1000 F/g), although these benefits are tempered by higher production cost. A comparative analysis with conventional activated carbon (AC) electrodes reveals MOFs' enhanced performance but also highlights cost as a significant barrier to widespread adoption. In carbon capture and storage (CCS), MOFs are contrasted with established liquid-amine technologies, with MOFs demonstrating environmental benefits, including the ability to achieve high-purity CO_2 collection (>99%), despite higher expenses. Similarly, in photocatalysis, while titanium dioxide remains dominant, MOFs are shown to offer competitive performance with a reduced environmental footprint, though cost considerations again play a decisive role. This review not only consolidates the current state of MOF research but also identifies critical gaps, particularly in cost-effectiveness, that must be addressed to enable broader application. The findings advocate for continued innovation in MOF synthesis and production, with an emphasis on achieving a balance between performance and affordability. In summary, this review highlights the pivotal role of MOFs in advancing material science and underscores the need for holistic approaches in material selection, with a forward-looking perspective on sustainable and economical production methods.

1. Introduction

97

98 The dawn of the 21st century marked the emergence of metal-organic frameworks (MOFs);

99 porous structures consisting of metal ions and organic linkers. Prior to MOFs, zeolites

100 (aluminium silicate crystals) were the world's most porous materials [1]. However, MOFs have

101 overcome zeolites' surface area by more than 100% in some cases. In addition to that, the

102 structure of the cavities and the size of the pore in MOFs can be tailored as a function of metal

103 ions, organic ligands, and synthesis conditions, and hence are thus amenable to engineering for

104 targeted applications [2], which catalyses exponential growth in research on their applications [3].

105 Due to their unique architectures and chemical or physicochemical properties, MOFs remain in

106 a class apart, with a wide reach of applications. Metal-containing nodes (SBUs) and organic

107 linkers are used to create very porous structures, which typically have surface areas greater than

108 7000 m^2/g [4]. Control over topology, dimensionality, and stability can be achieved by selecting

109 the right metal centers and organic ligands. For example, functional groups high in nitrogen can

110 enhance CO_2 absorption; certain MOFs can attain up to 40 cc/g [5].

111

112 On the other hand, sensitivity to humidity and thermal instability create practical problems, as

113 illustrated by ZIF-8, which swells at low pressure but phase transitions at higher pressures [6].

114 Synthesis conditions and metal-organic coordination bonds are key to the chemical stability and

115 reactivity of MOFs; high-throughput computational screenings have identified MOFs with high

116 gas adsorption capacities, such as methane storage up to 200 cm^3/cm^3 [4]. However, theoretical

117 predictions do not often match real-world performance, suggesting that somehow models and

118 real applications are detached from one another. It typically focuses on crystallinity and leaves

119 out the other forms, such as amorphous or semi-crystalline forms, which might also hold special

120 properties [7]. All this proves that there is a need to develop better characterization techniques

121 and insight into structure-function interplay to further advance the application of MOFs in

122 carbon capture, energy storage, and environmental remediation. The historical development of

123 MOFs shows the huge progress made in material science from exclusively inorganic or organic

124 structures to hybrid systems possessing new properties [8]. The necessity of material that shows

125 high porosity but custom architecture of the material developed during the late twentieth

126 century marked the starting point for the development of MOF [9]. Early studies, and mostly

127 those related to Prussian blue analogues, were the basis for the fast-growing interest in MOF

128 research in the late 1980s [10]. The "node-and-spacer" approach, proposed by Richard Robson,

129 enabled design of frameworks with well-defined coordination geometries and complex

130 structures. MOFs, like HKUST-1 and MOF-5, developed in the late 1990s and early 2000s,

131 represent advances in synthesizing large surface area materials that have high porosity and good

132 crystallinity [11].

133

134 In response to escalating energy demands and intensifying environmental challenges, the

135 development of advanced materials has become increasingly critical [12]. MOFs have emerged as

136 a highly versatile class of materials, offering exceptional properties that hold the potential to

137 revolutionize energy storage, environmental remediation, and photocatalysis [13]. As the global

138 population continues to grow and conventional energy sources dwindle, innovative approaches

139 to sustainable energy generation and environmental restoration are urgently needed. MOFs

140 present a promising solution due to their structural flexibility, large surface area, and tunable

141 properties. Energy storage, environmental remediation, and photocatalysis are key areas where

142 advanced materials have the potential to drive transformative change. Traditional materials,

143 such as metals, semiconductors, and polymers have historically played significant roles in these

144 applications. However, these materials often face in efficiency, stability, and versatility. MOFs,

145 with their exceptional characteristics, offer a promising alternative that could overcome these

146 limitations. While MOFs are very promising, there are several serious technological problems

147 to be overcome. Their structural stability is the first and foremost problem. Such interactions of

148 the proton and metal ion can result in degradation, and therefore most MOFs cannot be used

149 for an extended period of time in these environments [14]. Improvement of stability includes high-

150 valent metal ions and proper organic linkers, which generally decrease the diversity of possible

151 MOFs. On the other hand, most MOFs require comparatively high temperature and pressure for

152 synthesis and, therefore, are energy-consuming and expensive. In this regard, the search for

153 alternative synthesis techniques, including the solvothermal and microwave methods, or

154 recently mechanochemical methods, assumes the leading role among researchers to decrease

155 the price of synthesis and increase scalability [15].

156

157 Moreover, their generally low electrical conductivity limits the broad use of MOFs in

158 electrochemical applications. Strategies to enhance conductivity include embedding conductive

159 material carbon-based compounds or using highly conjugated organic linkers; however, these

160 add complexity and are more expensive to synthesize. For example, the MOF derivatives, such

161 as TMCs, have been designed to enhance conductivity and improve structural stability [16]. One

162 such example of improvement is the hybrid ZnS/MXene, which was reported to demonstrate

163 improved electron transfer and ion adsorption capabilities due to uniform anchoring of ZnS

164 nanodots onto the MXene nanosheets. The incorporation of a few metals into one MOF

165 structure has also shown some bright prospects in enhancing electrochemical performance but

166 adds more complications in terms of synthesis and scalability. For instance, sequential chemical

167 etching and sulfurization in the preparation of Zn-Co-S rhombic dodecahedral cages showed

168 enhanced specific capacitance because they hold a double-shelled structure [17]. Environmental

169 degradation stands as one of the foremost challenges of the 21st century. Increased awareness

170 of global warming, coupled with concerted efforts by governments and societies, is driving

171 research into environmental pollution mitigation. The United Nations has specified a series of

172   sustainable development goals, showcasing this assertion [18]. Recent research suggests that

173   MOFs demonstrate tremendous potential in capturing and detoxifying environmental toxins

174   across various media, such as water, air, and soil [19]. The increasing concentration of

175   atmospheric CO_2, primarily driven by the combustion of fossil fuels since the industrial

176   revolution, has been a major contributor to anthropogenic global warming [18]. The atmospheric

177   concentration of CO_2 has increased from 280 ppm in 1962 to 400 ppm in 2015 [20], a concerning

178   trend due to its links to global warming and associated environmental degradation, as well as

179   potential adverse health effects [19].   MOFs have shown significant potential in this regard,

180   particularly in carbon capture and storage (CCS) technologies. Their ability to selectively

181   adsorb CO_2 from the atmosphere makes them a viable candidate for reducing greenhouse gas

182   emissions [21].

183

184   In the realm of energy storage, MOFs' are being explored for their application in both

185   supercapacitors (SCs) and metal-ion batteries. MOFs can serve two main roles in these energy

186   storage devices: Primarily, they can function as direct electrode materials with modifiable

187   particle and pore dimensions. Secondly, they can serve as templates and precursors for

188   producing porous carbons and metal oxides. The resulting porous carbons and metal oxides

189   maintain the extensive surface area and highly porous structure of the MOF precursors, making

190   them ideal for implementation in electrical double-layer supercapacitors (EDLCs) and

191   pseudocapacitors [22]. Moreover, MOFs have garnered attention in photocatalysis owing to their

192   distinctive properties. Photocatalysis entails harnessing light energy to propel chemical

193   reactions [23], and MOFs' extensive surface area and porosity provide numerous active sites for

194   catalytic reactions. Researchers have incorporated various photocatalytic components, such as

195   metal nanoparticles or organic dyes, into MOF structures to enhance their photocatalytic

196   performance. MOFs can serve as photocatalysts themselves or as platforms to support other

197 catalytic materials. The tunable nature of MOFs allows researchers to modify their electronic

198 and optical properties, influencing their efficiency in light absorption and charge separation

199 critical factors in photocatalytic processes.

200

201 In this comprehensive and groundbreaking review, the report embarks on a pioneering journey

202 to assess the comparative advantages of MOFs over conventional materials. Delving into the

203 realm of energy storage, it investigates how MOFs can potentially revolutionize energy storage

204 technologies, including supercapacitors and metal-ion batteries, due to their exceptionally high

205 surface area, tunable electronic properties, and facile ion diffusion pathways. This new

206 approach to energy storage could enable previously unattainable levels of efficiency and

207 performance to be achieved. In the context of environmental challenges, the exploration focuses

208 on a remarkable novelty, namely the way MOFs display an unprecedented affinity for carbon

209 dioxide capture. This discovery offers a compelling and revolutionary alternative to

210 conventional adsorbents, with the potential to significantly mitigate greenhouse gas emissions.

211 Furthermore, in the domain of photocatalysis, MOFs have showcased a transformative capacity

212 to harness solar energy for driving chemical reactions with unmatched efficiency, representing

213 a major leap forward in sustainable energy conversion technologies.

214

215 This review tackles these issues by providing an in-depth analysis of case studies, experimental

216 results, and theoretical insights to illuminate the merits and limitations of MOFs compared to

217 conventional materials across three key applications: energy storage, carbon capture, and

218 photocatalysis. Tables summarizing the advantages and disadvantages of both conventional and

219 MOF materials are presented for each application, with a focus on performance, environmental

220 impact, and cost-effectiveness. Each broad factor receives a relative percentage weighting

221 based on importance, with the most critical factor assigned the highest percentage. Sub-factors

222   within each category are also identified based on the literature, assigning them scores out of 3

223   (3 correlating to high importance). After determining the weightings, both materials are

224   evaluated using a comparison matrix for each factor, using a scale of 1 to 5 (1 very bad, 2 bad,

225   3 suitable, 4 good, and 5 very good). The resulting scores allow a comparison of MOFs and

226   conventional materials for each of the three applications, helping identify which material offers

227   the most benefits based on the identified factors. Such a systematic approach will ensure that

228   all aspects are covered and that clear, actionable insights into practical benefits of MOFs in

229   addressing technological challenges in energy storage, carbon capture, and photocatalysis are

230   delivered. **Fig. 1** summarizes the methodology followed throughout this groundbreaking

231   literature review.

232
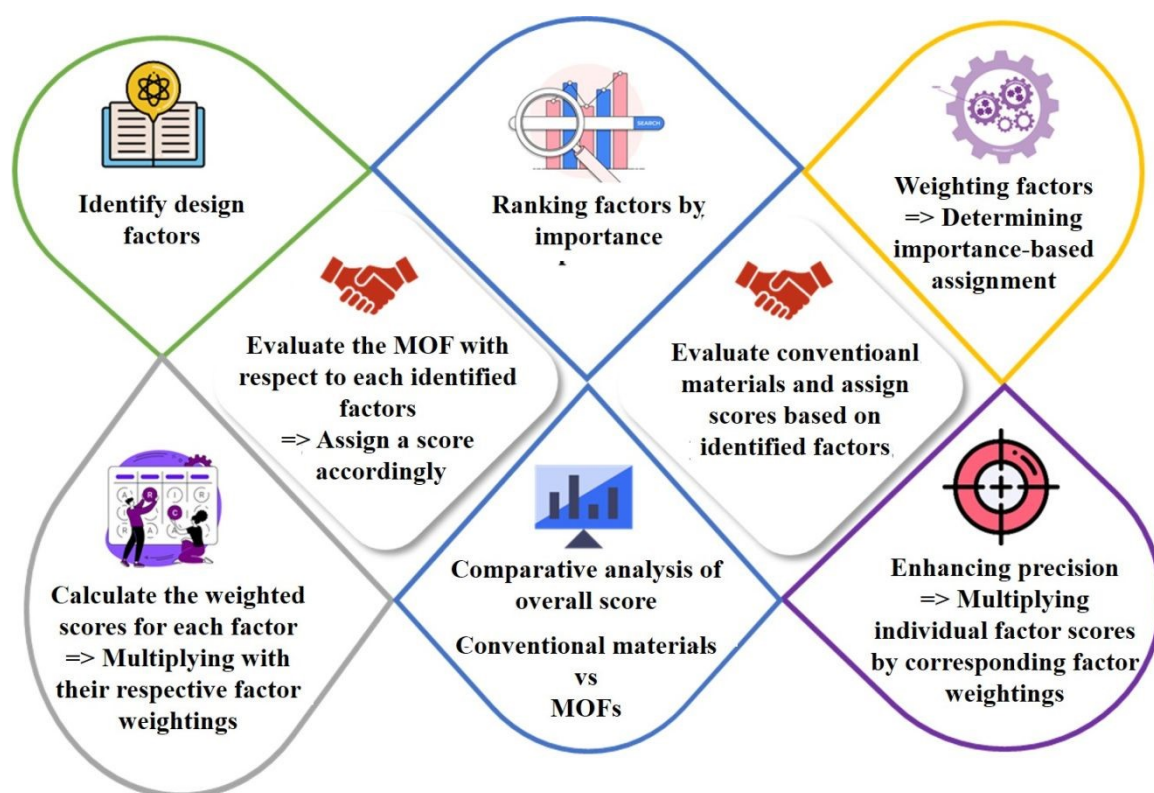
233   **Fig. 1.** Diagram explaining the adopted methodology for the present literature review. A
234   systematic comparison matrix is employed to assess the relative benefits of MOFs, offering
235   clear, actionable insights into their potential as a transformative material in critical fields.

2. Porous MOF and conventional materials for carbon capture

The argument presented by Mukherjee et al. [18] emphasizes humanity's reliance on gas as a critical component of energy and industrial processes. They contend that liquid fuels and feedstocks in the chemical industry have been largely replaced by gases. However, this viewpoint is challenged by the research conducted by Furukawa et al. [24] which shows a steady increase in all fossil fuels, both sources agree on the general trend of increasing CO_2 levels and their contribution to global warming and consequential environmental degradation. A sorbent's CO_2 selectivity is determined by comparing how much CO2 it can absorb to another gas while meeting certain predetermined parameters [18]. In the examination of a sorbent employed for post-combustion carbon capture, selectivity versus nitrogen (SCN) holds significant relevance. Selectivity is crucial as it impacts both the purity of the captured CO_2 and the concentration of CO_2 in the effluent gas discharged into the atmosphere. Mukherjee and colleagues [18] also suggest that increasing the SCN of a sorbent by five-fold could significantly reduce the cost of C-capture. Other important factors that influence sorbent selection for C-capture include stability, working capacity, regenerability and feasibility of scale-up.

2.1 Conventional liquid alkanolamine in carbon capture

For over half a century, liquid amine technology has remained at the forefront of carbon capture and storage (CCS) technologies [18]. This method of bulk-scale carbon capture operates through chemisorption, involving chemical reactions between CO_2 and the sorbent material. Originating in the 1930s, these processes were initially developed, and since the 1950s, they have been employed by gas-treating plants for the removal of acid gases like CO_2 and H_2S [19,25]onsequently, liquid amine processes are frequently recognized as the most mature CCS method and boast a high Technology Readiness Level (TRL) of 9 [25,26]. In two commercial-scale facilities housed within coal-fired power plants, post-combustion liquid amine CCS technology had been successfully installed as of 2018 [26]. The post-combustion liquid-amine CCS process

261 (**Fig. 2**(a)) involves exposing the flue gas stream to an aqueous amine solution, commonly a

262 member of the alkanolamine class, typically a 20–30 wt% aqueous monoethanolamine (MEA)

263 [27]. Subsequently, the amine undergoes a reaction with CO_2 in the flue gases, resulting in the

264 formation of carbamates or bicarbonate products, which can then be separated and removed.

265 The utilization of liquid amines is based on their capacity to achieve significant levels of

266 purification and separation through the chemisorption process [18].

267

11
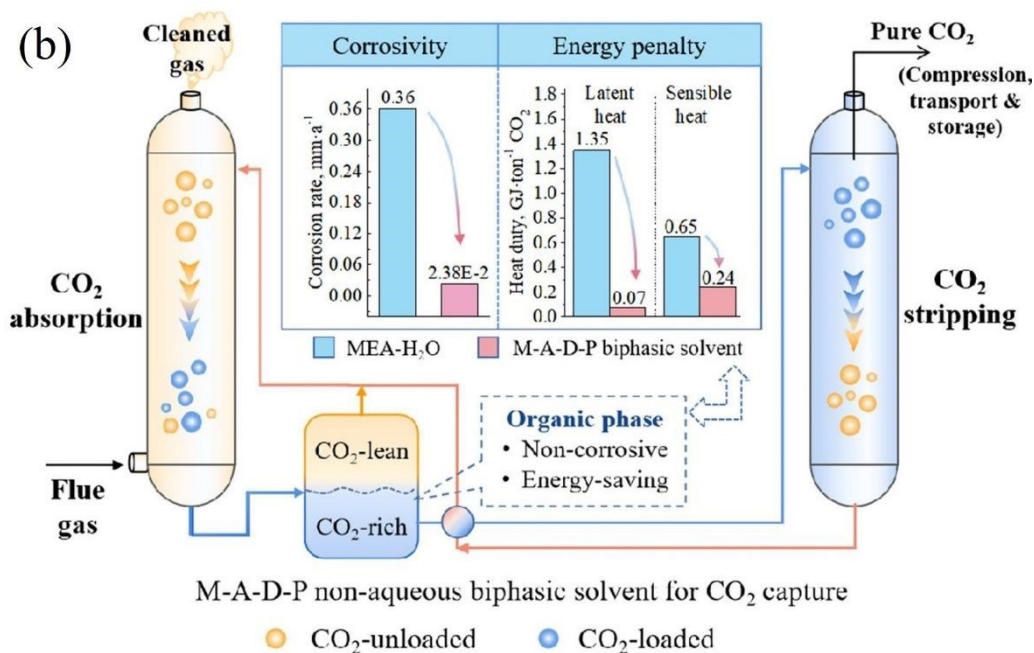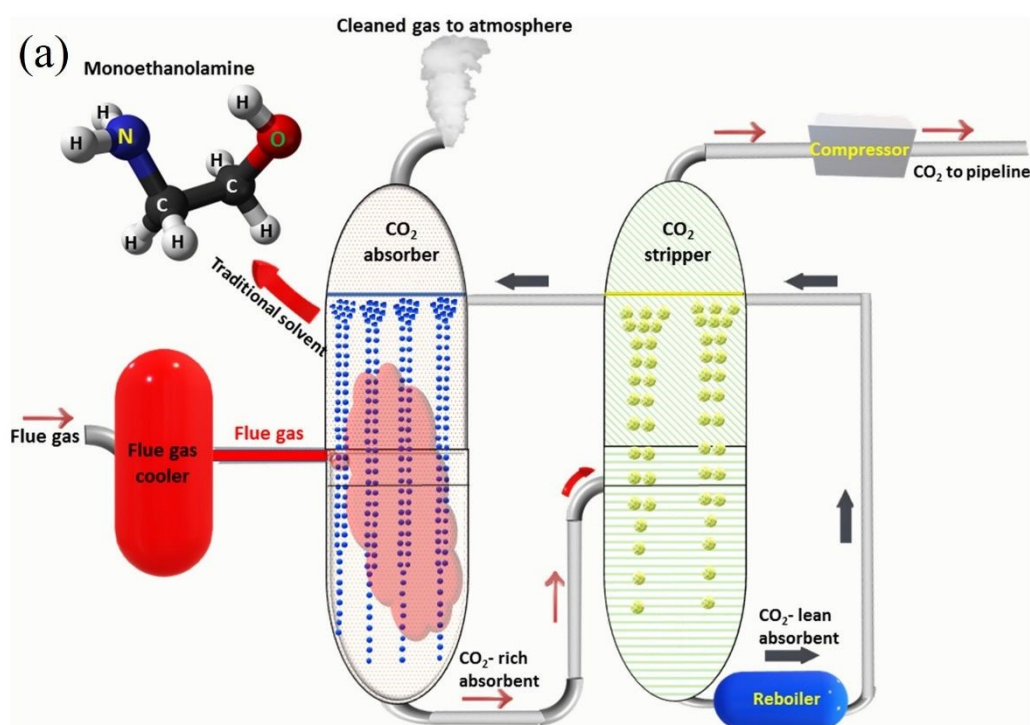
268 **Fig. 2.** (a) Post-combustion technology involves cooling hot flue gas before directing it to an
269 absorber unit that typically contains a monoethanolamine solvent as the traditional sorbent. The
270 CO_2-rich absorbent is then sent to a stripper unit to release the CO_2 gas, while the CO_2-lean
271 absorbent is recycled back to the absorber unit. Finally, the pure CO_2 is compressed and
272 dehydrated for transport via pipelines and for storage purposes. Adopted from Ref. [28] with
273 permission. (b) A schematic illustration of a reactor containing a nonaqueous
274 monoethanolamine-based biphasic solvent for reduced energy penalty and corrosion of carbon
275 dioxide capture. Adopted from Ref. [29] with permission.

277 Monoethanolamine (MEA) offers several advantages, such as a substantial CO_2-carrying

278 capacity, biodegradability, and rapid adsorption rates [26,27]. Additionally, it is well-suited for

279 carbon capture applications with low CO_2 partial pressures. Because of this, MEA has become

280 the industry standard for carbon capture amines despite having modest degrees of toxicity and

281 oxidative and thermal degradation [26]. In the context of standard post-combustion flue gas CO_2

282 separation, employing a 30 wt% MEA solution at pressures ranging from 10–15 kPa, a

283 temperature of 40 °C, and targeting a 90% CO_2 removal rate, it is typically estimated that a

284 reboiler would necessitate approximately 3.6–4.0 GJ per tonne of captured CO_2 [26]. This value

285 has been verified by a number of small- and medium-sized pilot studies [30]. While it's important

286 to acknowledge that reducing reboiler energy is just one of several performance considerations,

287 it is often regarded as a primary focus in the realm of chemical sorbent research. Liquid amines

288 offer a notable advantage for CCS due to their often-high selectivity. Liquid amine CCS

289 technology does have several disadvantages, though. Chemisorbents form strong covalent

290 connections, in contrast to physisorbents, which work through van der Waals interactions [18].

291 Consequently, the regeneration of sorbents in the case of chemisorbents demands more energy,

292 resulting in a larger energy footprint. Furthermore, in situations with low CO_2 concentrations,

293 the kinetics of the chemisorption process are likely to be sluggish, which is less than ideal for

294 CCS.

296   In a study conducted by Li et al. [29], a novel approach to advance CO_2 capture technology aims

297   to reduce energy penalties and mitigate equipment corrosion simultaneously (**Fig. 2**(b)). A new

298   biphasic solvent system was developed for carbon dioxide (CO_2) capture, comprising

299   monoethanolamine (MEA), 2-amino-2-methyl-1-propanol (AMP), dimethyl sulfoxide

300   (DMSO), and N,N,N',N'',N''-pentamethyldiethylenetriamine (PMDETA). Performance

301   evaluation revealed that the optimized solvent achieved a high CO_2 loading of 0.88 mol/mol,

302   with 95.3% of absorbed CO_2 stored in the rich phase, occupying only 56.8% of the total volume.

303   Both MEA and AMP could absorb CO_2 to generate mostly carbamic acid species, according to

304   13C nuclear magnetic resonance (NMR) studies and quantum chemical calculations. Sufficient

305   mutual solubility was guaranteed by hydrogen bonding with the polar DMSO. Only the CO_2-

306   rich phase needed to regenerate since the less polar PMDETA remained isolated and caused

307   phase separation. The M-A-D-P biphasic solvent dramatically reduced sensible heat and

308   vaporisation heat by 63.1% and 94.8%, respectively, when compared to the MEA benchmark.

309   Corrosion tests demonstrated that M-A-D-P exhibited virtually no corrosion to carbon steel,

310   outperforming the MEA solution. Although liquid-amine technologies have proven effective as

311   "wet scrubbers", their industrial-scale deployment has been hindered by several drawbacks.

312   Grande et al. [31], in their report, emphasize the need to advance CCS technology beyond liquid

313   amine approaches to ensure sustainability, primarily due to the substantial regeneration energy

314   requirements associated with liquid amine-based wet scrubbers, which can exceed 140 °C. The

315   increased energy requirements result from the high stability of the carbamate/bicarbonate

316   species generated during the amine-CO_2 reaction [32]. It is worth noting that the energy required

317   to reverse an amine-CO_2 reaction varies depending on the specific amine used. Ghosh et al. [19]

318   elucidate that this discrepancy is a consequence of bicarbonates demanding less energy

319   compared to carbamates when regenerating the constituent amine.

320

321 Various additional drawbacks associated with liquid-amine technologies have been also

322 highlighted [31]. Equipment requirements pose limitations as it is prone to corrosion over time,

323 and retrofitting can prove challenging due to its substantial size. This perspective is

324 substantiated by Vega et al. [25], who propose a potential solution to mitigate equipment corrosion

325 through the use of corrosion-resistant materials and inhibitors, albeit at an added cost. Vericella

326 et al. [27]ggest an alternative approach by proposing the microencapsulation of the amine. This

327 approach seeks to avoid direct contact between the amine and the equipment, as well as effluent

328 gases, potentially mitigating equipment corrosion and decreasing evaporative losses. Moreover,

329 it has been reported by several sources that liquid amines are susceptible to deterioration and

330 breakdown when they come into contact with dust, HCL, HF, SOx, NOx, and oxygen, among

331 other contaminants [25]. Concerns have been expressed regarding the elevated volatility and

332 limited stability of liquid amines. As per the findings of Williams and their research team [33],

333 conducting multiple capture-release cycles leads to notable losses of amine sorbent,

334 subsequently causing a decrease in efficiency and performance. The collective impact of these

335 factors can also negatively affect the overall efficiency of a power plant utilizing post-

336 combustion liquid amine carbon capture and storage technology. A recent report attributed a

337 30–40% reduction in the overall efficiency of power plants to the difficulties associated with

338 implementing CCS technology [19].

339

340 Furthermore, an associated cost was estimated to range from €70 to €100 per ton for this

341 reduction in efficiency. Concerns have been also raised regarding the industrial scalability of

342 liquid-amine technology, with certain publications questioning its suitability for large-scale

343 implementation. Vega et al. [25] contend that, until the CO_2 capacity can be expanded from its

344 present 800 tons per day to the necessary 8000 tons per day, the technology may not be suitable

345 for large-scale CO_2 emission mitigation on an industrial level. Additionally, one of the most

346   significant challenges associated with liquid-amine processes is their restricted scope for

347   performance enhancement [18]. Much of the existing literature underscores the significance of

348   creating novel technologies with enhanced capabilities to supplant current liquid-amine

349   processes. Conversely, the Energy Technologies Institute (ETI) argues that liquid-amine

350   technologies still offer opportunities for future advancements [34]. They cite the development

351   progress of bi-phasic systems as evidence of this potential.

352

353   Moreover, the environmental impact of amines has raised significant concerns. Williams et al.

354   [33] argue that, owing to their highly toxic nature, amines are unsuitable for direct air capture

355   (DAC) applications and could potentially pose an environmental threat if employed in such

356   contexts. Vericella et al. [27] corroborate this viewpoint, noting that the commonly used amine

357   for CCS, monoethanolamine (MEA), generates toxic degradation byproducts. Furthermore,

358   there are apprehensions that the decrease in power plant efficiency resulting from the presence

359   of liquid-amine post-combustion technologies may partially offset the technology's advantages

360   [18]. Another foremost issue with liquid-amine CCS is the high cost; with some sources claiming

361   the capture of 1 ton of CO_2 costs around 50–100 USD (as a conservative estimate) [18].

362   Contrarily, an earlier report from 2015 provided an estimate of the maximum cost of post-

363   combustion amine CCS as $110/tCO_2$ [35]. As a result, numerous sources contend that the

364   technology is not yet commercially feasible for widespread use. Another problem is the extra

365   expense associated with the post-combustion C-capture system because it needs electricity to

366   operate. Liquid-amine CCS (L-A CCS) technology typically causes a large rise in capital costs

367   along with a decrease in power plant efficiency [34].

368

369   There are indications that beyond 2030, continuous technological advancements may lead to

370   cost reductions in liquid-amine technology, ultimately enhancing its viability for large-scale

371   implementation. Developers in the US, Canada, and the UK have committed to sharing publicly

372 all knowledge, data, and designs related to CCS technology, which should foster innovation.

373 According to the ETI, larger projects will enable the exploitation of economies of scale, which

374 will lead to additional cost reductions [34]. One recommended approach is the sequential

375 deployment of existing C-capture technologies in 3 or more full-scale power plants. The ETI

376 suggests that sequential deployments will result in a reduction in risk [34]. Reduced finance costs,

377 larger scale, and infrastructure sharing all work together to potentially cut the cost of output

378 energy by about 45%. Because it might result in more affordable financing solutions, risk

379 minimisation reduces financing costs.

2.2 Metal-organic frameworks in carbon capture

2.2.1 Performance and challenges

382 Solid sorbents such as MOFs are exciting candidates for low-temperature C-capture [32]. Their

383 intrinsic properties such as their high porosity and their customizable chemistry provide the

384 potential to tune MOFs for improved CO_2 uptake capacity and selectivity [26]. Despite their

385 benefits, MOF sorbents face several hurdles. It is generally agreed that the thermal conductivity

386 of sorbents affects the C-capture operation and regeneration process's cost and cycle time [36].

387 MOFs, however, tend to have poor thermal conductivities (at T = 25 °C, the thermal

388 conductivity of MOF-5 single crystal stands at a mere 0.32 W/m K) [37]. The enhancement of

389 MOFs' thermal conductivity is presently the subject of relatively few studies, thus perhaps more

390 research in this field is warranted. Opt-UiO-66(Zr)-$(OH)_2$ (2.50 mmol/g) is one of the best-

391 performing pristine MOFs [38]. This MOF is both water-stable and shows a CO_2 uptake higher

392 than that of MEA [38]. Based on their functional characteristics, modified metal oxide fragments

393 (MOFs) for C-capture can be broadly categorised into three groups: MOFs with amine-

394 functionalized sites (AFSs), unsaturated metal centres (UMCs), and saturated metal centres

395 (SMCs)[18]. Reports suggest that, while able to provide a significantly improved working

396 capacity, the UMC-rich MOFs with the highest capacities suffer from modest selectivity versus

397   nitrogen (SCN) [18]. UMCs can be generated by removing the solvent molecules responsible for

398   the partially coordinated metal atoms in some MOFs. This can be done through heating the

399   material or vacuuming. These UMCs exhibit an excellent CO_2 affinity, and can therefore be

400   used to enhance the capture capacity of a MOF at low pressures [39].

401

402   A new bimetallic MOF, functionalized with pyrazine and used in combination with polysulfone

403   (PSf), was employed to create a mixed matrix membrane (**Fig. 3(A)**) [40]. This innovative

404   membrane demonstrated adaptable interfaces facilitated by the incorporation of the interfacial

405   plasticizer, polyethylene glycol (PEG). The inclusion of the MOF filler notably boosted the

406   CO_2 capture capacity of both pristine PSf membranes and PSf/PEG blend membranes.

407   Specifically, with the PSf/PEG/Pyrazine-MOF membrane, the CO_2 permeability rose

408   dramatically from 6.82 Barrer for the pure PSf membrane to 17.13 Barrer [40]. Bhatt et al. [41]

409   detailed the development of a hydrolytically stable fluorinated metal-organic framework

410   (MOF) referred to as NbOFFIVE-1-Ni. Remarkably, this synthesized MOF exhibits significant

411   CO_2 adsorption capacities, measuring approximately 1.3 mmol/g gravimetrically and 51.4 cm^3

412   (STP) cm^3 volumetrically when exposed to 400 ppm of CO_2 at 298 K (**Fig. 3(B)**). Furthermore,

413   a methyl-functionalized aluminium-based MOF (ZJU-620(Al)) with remarkable chemical-

414   thermal stability and a high specific surface area of 1347 m²/g has been recently developed [42].

415   This MOF has emerged as a highly promising candidate for CO_2 capture due to its exceptional

416   recyclability and impressive capacity, reaching up to 4.25 mmol/g at 298 K and 1 atm. CO_2

417   molecules are primarily captured within two distinct sites. The first site (I) is situated in close

418   proximity to the AlO_6 clusters, while the second site (II) is positioned between two parallel

419   benzene rings, separated by a distance of 6.64 Å (**Fig. 3(C)**). While MOF technology has held

420   great promise to date, the performance data from **Fig. 3(D)** raises some deeply troubling

421   questions about realistic applicability [43]. Specifically, it constructs bond dissociation energy

422   from the noisy-prone measurements of emulated hardware under two error mitigation schemes:

423   state preparation and measurement (SPAM) error mitigation and post-measurement symmetry

424   verification (PMSV). A variational outcome of up to ±1 mHa based on noise alone illustrates

425   the practical challenges in reliably predicting MOF performance under more realistic conditions

426   [43].

427

Journal of Materials Chemistry A Accepted Manuscript
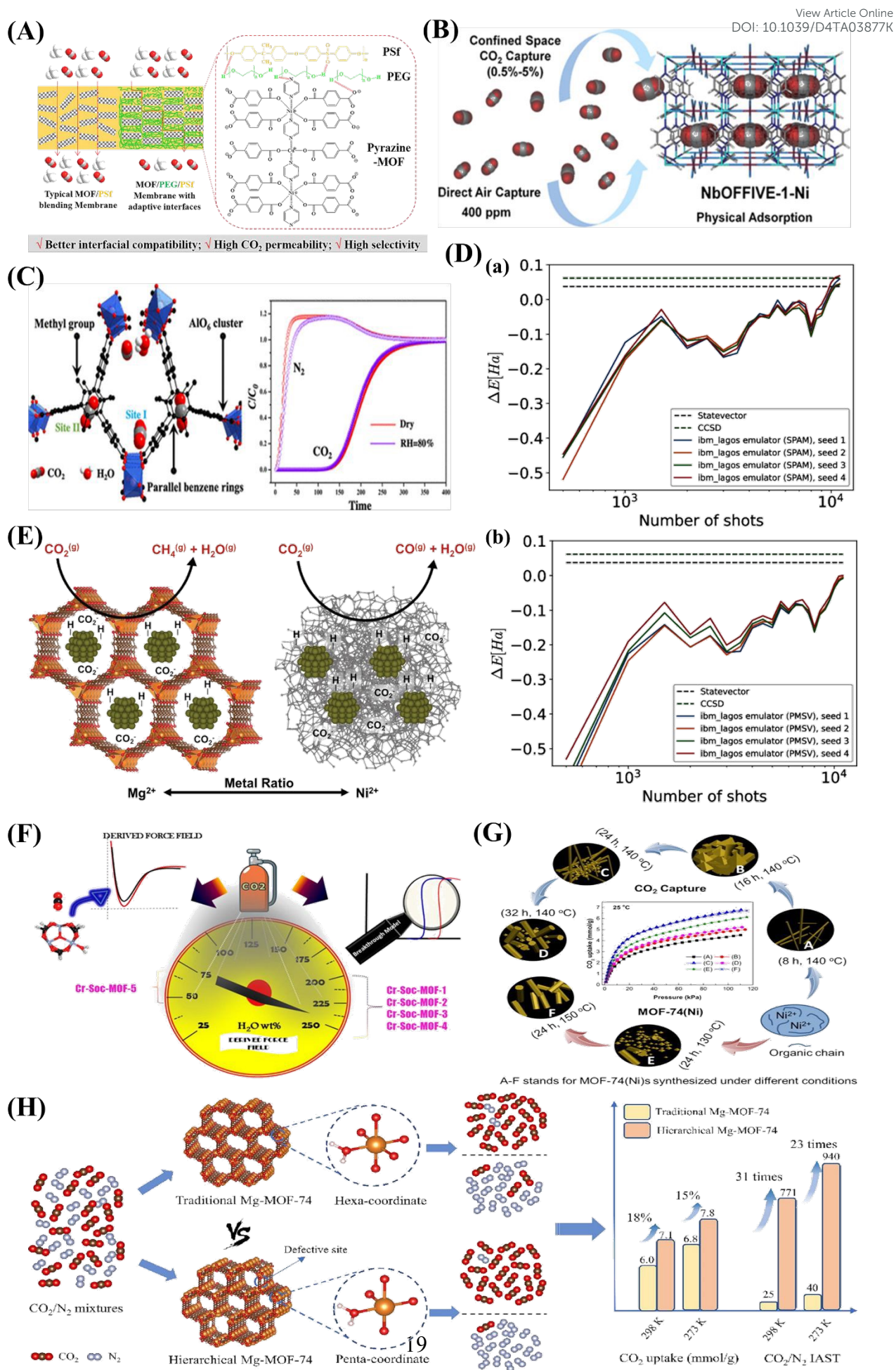
429 **Fig. 3.** (A) An illustration of the interactions and interfacial structure of the PEG/PSf mixed
430 matrix membrane with pyrazine-MOF incorporation for the separation of CO_2 from CH_4.
431 Adopted from Ref. [40] with permission. (B) Fluorinated MOF, NbOFFIVE-1-Ni, for trace CO_2
432 removal and air capture. Adopted from Ref. [41] with permission. (C) Methyl-functionalized Al-
433 based MOF ZJU-620(Al) for CO_2 capture. The two main types of sites where CO_2 molecules
434 are adsorbed are Site I, which is close to the AlO_6 clusters, and Site II, which is between two
435 parallel benzene rings. Adopted from Ref. [42] with permission. (D) Calculate bond dissociation
436 energy using noisy emulated hardware data for 2 noise rates. Demonstrating two error
437 mitigation approaches: (a) state preparation and measurement (SPAM) error mitigation, and (b)
438 post-measurement symmetry verification (PMSV). Both approaches use the same set of 4
439 randomization seeds results in order of the number of measurement shots. Adopted from Ref.
440 [43] with permission. (E) Catalysts with MOF-74 templating comprising mixed metals for
441 effective carbon dioxide capture and methanation. The resultant support material influences a
442 qualitative CO_2 hydrogenation reaction pathway involving the reverse water-gas shift and
443 Sabatier reactions. Adopted from Ref. [44] with permission. (F) Coordinatively unsaturated MOF
444 with square octahedral (Soc) topology (Cr-Soc-MOF) for super-adsorption of CO_2 under humid
445 conditions. Adopted from Ref. [45] with permission. (G) MOF-74(Ni) synthesized under different
446 conditions for carbon capture and storage. Adopted from Ref. [46] with permission. (H) A
447 schematic diagram showing how defect-rich hierarchical porous Mg-MOF-74 and conventional
448 Mg-MOF-74 are prepared differently and their application in CO_2 adsorption. Adopted from
449 Ref. [47] with permission.
450

451 Mg-MOF-74 is often used as a benchmark for other physisorbents, as it has an excellent CO_2

452 adsorption capacity in dry conditions at low pressures (5.5 mmol/g at 0.15 bar, 313 K [18,48] and

453 up to 8 mmol/g at 1 bar and 298 K [39]). The high density of UMCs is largely responsible for the

454 remarkable CO2 uptake values. It is created by reacting 2,5-dihydroxyterephthalic acid with

455 magnesium metal salts, which produces a large amount of UMCs within the MOFs framework.

456 Bahamon and associates compare a number of MOFs to zeolites in their report [49]. Because Mg-

457 MOF-74 performs well in TSA operating settings, they present it as having good potential for

458 TSA separation. According to their findings, Mg-MOF-74 outperformed zeolite 13X, a zeolite

459 that is frequently utilised [49]. In the same context, a mixed-metal metal-organic framework

460 (MOF) referred to as NiMg-MOF-74 was utilized as a template to achieve the even distribution

461 of small nickel nanoclusters within the native MOF framework [44]. Through the adjustment of

462 the Ni-to-Mg ratio within the initial MOF, it is possible to modulate both the available surface

463 area and crystallinity after thermal treatment (**Fig. 3(E)**). This, in turn, has an impact on the

464 capacity for CO_2 adsorption and the selectivity of hydrogenation.

465

466　On the other hand, critics have often pointed out the poor performance of MOFs in gas

467　separation, particularly under humid conditions. Palakkal et al. [45] examined coordinatively

468　unsaturated MOF (CUS-MOF) with square octahedral (Soc) topology. The research

469　encompassed examinations of both co-adsorption (CO_2/N_2) and single-component (CO_2, N_2)

470　adsorption with moisture at 298 K and pressures between 0 and 10 bar. The authors focused on

471　five different Cr-Soc-MOFs, which exhibited experimentally established iso-structural

472　topologies but differed in polynuclear aromatic ring size and N-heteroatom content within their

473　pore walls (**Fig. 3(F)**). Remarkably, Cr-Soc-MOFs with larger pore volumes exhibited CO_2

474　uptake ranging from 23 to 35% by weight, with selectivity levels ranging from 20 to 50%, even

475　up to 70% relative humidity (RH) [45]. A Ni-based metal–organic framework, MOF-74(Ni), was

476　synthesized using a straightforward condensation reflux method [46]. By adjusting the synthesis

477　duration at different temperatures, both the structure and CO_2 adsorption isosteric heat of MOF-

478　74(Ni) could be customized (**Fig. 3(G)**). After being produced at 140 °C for 24 hours, the

479　optimised MOF-74(Ni)-24-140 demonstrated remarkable CO_2 adsorption capacity, attaining

480　8.29/6.61 mmol/g at 273/298 K with a pressure of 1 bar. This capacity surpassed that of

481　previously reported MOF-74-Ni, UTSA-16, and DA-CMP-1 under similar conditions by

482　factors of 2.0/2.1, 1.5/1.6, and 3.6/4.9, respectively. An et al. [47] reported the synthesis of a

483　defect-rich hierarchical porous Mg-MOF-74 (**Fig. 3(H)**). The defect-rich hierarchical porous

484　Mg-MOF-74 exhibits an increased adsorption enthalpy of CO_2 at zero load, rising from 36 to

485　46 kJ/mol compared to conventional Mg-MOF-74. Moreover, the saturated CO_2 adsorption

486　capacity under ambient pressure has seen a significant improvement of 15%.

487

488　Despite high performance of Mg-MOF-74, their application is hindered by several factors

489　including its relatively poor CO_2 selectivity over other gases such as O_2, N_2, and CH_4 (all of

490   which are abundant in the flue gas mixture) [18]. Additionally, whereas CO_2 molecules are

491   strongly attracted to UMCs, H_2O molecules would preferentially occupy the open metal sites

492   [50]. As a result, Mg-MOF-74 absorbs substantially less CO_2 when it is exposed to moisture. This

493   is troublesome since there is a significant amount of $H_2O(g)$ (5–7%) in flue gases [50]. Hence, it's

494   crucial to explore and devise methodologies for enhancing the selectivity over nitrogen of the

495   MOF, particularly in the presence of water. An example of the ongoing research into this issue

496   includes the introduction of amines into MOFs in an effort to emulate the chemisorption of CO_2

497   used by conventional liquid-amine technologies [51]. In a recent study conducted by Kim et al.

498   [52], MOFs modified with diamines (nitrogen compounds) were investigated. The modified

499   MOFs can capture and release CO_2 at lower temperatures than those used by existing carbon

500   capture materials [52]. As a result, the CCS process requires far less energy than it does with

501   existing technology, which lowers the process's cost [52]. Amine-modified MOFs are produced

502   by grafting amine functional groups onto MOFs [18]. This can improve the MOF's SCN and

503   operating capacity, but regrettably, there is frequently a significant regeneration energy penalty

504   [53]. Nonetheless, under capture conditions, some alkylamine-modified MOFs have good CO_2

505   working capabilities, SCN, and moderate regeneration [39]. There have been successful reports

506   of functionalizing $Mg_2(dobpdc)$ with N,N'-dimethylethylenediamine (mmen). Coordination

507   bonds form between the amine groups and the unsaturated metal centers (UMCs) on

508    $Mg_2(dobpdc)$. The resultant MOF, mmen-$Mg_2(dobpdc)$, boasts a high density of amine groups,

509   leading to enhanced selectivity versus nitrogen (SCN) even in the presence of water. At 313.15

510   K and 0.15 bar, the CO_2 adsorption capacity reaches 3.5 mmol/g. Moreover, this MOF

511   effectively mitigates the substantial energy requirements for regeneration, further bolstering its

512   potential for carbon capture applications [39]. **Table 1** summarizes adsorption data for a variety

513   of functionalized MOF sorbents at different pressures and temperatures.

514

515   **Table 1.** CO_2 adsorption data for a variety of functionalized MOFs at different experimental
516   conditions.

		CO_2 uptake (mmol/g)					
Adsorbent	**Functionality**	**Low pressure (mbar)**	**0.15 bar**	**1bar**	**Temperature (K)**	**Selectivity (S_{CN})**	**References**
Mg-MOF-74	UMC	NA	5.35	8.1	296	182 (IS) (15:85)	[18]
Mg_2(dobpdc)	UMC	NA	4.85	6.42	298	NA	[53]
UiO-66-$(CH_3)_2$	UMC	NA	1.3	4.01	293	58 (IS) (15:75)	[54]
UiO-66	UMC	NA	NA	1.8	298	23 (IAST) (14:57)	[18]
Co-MOF-74	UMC	NA	2.76	6.69	296	NA	[18]
mmen-Mg_2 (dobpdc)	Amine-modified	2.05 at 0.4mbar	3.13	3.86	298	200 (IS) (15:75)	[55]
[Mg_2(dobdc) $(N_2H_4)_{1.8}$]	Amine-modified	3.89 at 0.4mbar	5.18	5.51	298	NA	[56]
UiO-66-NH_2	Amine-modified	NA	1.15	2.6	298	32 (IS)	[18]
MOF-5	Pristine MOF	NA	NA	2.1	298	10.1 (IS)	[57]
MOF-505	Pristine MOF	NA	0.4	1.5	304	NA	[18]

517

2.2.2   Manufacturability, stability and cost

519   Mukherjee et al. [18] emphasize the importance of the industrial-scale production of candidate

520   sorbents to meet the quantity demands of later-stage pilot-scale testing and wide-scale rollout.

521   Most MOFs are not yet manufactured on a large scale, and the few that can be, are synthesized

522   as powders [26]. MOFs need to be structured sorbents to be incorporated into the C-capture

523   procedure. Therefore, it is necessary to look for ways to turn MOFs into pellets, beads, fibres,

524   or monoliths. The absence of methods for transforming microcrystalline MOF powders into

525   devices has given rise to numerous problems [18]. Some studies explore the incorporation of

526   MOFs into support structures (monoliths or pellets) but these are still in the early development

527   stages [58]. Generally, research into the pelletizing MOFs without binders has shown a reduction

528   of approximately 5% in the MOF's CO_2 uptake capacity [59]. Research conducted by Peterson et

529   al. [60] employed octane adsorption experiments to investigate the effect of pelletization pressure

530   on the properties of UiO-66. Results showed that pelletization at 68.94 bar led to an 8%

531   reduction in octane adsorption and pelletization at 689.5 bar led to a larger reduction of 16%.

532   However, results for the pelletization of HKUST-1 reported by Asadi et al. [61] show a 20%

533   decrease in CO_2 uptake capacity. This suggests that sorbents may have varying uptake capacity

534   responses to pelletization. Hu et al. [62] argue that, given the complexity of pelletization, an

535   empirical approach involving practical investigations is necessary.

536

537   The current synthesis of MOF powders is typically done via solvothermal batch processes.

538   These processes are time-consuming, require the use of expensive organic solvents, and involve

539   complex purification methods [62]. These problems lead to high manufacturing costs, which may

540   reduce their attractiveness as possible sorbents from an economic standpoint. Although more

541   work needs to be done, some progress has been made recently, such as the utilisation of twin-

542   screw extrusion (TSE) kg per hour-scale MOF synthesis without the use of ore-reduced

543   solvents. When suggesting uses for newly created materials, a variety of considerations,

544   including toxicity, life-cycle assessment studies, and economic implications, must be taken into

545   account in addition to the previously mentioned concerns. On the other hand, one prominent

546   drawback that has hampered the applicability of MOFs in this domain is their stability under

547   the conditions of CCS operation, with many MOFs exhibiting poor hydrolytic stability [18]. This

548   means that when MOFs are exposed to moisture, they are prone to decompose. There have been

549   developments in the field to address this issue and recent research shows promise of progress.

550   Investigated strategies include doping MOFs with alkyl amines (or other chemical functions)

551 and improving the MOF's hydrophobicity [62]. Studies on doping MOFs with N,N-

552 dimethylethylenediamine, hydrazine (N_2H_4), and 2,2-dimethyl-1,3-diaminopropane (dmpn)

553 have shown that the CO_2 absorption capability is nearly entirely retained when there is moisture

554 present [63]. However, it is important to note that doped MOFs may still struggle with poor

555 chemical, mechanical, and thermal stability [53]. Research by Dalvi and Rossky [64] showed a

556 marked improvement in hydrophobicity from MOFs decorated with fluoro or alkyl groups,

557 suggesting this could be an alternative solution.

558

559 Another method of preparation that has been explored is wet granulation. This method,

560 proposed by Chang and colleagues [65], mixes the MOF with a mesoporous γ-alumina (MRA)

561 binder to produce millimeter-scale spheres (**Fig. 4(a)**). Numerous MOFs, including MIL-

562 101(Cr), UiO-66(Zr)-NH2, MIL-100(Fe), and UiO-66(Zr), have shown effectiveness with this

563 strategy. After shape, the MOF's natural characteristics are preserved with the aid of a binder.

564 Furthermore, tiny businesses like Mosaic Materials and NuMat are making a concerted effort

565 to satisfy these needs [26]. In the research conducted by Das et al. [66], the authors detailed formation

566 of a hydrogen-bonded three-dimensional (3D) framework involves a zinc (II) center, a partially

567 fluorinated elongated dicarboxylate ligand, and an amine-rich melamine co-ligand (**Fig. 4(b)**).

568 Notably, this framework exhibits two distinct types of 1D channels adorned with CO_2-attractive

569 ($-NH_2$ and $-CF_3$) groups that facilitate the framework's exceptional selectivity for CO_2

570 adsorption (uptake of 49.88 and 31.16 cm^3/g at 273 and 298 K, respectively) [66]. Furthermore, a

571 straightforward and comprehensive room-temperature procedure has been established for the

572 fabrication of (111)-oriented UiO-66 membranes [67]. This method utilizes a ZrO_2 buffer layer-

573 modified porous α-Al_2O_3 substrate and a $Zr(n-OPr)_4$ source (**Fig. 4(c)**). Experimental findings

574 revealed that conducting the reaction at room temperature (RT) increased the number of missing

575 linkers within the UiO-66 framework (1.5 per Zr_6 formula unit). Consequently, this resulted in

576 enhanced CO_2/N_2 adsorption selectivity due to a stronger affinity interaction between CO_2 and

577 the defective sites in the Zr6-oxo cluster nodes [67].
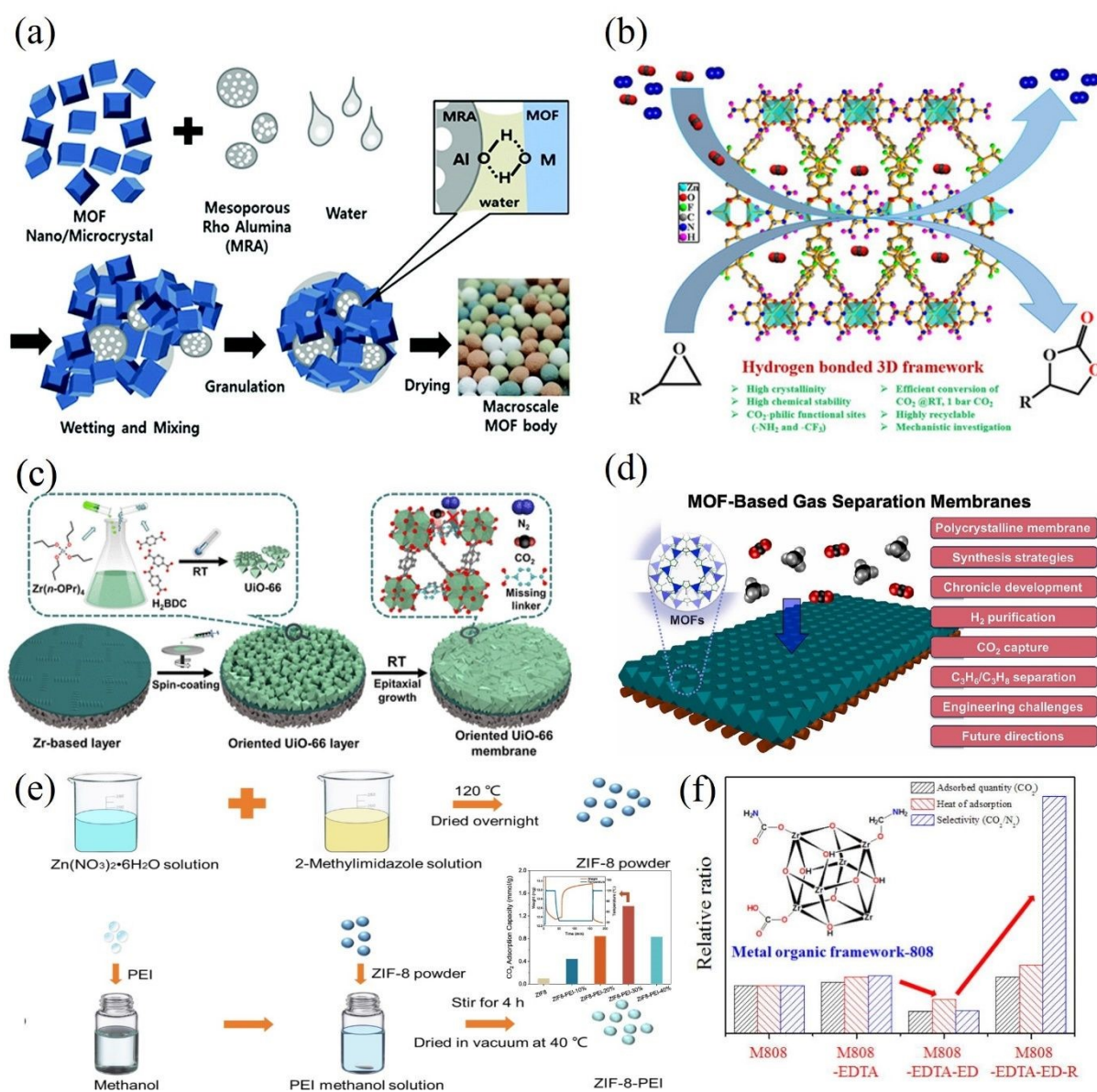
578

579 **Fig. 4.** (a) Creating MOF granules or spheres via the wet granulation process by aggregating
580 MOF and MRA particles. Adopted from Ref. [65] with permission. (b) The rational design of a
581 porous Zn(II)-MOF with several functional sites that can be used, under moderate conditions,
582 for extremely effective CO_2 fixation with internal and terminal epoxides. Adopted from Ref. [66]
583 with permission. (c) A schematic diagram depicting the entire room temperature preparation
584 process for defect-engineered (111)-oriented UiO-66 membranes. A higher CO_2/N_2 adsorption
585 selectivity was demonstrated and attributed to the stronger affinity interactions between CO_2
586 molecules and the defective sites in the Zr_6-oxo cluster nodes. Adopted from Ref. [67] with
587 permission. (d) Diagram showing the in-situ growth process for homochiral MOF membrane
588 production on nickel net and its use for molecular separations. Adopted from Ref. [68] with
589 permission. (e) A synthesis process of unmodified and PEI-modifed ZIF-8 and the
590 corresponding adsorption capacity at different PEI loadings. Adopted from Ref. [69] with
591 permission. (f) Zr-based MOF functionalized with ethylenediaminetetraacetic acid (MOF-808-

592   EDTA), ethylenediamine (MOF-808-EDTA-ED), and lithium aluminium hydride (MOF-808-
593   EDTA-ED-R) for selective CO_2 adsorption. Adopted from Ref. [70] with permission.

594

595   Conversely, many research endeavours have focused on MOF-based gas separation

596   membranes, with particular attention to ZIF-8 [68] (**Fig. 4(d)**). The exploration of MOF

597   membranes for gas separation traces back to 2009 [71], with the milestone achievement of the

598   first continuous MOF-5 membrane via an in-situ growth method. This milestone marked the

599   beginning of MOF membrane development for gas separations. Other methods include layer-

600   by-layer growth, electrochemical synthesis, vapour phase synthesis, seeding and secondary

601   growth, and contra-diffusion also appeared in the ensuing ten years. Particularly noteworthy is

602   the considerable focus on ZIF-8 in MOF membrane research due to its exceptional C_3H_6/C_3H_8

603   separation capabilities, straightforward synthesis, and the potential for producing high-quality

604   membranes. A recent study involved the synthesis and characterization of ZIF-8 with varying

605   weights of polyethyleneimine (PEI) [69]. The results indicated that ZIF-8 with 30 wt.% PEI

606   achieved the highest CO_2 uptake of 1.4 mmol/g under dry conditions and demonstrated

607   remarkable CO_2/N_2 separation performance (**Fig. 4(e)**). The CO_2 adsorption capacity of ZIF-8-

608   PEI30% notably rose to 1.7 mmol/g when exposed to humid flue gas with 50% relative

609   humidity (RH). Furthermore, even after undergoing 50 adsorption/desorption cycles, only a

610   slight decrease in adsorption capacity was observed. Park et al. [70] have directed their efforts

611   towards improving the efficiency of Zr-based metal-organic framework (MOF-808) for CO_2

612   capture by introducing various functional groups onto the MOF surface. Notably, reducing the

613   MOF-808-EDTA-ED compound with lithium aluminium hydride (LAH) led to a significant

614   enhancement in performance, including higher CO_2 adsorption capacity, CO_2/N_2 selectivity,

615   and isosteric heat of adsorption. For example, under conditions of 298 K and 1 atm, MOF-808,

616   MOF-808-EDTA, MOF-808-EDTA-ED, and MOF-808-EDTA-ED-R demonstrated CO_2/N_2

617   selectivity of 40, 48, 19, and 197, respectively (**Fig. 4(f)**). This significant enhancement is

618 attributed to the contribution of functional groups and porosity. The introduction of amides

619 during the reaction with ED resulted in decreased MOF porosity, negatively impacting CO_2

620 capture. However, subsequent reduction of amides to amines improved adsorption effectiveness

621 [70].

622
623 Regarding the cost, it can vary widely depending on several factors, including the specific MOF

624 composition, synthesis method, scale of production, and market demand. Generally, MOFs are

625 more expensive to produce compared to traditional adsorbents like activated carbon due to their

626 complex synthesis processes and sometimes costly precursor materials. At present, the

627 production of MOFs typically involves expensive starting materials and specialized synthesis

628 techniques, which contribute to higher production costs. Additionally, the purity and quality of

629 MOF materials also affect their cost, with higher-purity MOFs often commanding a premium

630 price. As was previously said, the creation of MOFs that require less temperature to absorb and

631 release CO_2 will probably lead to lower process costs over time [52]. However, MOF sorbent costs

632 are still considered the limiting factor for their commercial application [62]. Since MOF sorbents

633 for post-combustion C-capture have not been subjected to real-world trials, prices can be

634 estimated in part by considering the price of the substrates or raw sorbent utilised in the

635 preparation [18]. The metal ions or clusters are often inexpensive, consequently, the main factor

636 affecting the cost of a MOF sorbent is the linker cost. Whilst most sorbents use polycarboxylate

637 ligands, there is a variety of inexpensive and commercially available ligands, for example, one

638 of the most common ligands, 4,40 -bipyridine (bipy) [72]. Commercial MOF vendors still charge

639 significantly more than more conventional porous materials like zeolites, even though MOFs

640 are synthesised from comparatively cheap ingredients [62]. This is often attributed to high

641 manufacturing costs which are the result of a shortfall in large-scale production methods.

3. Energy storage devices

642

643   Currently, supercapacitors (SCs) are among the most popular energy-storage devices [73], which

644   have already found applications in consumer electronics, memory backup systems as well as

645   industrial-scale power and energy management devices [74]. Although conventional capacitors

646   have a larger energy density, SCs are seen to be better because of their many benefits, including

647   flexible packaging, low weight, minimal heating, and strong device stability [75]. Furthermore,

648   SCs have proven to be both safe and reliable, as Sundriyal et al. [74] highlight in their recent

649   application in the emergency doors of the Airbus A380. In addition, one of the most intriguing

650   uses of SCs is in contemporary transportation systems like electric cars. The sales ban on

651   internal combustion engines (IC) engines will be accelerated from 2040 to 2035 as a result of

652   growing social and governmental pressure to reduce fossil fuel consumption. As a result, the

653   electrical energy storage (EES) devices used in these transportation systems must be able to

654   provide a high enough power density to expedite vehicle charging times [74]. SCs' high-power

655   densities (up to 15 kW/kg) give them the ability to charge and discharge rapidly, which would

656   enable fast charging of electric vehicles and their good cyclic stability would ensure that their

657   performance wouldn't degrade significantly over time. However, their largescale usage is

658   hindered by low energy densities meaning that they are unable to hold large amounts of energy

659   [75].

660
661   In the same context, electrodes play a critical role in SC performance, therefore selecting an

662   electrode design and material is key to ensuring effective energy storage. Sundriyal et al. [74]

663   suggest several critical electrode parameters that determine the performance of the SC including

664   specific capacitance, power and energy densities, cycle life, and stability in bending. Forse et

665   al. [76] also offer a range of critical electrode material properties that require consideration,

666   including a large specific surface area, good stability at high temperatures, pores size and

667   distribution, high corrosion resistance, high conductivity, and cost-effectiveness. Research by

668 Huang et al. [73] supports this but summarises the performance criteria under the broad umbrella

669 of material properties that allow for a short ion or charge transfer channel whilst also providing

670 many active sites.

671

672 Many sources discuss the relationship between the specific surface area (SSA) and capacitance

673 as though it were linear, with higher SSAs resulting in a higher capacitance [73]. Whilst this is

674 true for certain SC electrodes, Wu and Cao [77], highlight that in some instances, a higher SSA

675 will not guarantee a greater capacitance. Effective surface area (ESA) is a surface area that is

676 directly utilised for charge absorption and is associated with the distribution of pore sizes. As

677 previously mentioned, the low energy density of SCs is currently impeding their practical

678 deployment [78]. Energy density denotes the quantity of energy that a SC can store per unit

679 volume of SC [74]. On the other hand, power density describes the amount of power transferred

680 per SC volume. The difference between SSA and the attained specific capacitance is a topic

681 covered in a number of studies. Some reports indicate that during charge storage, not all of the

682 pores are used [75]. Consequently, Forouzandeh et al. [75] argue that while SSA is an important

683 performance parameter for EDLC design, other factors such as pore size distribution and ESA

684 will also influence the SC's electrochemical performance. In their research paper, Wu and Cao

685 [77] state that the electrode surface area is the main influencer on the electrochemical properties

686 of the SC.

687

688 Phiri et al. [79] highlight the important role played by ion-transport kinetics in SC electrode

689 performance. According to their research, the material's surface area and pore structure affect

690 the electrode's ion kinetics. Consequently, the authors suggest a material that combines a high

691 SSA with a combination of micropores and mesopores (to raise the ESA) while thinking about

692 ways to improve the electrochemical performance of electrodes. They suggest that the

693   mesopores may serve as a quick pathway for the SC electrolyte to move, boosting the

694   capacitance of the SC and that the micropores offer a sizable SA for quick ion adsorption. Wu

695   and Cao [77] also propose other factors for consideration such as the electrical conductivity of the

696   electrode material and the presence of surface functional groups. Overall, factors such as power

697   and energy densities, cyclability, specific capacitance and morphology require consideration

698   during the material selection process for SC electrode capacitors. Moreover, cyclability pertains

699   to the count of charge and discharge cycles a supercapacitor can undergo before experiencing

700   electrode degradation and notable performance decline. [77]. Often, degradation only becomes

701   evident after prolonged cycling. Consequently, estimating the cyclability can be difficult.

702   Weinstein and Dash [80] warn that laboratory-based testing of cyclability often relies on "beaker

703   tests". During these tests, the SC electrodes are placed in a beaker and submerged in the

704   electrolyte. This kind of approach reduces the effect of contaminants on cyclability by allowing

705   them to diffuse into the huge volume of electrolyte that causes errors. On the other hand,

706   because of the device's real operating circumstances, there is minimal room for diffusion

707   because the electrolyte volume is rather tiny [80]. Therefore, the cycle life obtained through

708   laboratory tests is likely to be different from values obtained from testing the real fabricated

709   SC. Cyclability is an important factor for the assessment of both the performance and the

710   environmental impact of the design. If the electrode degrades quickly, more material will be

711   required over the lifetime of the device or the device will require replacing.

712

713   In another context, Forouzandeh et al. [75] highlight a series of considerations for assessing the

714   environmental impact of an electrode including the toxicity, reusability (reformation prospects),

715   and energy requirements for the primary manufacturing (processing raw materials).

716   Furthermore, Weinstein and Dash [80] postulate that, because SCs are often relatively small

717   compared to the device they power, there is little incentive to reduce the size and weight of the

718   SC if it results in higher costs. Manufacturers of SC are more concerned with controlling costs

719   than with making incremental performance advances. Price is acknowledged as significant, but

720   it is not given more weight than the other factors [75]. Contrarily to Weinstein and Dash,

721   Pongprayoon and Chaimanatsakun [81] argue that the two most important design requirements

722   for SCs are tuning the electrode material morphology (pore shape and size) to optimize the

723   transportation of electrolyte ions and a high SSA to increase the availability of

724   electrochemically active sites. Both are relevant for improving performance rather than

725   reducing cost.

3.1   Porous carbonaceous materials for supercapacitors

726

727   Porous carbonaceous materials stand out as highly versatile materials for supercapacitor

728   electrodes, particularly due to their diverse applications in various biomass sources. In recent

729   scientific research, there has been a notable emphasis on synthesizing carbonaceous materials

730   from biowaste, which produces a variety of morphologies and surface textures. The typical

731   synthesis process involves carbonization and activation steps, leading to activated carbon with

732   tunable pore sizes and exceptionally high specific surface area compared to other carbonaceous

733   materials. This renders activated carbon a preferred choice for supercapacitor electrodes. Prior

734   to the rise of MOFs, most studies on supercapacitor electrode materials were concentrated on

735   carbon-based materials [82]. Activated carbon (AC) is used in almost all electrochemical

736   capacitors (ECs), and many producers of SC choose to use coconut shell AC as their active

737   electrode material [80]. Phiri et al. [79] note that while graphene and carbon nanotubes (CNTs) are

738   also common material choices for SC electrodes, their wide-scale deployment has been

739   hindered by their high production costs and disposition to nanoparticle aggregation which limits

740   their effective SSA.

3.1.1 Performance and properties

Carbon SC electrodes usually work via charge adsorption, resulting in large power densities and long cycle life [73]. In addition to this, carbon electrodes often present superb chemical stability and electrical conductivity. An AC fabricated electrode in a study by Li et al. [83] displayed a specific capacitance of 207.5 F/g and a cycle life of over 3000 cycles when tested at a current density of 0.5 A/g. Another study reports an energy storage density of about 28 Wh/kg, but it also mentions that the device's charge supply rate limits the amount of power that can be produced [84]. Research by Ajay and Dinesh [85] yielded a specific capacitance of 107.6 F/g for commercially available AC measured at a 5 mV/s scan rate. However, Phiri et al. [79] argue that biomass-derived ACs also have disadvantages, including discrepancies in the structures of the biomass sources. Because of this, the ideal circumstances for the synthesis of AC from one biomass source might not be appropriate for another. According to their studies, this can also apply to a single biomass source that is used intermittently. As a result, a biomass source needs to have a predictable and consistent structure to be taken into consideration for large-scale practical applications.

AC-based SC electrodes are well suited for this purpose, not only do they have a high thermal and electrochemical stability, but they also benefit from a large SSA. Available values of AC SSA vary with most papers agreeing on a value within the range of 1000–3000 m^2/g [86,87]. Conversely, a study by Weinstein and Dash [80] suggests a theoretical maximum SSA of 2000 m^2/g. Carbon materials have a high SSA in addition to being relatively simple to produce, modify, and optimise [87]. The premium-grade AC utilised for SC electrodes has been refined to guarantee that the ash level is less than 1% and the halogen and iron impurities are fewer than 100 ppm [80]. This purification helps to improve the cycle life of the electrode. Despite this, ACs are still comparatively cheap. ACs also benefit from high pore volumes in the range of 0.5–2

766 cm^3/g [87]. As previously stated, other literature suggests that the SSA is not as important as the

767 pore size and its impact on the effective specific surface area (ESSA) [75]. Research by Arenillas

768 et al. [88] supports this, suggesting that for AC electrodes, the whole SSA is not used for charge

769 storage as the larger electrolyte ions are unable to enter the small micropores. The largest

770 obtainable SSA for AC is estimated at 3000 m^2/g, whilst the obtainable ESSA ranges from 1000

771 to 2000 m^2/g [75]. Forouzandeh et al. [75] also examine the potential drawbacks associated with

772 large specific surface areas (SSAs), noting in their report that, in some scenarios, augmenting

773 the SSA can induce electrolyte decomposition and create dangling bond positions. Additionally,

774 a high pore volume may arise from attempts to raise the SSA through excessive activation. Poor

775 conductivity and low material density, which resulted in low energy and power densities, were

776 among the effects of these huge pore volumes that were investigated [89]. The impact of various

777 electrolytes on the obtained capacitance of AC electrodes has also been studied. It was shown

778 that the capacitive performance of AC electrodes was enhanced when an aqueous electrolyte

779 was used instead of an organic electrolyte.

780

781 The performance and characteristics of activated carbon as electrode materials for

782 supercapacitors are very well presented in **Fig. 5A (a, b)**. The latter presents the CV curves of

783 the electrodes at a scan rate of 50 mV/s and gives an idea about their capacitive behaviour and

784 electrochemical performance. That nearly rectangular shape of the CV curve indicates ideal

785 capacitive properties; among them, better performance is obtained for the AC-HF sample [90].

786 **Fig. 5A(b)** shows the galvanostatic charge-discharge curves of the electrodes at a current

787 density of 1.5 mA/cm², which provides the potential for energy storage. The GCD curves are

788 overlapping linearly and symmetrically, which further testifies to the high reversibility and

789 efficiency of the activated carbon electrodes, especially AC-HF, with the longest charging time

790 and discharge time and thus indicative of higher energy storage capacity [90]. A recent

791   breakthrough introduced a straightforward and cost-effective technique for producing high-

792   performance cellulose-based activated carbon fibre papers (ACFPs), capable of serving as self-

793   supporting supercapacitor electrodes without the need for binders [91]. This innovative approach

794   combines wet papermaking, thermal carbonization, and double activation processes, enabling

795   the on-site conversion of fibrillated pulp fibres into cellulose-derived activated carbon,

796   seamlessly integrated with carbon fibres (CFs) (**Fig. 5(B)**). The electrochemical evaluations

797   demonstrated that the ACFPs exhibited outstanding electric double-layer capacitive behaviour

798   (**Fig. 5(C)**), with coulombic efficiency and capacity retention remaining at 98.58% and 100%,

799   respectively, even after 10,000 cycles (**Fig. 5(D)**). The authors further elucidated the schematic

800   representation of charge transfer and electrolyte ion transfer within ACFP [91]. The configuration

801   presented in **Fig. 5(E)** demonstrates a stable three-dimensional conductive network structure

802   through the close interweaving of CFs within the ACF matrix. This arrangement facilitated

803   swift electron migration along the CFs and enhanced the adsorption of electrolyte ions by the

804   ACFs [91].
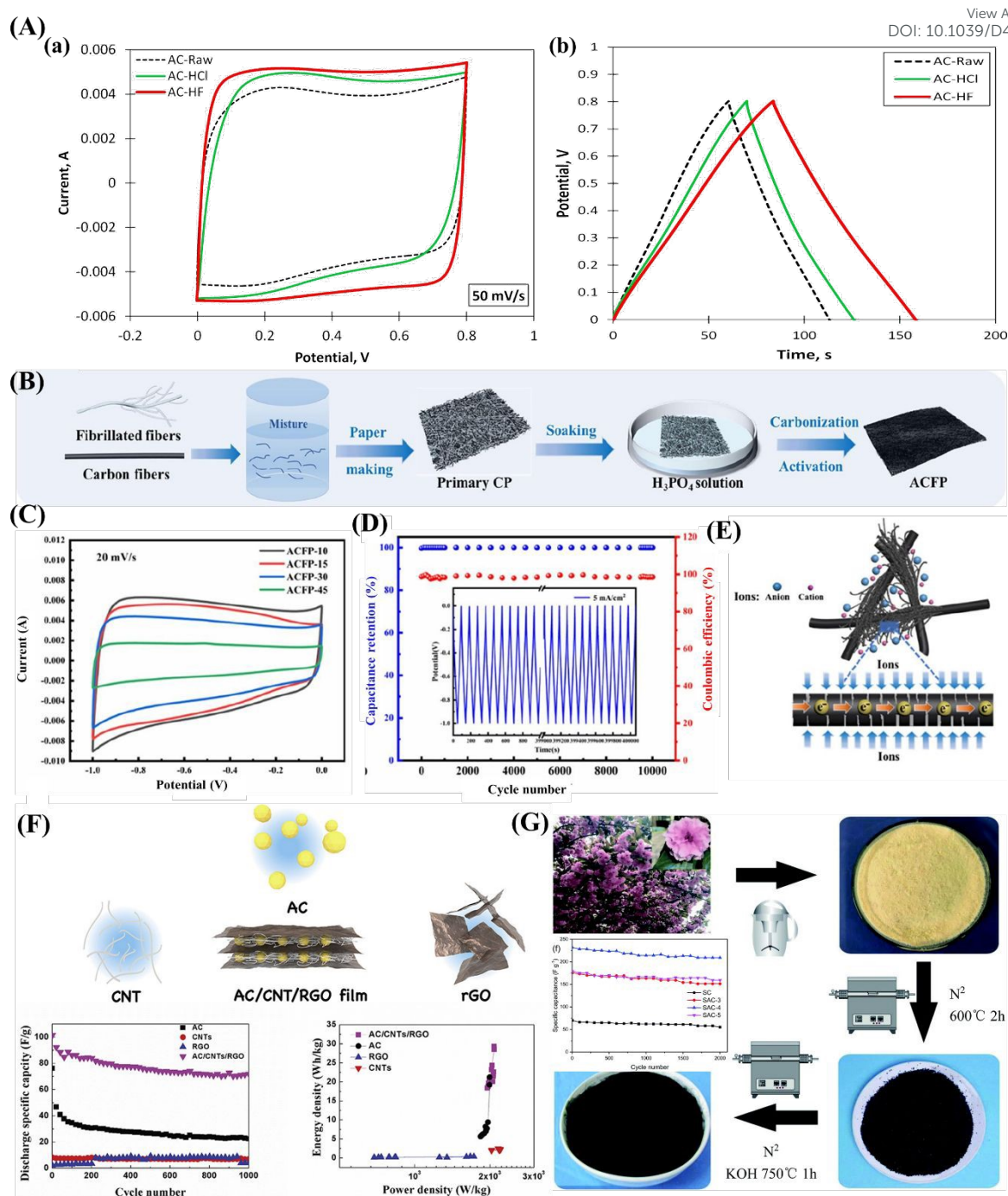
Fig. 5. (A) (a) Cyclic voltammetry curves measured at a scan rate of 50 mV/s; (b) galvanostatic charge discharge curves measured at a current density of 1.5 mA/cm². Adopted from Ref. [90] with permission. (B) Illustration depicting the production process of cellulose-based activated carbon fibre papers (ACEPs), (C) Cyclic voltammetry curves recorded for ACFPs with varying CFs content using a 20 mV/s scan rate, (D) Retention of capacitance and coulombic efficiency measured at a current density of 5 mA/cm², and (E) Schematic diagram illustrating the charge transfer and electrolyte ion transfer within the conductive networks in ACFP. Adopted from Ref. [91] with permission. (F) A flexible electrode consisting of self-supporting activated carbon, carbon nanotube, and reduced graphene oxide and its SCs performances show a high specific capacitance of 101 F/g at the current density of 0.2 A/g. Adopted from Ref. [92] with permission. (G) Schematic representation illustrating the production process of porous carbon derived from

817 sakura, along with its corresponding long-term cycling performances. Adopted from Ref.[93]

818 with permission.

819

820 In the work of Li et al. [92], a deliberately engineered self-supporting and flexible film composed

821 of activated carbon, carbon nanotubes, and reduced graphene oxide (AC/CNT/RGO) has been

822 developed (**Fig. 5(F)**). The AC/CNT/RGO electrode demonstrates an impressive specific

823 capacitance of 101 F/g when operated at a current density of 0.2 A/g, resulting in a remarkable

824 maximum energy density of 30 Wh/kg. Conversely, three-dimensional porous carbon materials

825 were synthesized by utilizing sakura petals as the source material and employing a combination

826 of pre-carbonization and KOH activation techniques (**Fig. 5(G)**) [93]. The synthesized porous

827 material exhibited a high specific surface area (up to 1785.41 m^2/g), leading to a maximum

828 specific capacitance of 265.8 F/g at a current density of 0.2 A/g. Additionally, under continuous

829 cycling for 2000 cycles, the capacitance retention rate remains excellent, reaching an impressive

830 90.2%, demonstrating outstanding cycling stability [93]. Recently, AC was prepared using biochar

831 derived from date seeds via pyrolysis and activated with H_2SO_4 [94]. The elaborated samples

832 demonstrated a specific capacitance of 487.5 F/g at a current density of 1 A/g. Additionally,

833 galvanic charge and discharge trends indicated a higher charge storage capacity with reduced

834 discharge. Another study focuses on converting inexpensive Cilantro plants (C. sativum) into

835 AC aiming to produce a cost-effective AC material that shows promise in supercapacitors for

836 energy storage [95]. The material that was synthesised at 700 °C showed ideal specific surface

837 area (SSA) and surface functionalities, which promoted surface redox processes, electrode

838 wetting, and ion diffusion-induced pseudo-capacitance. At 1 A/g, its specific capacitance was

839 162.4 F/g. Particularly noteworthy is the remarkable performance of the activated carbon (AC)

840 symmetric supercapacitor, delivering a high-power density of 243.94 W/kg and maintaining

841 minimal capacitance loss over 5000 cycles at 10 A/g, indicative of excellent cycling stability.

3.1.2 Environmental impact

842

843 Numerous commercially available ACs are produced from precursors such as coal and

844 polymers, which are fossil fuel-based, making them both expensive and environmentally

845 unfriendly [79]. However, ACs derived from biomass are still promising candidates for SC

846 electrode materials [86]. Large pore volume and surface area (which can surpass graphene's), ease

847 of preparation, and a customised architecture that has been deemed feasible for commercial

848 usage are some of their potential qualities. Gao et al. [96] also draw attention to the other

849 environmental benefits of bio-mass-derived ACs including the renewability and abundance of

850 raw materials that can be used to make ACs. Furthermore, AC-based electrodes show good

851 potential for recyclability. The recycling process for activated carbon was investigated by Jiang

852 and Pickering [97]. The recycling procedure is assumed to be capable of recovering 90% of the

853 electrode's active materials [84]. The measured surface area of the AC that was recovered by this

854 technique is only 95% of its original, pristine value. This indicates a little decline in the content's

855 quality [97].

856

857 Considering the environmental impact of recycling/recovering materials, Cossutta et al. [84]

858 suggest using the substitution model. This model's underlying idea is that material recovery

859 reduces the need to generate additional virgin material, which benefits the environment. The

860 quality of the recycled product determines how much virgin material may be substituted (0.95

861 g of virgin AC can be replaced by 1 g of recovered material) [84]. This is not a 1:1 substitution

862 due to the degradation of material quality/properties. Research by Ke and Wang [98] provides a

863 value for the theoretical specific capacitance for used AC as 200 F/g (this value is based on

864 results for maximum actual SSA). Cossutta et al. [84] highlight that, while the production of AC

865 requires energy, it is not as greenhouse gas (GHG) intensive as other electrode materials (such

866 as graphene). AC production produces around 5 g CO_2 eq./g (compared to ~80 g CO_2 eq./g).

867 Furthermore, since the emissions from the recycling process are lower than the emissions

868 connected to the sourcing and initial production of ACs, recycling AC supercapacitors can

869 result in a net reduction in GHG emissions. Research by Ntuli and Hapazari [99], also suggests

870 that the use of agricultural by-products or lignocellulosic materials (such as coconut shells) as

871 feedstocks for AC production would further reduce GHG emissions as processing would avoid

872 the emission of GHGs when they rot or burn. However, the lifecycle analysis (LCA) of the AC

873 as electrode materials for supercapacitors manifests a fundamental environmental performance.

874 From here, it is observed that following the ISO framework, 1 kg of AC from coconut shells

875 contains 34.4 MJ of energy use and 5.68 kg of CO_2, char production and activation account for

876 86% of the CO_2 emissions at 97% [100]. New AC electrodes exhibit competitive environmental

877 performance in comparison with coal-derived AC, reduced graphene oxide, and algae-derived

878 biochar aerogel electrodes, though they have larger impacts on land and water use as a function

879 of the agricultural intensity of coconut production. They have lower impacts in regard to

880 terrestrial ecotoxicity and freshwater eutrophication [101].

881

882 The AC production process involves high temperatures and activation agents such as potassium

883 hydroxide, hence is highly energy-intensive with chemical wastes as by-products. The specific

884 surface area for mesophase-derived AC, for example, is 2000 m²/g, reducing to 1600 m²/g when

885 treated thermally but improving its stability by 99% [102]. During usage, AC-based

886 supercapacitors show excellent performance, with thermally treated AC (AC-1000) exhibiting

887 only a 5% reduction in specific capacitance after 10,000 cycles, compared to untreated AC's

888 reductions of 12% and 17% [103]. An asymmetric capacitor using AC and AC-1000 shows a

889 capacitance decrease from 220 F/g to 210 F/g after 10,000 cycles, and to 198 F/g after 20,000

890 cycles [104]. These efficiencies translate into reduced energy losses and extended lifetimes for

891 devices. However, some of the challenges are in disposal and recycling, wherein exposure to

892 residual chemicals from AC materials may contaminate the environment. Overall, AC materials

893 enjoy huge technical advantages, but their lifecycle environmental impact implores that the

894 production methods used should be as clean and green as possible, the usage as efficient as can

895 be, and the disposable or recyclable end-of-life-time processes as innocuous as can be to avoid

896 adverse impacts on the environment.

897 ### 3.1.3 Recent developments in AC electrodes

898 Recent literature provides a range of strategies for the improvement of AC electrochemical

899 performance. In their 2020 research paper, Grishchenko and colleagues [105] explored modifying

900 the surface of the AC electrodes through oxidation, and while there was a significant reduction

901 in the SSA of oxidized material, they achieved a 1.4 times higher specific capacitance in a

902 symmetric SC electrode compared to a pure AC electrode. Another example of the continuing

903 improvement of AC electrodes can be seen in the work by Cheng et al. [106]. To create a new

904 class of nanocomposite electrodes, the scientists examined the synergistic effects of combining

905 ACs and carbon black (CB) with other species such as carbon nanofibers (CNFs) and carbon

906 nanotubes (CNTs). The study demonstrated that, in comparison to pure AC electrodes, the

907 electrochemical performance was significantly improved by mixing the species employed in

908 the SC electrode. The weight percentage composition of the optimised nanocomposite electrode

909 was 1.25% CB, 3.75% CNT, 1.25% CNF, and 88.75% AC. The completed SC demonstrated

910 good cyclability (capacitance retention of 91.4% over 30000 cycles) and volumetric

911 performance (high capacitance of 66.1 F/cm^3, power density of 101.7 kW/L, and energy density

912 of 29.6 W h/L).

913

914 The improved performance is the result of the obtained morphology, as the added CB particles

915 fit into the voids between AC particles and it was found that the flexible CNTs wrap tightly and

916 uniformly around the AC particles. The CNFs were added, which helped to lessen the CB

917 particles' tendency to aggregate. By acting as a bridge between CB and CNT-wrapped AC

918   particles, CNFs' relative stiffness (as compared to CNTs) enhances the structural stability of the

919   nanocomposite. The final electrode featured a three-dimensional electrical conduction network

920   that enhanced capacitive behaviour and packing density. Furthermore, the nanocompositing

921   approach employed by Cheng et al. [106] utilizes readily available materials to synthesize the

922   nanocomposites. These can then be used to mass-produce large-scale high-performance SC

923   electrodes via the cost-effective industrial slurry process. A recent study focuses on

924   synthesizing graphene oxide (GO) using a modified version of the Hummers' method [107]. The

925   produced GO is then incorporated into an activated carbon slurry to create electrodes for

926   supercapacitors. The addition of an appropriate amount of graphene oxide (GO) into the

927   electrode renders it hydrophilic, thereby enhancing the interfacial contact between the electrode

928   and the hydrogel electrolyte. The oxygen-containing functional groups present on GO attract

929   cations and facilitate ion dissociation, thereby improving ion mobility. However, as an insulator,

930   GO affects electrode conductivity. Remarkably, utilizing GO with weight ratios of 5% achieves

931   a balance, providing a sufficient free ion ratio for good ion conductivity while maintaining

932   acceptable electronic conductivity. Supercapacitors incorporating GO5 exhibit minimal

933   equivalent series resistance (ESR) of 4 Ω and a maximum specific capacitance of 117.7 F/g. In

934   a similar context, biowaste from litchi seeds was utilized to synthesize 3D activated carbon

935   (3D-AC), which was further combined with reduced graphene oxide (rGO) and multi-walled

936   carbon nanotubes (MWCNT) to create a multidimensional carbonaceous material [108]. This

937   composite exhibited a specific capacitance of 320 F/g at 1 A/g. Additionally, 3D-AC served as

938   a supporting matrix for the growth of zinc cobalt sulfide nanoparticles, leading to promising

939   electrochemical performance in both asymmetric and symmetric devices.

940

941   Other recently explored strategies include using ultrasonic radiation for Fermi-level position

942   modification of the activated carbon [109], sulphur and oxygen functionality doping of the porous

943 AC [110], and the formation of composite electrodes via the insertion of polymers into the AC

944 substrate [111]. The price of AC has decreased dramatically over time, and this has been ascribed

945 to the SC carbon market's strong price sensitivity relative to performance. Suppliers such as

946 Kuraray, whose prices have dropped from \$150–200 USD per kilogramme to \$15 USD per kg,

947 are an example of this price reduction [80]. More recent works provide a lower value of \$4.15

948 USD per kg and also emphasize the manufacturing economic benefits of coconut shell AC by

949 highlighting their abundant supply [87,112]. Activated carbon, while a popular material in

950 supercapacitors, has several limitations that impact its performance. One of the main issues is

951 its broad and irregular pore size distribution that is predominantly microporous (<2 nm). These

952 small pores can limit the accessibility of electrolyte ions, particularly larger ions in organic

953 electrolytes, resulting in reduced capacitance and inefficient ion transport. Despite its high

954 surface area, activated carbon often exhibits low specific capacitance because not all of its

955 surface area is effectively utilized due to the presence of micropores that are too small for ion

956 penetration. Additionally, the properties of activated carbon are less tuneable compared to

957 materials MOFs. This lack of tunability restricts the ability to optimize its surface chemistry,

958 pore structure, and functional groups for specific applications.

959 ### 3.2 Metal organic frameworks as supercapacitors

960 **Table 2** presents a selection of functionalized MOFs investigated for their suitability as

961 supercapacitor electrodes and compared to activated carbon. The table demonstrates a wide

962 range of potential specific capacitances, with some MOFs showing values higher than those of

963 AC, indicated at the bottom of the table. Additionally, MOFs exhibit the potential for enhanced

964 cyclability compared to ACs, highlighting their promise for supercapacitor applications.

965

966 **Table 2.** Supercapacitor's performance of functionalized MOF compared to AC electrodes.

Electrode material	Cycle life	Specific surface area m²/g	Current density /scan rate	Specific capacitance F/g	Reference
ZIF-8 (HNC) MOF derived porous carbon	20000	1215	536 mA/hg 1 mV/s	253.6	[73]
ZIF-8 (NPCF) MOF derived porous carbon	5000	NA	1 mV/s (rate)	332	[22]
ZIF-8 (NCF) MOF derived porous carbon	10000	NA	5 mV/s (rate)	264	[22]
Co-MOF MOF directly used	NA	2900	0.6 A/g	206.76	[74]
Zr-MOF (1) MOF directly used	NA	1047	5 mV/s	1144	[22]
ZIF-8 (NPC) MOF derived porous carbon	NA	1523	5 mV/s	251	[22]
MOF-5 (NPC) MOF derived porous carbon	NA	2872	1 mV/s	312	[22]
Ni-MOF	49.1% (5000)	295.7	1 A/g	1024.4	[74]
NiOx@NP 3-electrode system. From waste PET	(91.5% retention after 5000 cycles	1523	5 mV/s	581.30	[113]
3D) Ni-MOF	5000	NA	1 A/g	2150	[114]

43

Fe-MOF@AC	10000	180.7	1 A/g 1 mV/s	470.05	[115]
NiO@Ni-MOF	3000	433	1 A/g 1 mA/cm^2	144	[116]
Cu-MOF and Co-MOF	1000	NA	3 mV/s	451 and 103 C/g	[117]
Activated carbon	> 3000	NA	0.5 A/g	207.5	[83]

967

3.2.1 Pristine MOFs and their composites

969 From the available literature, it can be observed that the use of pristine MOFs for

970 electrochemical applications, such as SC electrodes, is rare [118]. As previously mentioned, this

971 is predominantly due to their inherent insulating properties which result in low capacitance,

972 often regarded as insufficient for most electrochemical applications [119]. One report explores the

973 use of Fe-MOF and its variants (MIL-88B, MIL100, and MIL-53) as SC electrodes coupled

974 with an aqueous and neutral electrolyte [120]. The device's performance is significantly impacted

975 by the material properties of the electrode, such as the size of the pellet and the pore diameters.

976 Using an aqueous 0.1M Na_2SO_4 electrolyte, it was discovered that the MIL-100 sample only

977 produced a specific capacitance of 34 F/g. The irritating nature of the Fe-MOF and insufficient

978 mixing between the conductive and non-conductive phases of the Fe metal centres were the

979 authors' explanations for this very low specific capacitance. This stops the material's electrons

980 from moving through it in the best possible way when the iron centre is being reduced or

981   oxidised. The Fe-MOF was deemed unsuitable for use as an electrode due to the limited quantity

982   of redox-active Fe ions in the structure. The use of bare Fe-MOF electrodes has also proven

983   problematic, as experiments have shown that during the reduction cycle, the electrode is subject

984   to some degree of dissolution.

985

986   Despite their limitations, MOFs exhibit a rapid diffusion of electrolyte ions into the pores of

987   electrode materials. Consequently, research into utilizing pristine MOFs as SC electrodes has

988   experienced a noticeable uptick. These MOFs often work as pseudocapacitors via faradaic

989   redox reactions between the electrodes and the electrolyte. As the work by Wang et al. [121] shows,

990   these fabricated electrodes yield theoretical values for capacitance as high as 2000 F/g [121].

991   However, Ramachandran et al. [122] argue that these benefits come at the cost of the electrode's

992   cycle life. In their investigation, they discovered that the cyclic stability of pseudocapacitive

993   MOFs was weakened by frequent charging and discharging cycles. This results from the

994   occasional dissolving of MOF electrode material during the reduction reactions, as well as

995   incompatibility between the electrode and electrolyte. A prominent example of the use of

996   pristine MOFs as SC electrodes is the work done by Lee et al. [123] in their paper. During their

997   experiments with a Co-based MOF electrode in an aqueous electrolyte of 1 M LiOH, the authors

998   were able to achieve a specific capacitance of 206.76 F/g with a current density of 0.6 A/g.

999   After the electrode's cycle life was examined, it was discovered that, after 1000 cycles of testing,

1000   its capacitance retention could reach 98.5%. However, the Co-based MOF electrode's

1001   performance significantly decreased and was ultimately declared unsatisfactory when tested in

1002   different electrolytes (such as KOH and KCl). An investigation was conducted into how the

1003   temperature of the synthesis reaction affected the performance, degree of crystallisation, and

1004   particle size of a zirconium-based MOF (UiO-66) [124]. It was observed that a sample with the

1005   smallest particle size and a synthesis reaction temperature of 50 °C achieved the highest specific

1006   capacitance (1144 F/g at a 5 mV/s scan rate). However, the cost may prove to be a limiting

1007   factor as 1 kg of UiO-66 has been priced at around $25000 USD [125].

1008

1009   Other research into altering MOF morphology to improve SC performance includes the

1010   synthesis of a superstructure electrode from "accordion-like Ni-MOF" [126]. Whilst being tested

1011   at current densities of 1.4 and 7 A/g, the electrode achieved enhanced specific capacitances

1012   (988 F/g and 823 F/g respectively). Additionally, after 5000 cycles, the capacitance retention

1013   was 96.5%, which was a respectable retention rate. Highly elevated specific capacitances have

1014   also been seen with Ni-MOF electrodes in combination with a 6 M aqueous KOH electrolyte.

1015   Yang et al. [127] report that, with current densities of 0.5 A/g and 10 A/g, specific capacitances of

1016   1127 F/g and 668 F/g respectively could be achieved. The high specific capacitances were

1017   explained by the authors as the result of the electrode's pseudocapacitive nature. Additionally,

1018   it was discovered that this electrode had improved cyclic stability, demonstrating 90% after

1019   3000 cycles. The MOF's layered structure and sizable open facets were both credited with its

1020   cyclic stability and quick surface redox reactions.

1021

1022   Rahmanifar et al. [128] reported a one-pot co-synthesis method for creating a novel, water-stable

1023   Ni-MOF in combination with a Co-MOF. They also developed a dual Ni/Co-MOF-reduced

1024   graphene oxide (rGO) nanocomposite (**Fig. 6(a)**). The asymmetric device comprising activated

1025   carbon//Ni/Co-MOF-rGO demonstrated impressive performance, delivering a specific energy

1026   of 72.8 Wh/kg at 850 W/kg and maintaining a capacity of 15.1 Wh/kg even under the high

1027   specific power of 42.5 kW/kg. Furthermore, it exhibited exceptional cycle life, retaining 91.6%

1028   capacitance after 6000 charge-discharge cycles at 1 A/g [128]. In the work of Li et al. [129], a

1029   controlled and straightforward two-step method was introduced for cultivating Ni-MOF arrays

1030   on the surface of NiCo2O4 nanowires by regulating the MOFs' formation reaction (**Fig. 6(b)**).

1031 The NiCo2O4@Ni-MOF hybrid electrode, after optimization, demonstrates improved

1032 electrochemical performance. It presents a notable specific capacity of 208.8 mA h/g at a

1033 current density of 2 mA/cm^2, alongside exceptional rate capability [129].

1034

1035 Recent research focused also on the potential of using waste polyethylene terephthalate (PET)

1036 derived Ni-MOFs in the synthesis of NiOx@NPC nanocomposite (NiOx nanoparticles with

1037 nitrogenous porous carbon) [113]. The simple solvothermal route used to synthesize this porous

1038 carbon composite has been described as cost-efficient. A schematic of the process can be seen

1039 in **Fig. 6(c)**. The BDC (benzene-1,4-dicarboxylic acid) utilised in this report's synthesis of the

1040 NiOx@NPC came from discarded PET bottles. The final product showed good specific

1041 capacitance, cyclic stability, and a high specific surface area (1523 m^2/g). But nothing about

1042 whether it's appropriate for widespread implementation is mentioned [113]. In another context, a

1043 novel electrode material comprising MOFs (Zr-TAA, where TAA stands for trans-aconitic acid)

1044 and multi-walled carbon nanotubes (MWCNTs) was easily synthesized using a one-pot reflux

1045 method and subsequently employed in a high-performance supercapacitor (**Fig. 6(d)**). Due to

1046 its improved conductivity and even distribution of pore sizes, this composite material exhibits

1047 outstanding electrochemical performance, achieving a specific capacitance of 562.06 F/g.

1048 Moreover, it retains nearly all of its initial capacitance even after undergoing 1000 cycles of

1049 testing with a 6 M KOH electrolyte [130].

1050
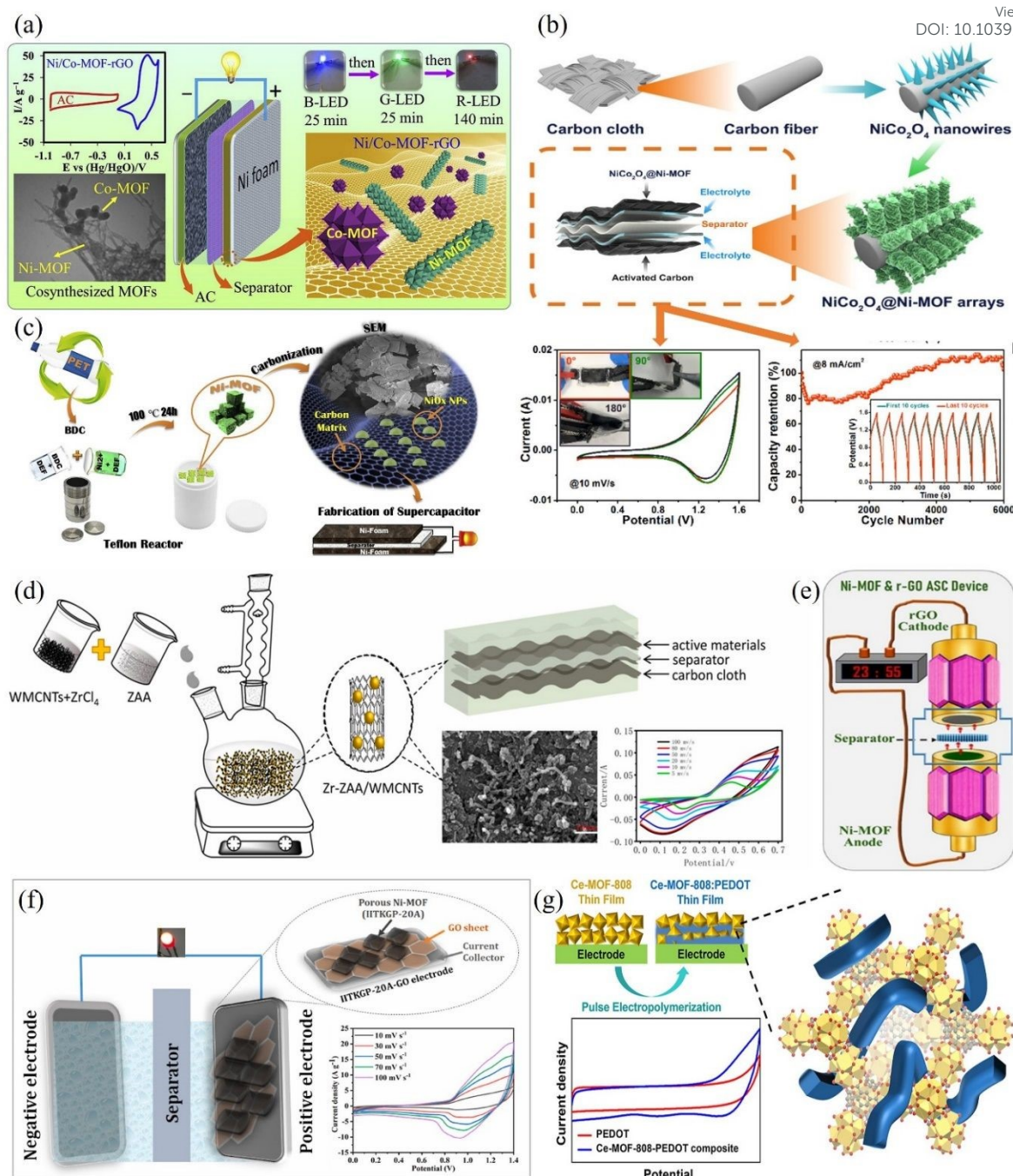
Fig. 6. (a) An asymmetric AC//Ni/Co-MOF-rGO device showing a capacitance of 860 F/g@1.0 A/g in a 3E cell setup. Adopted from Ref. [128] with permission. (b) A schematic depiction of the synthetic method employed to create core/shell hybrid arrays of NiCo$_2$O$_4$@Ni-MOF on a carbon cloth substrate and the corresponding CV curves, and cycling stability tested at 8 mA/cm^2. Adopted from Ref. [129] with permission. (c) Schematic diagram of the proposed method of synthesizing NiOx@NPC nanocomposites using waste PET with enhanced electrical conductivity and stability and improved charge relocation operation for a better performance of supercapacitor devices. Adopted from Ref. [113] with permission. (d) A novel electrode material, composed of MOFs (Zr-TAA, where TAA is trans-aconitic acid) and MWCNTs synthesized using a simple one-pot reflux method and applied to high-performance supercapacitors. Adopted from Ref. [130] with permission. (e) A three-dimensional Ni-MOF used as an anode electrode in a two-electrode asymmetric supercapacitor device setup. Adopted from Ref. [114]

1064   with permission. (f) Highly scalable and pH stable 2D Ni-MOF-based composites (IITKGP-
1065   20A-GO) for high-performance supercapacitors exhibiting a specific capacitance of ~ 840 F/g
1066   at 2 A/g current density. Adopted from Ref. [131] with permission. (g) A cerium-based
1067   MOF@conducting polymer (PEDOT) nanocomposites for supercapacitors. Adopted from Ref.
1068   [132] with permission.

1069

1070   A recent study has concentrated on developing a 3D Ni-MOF with an outstanding capacitance

1071   of 2150 F/g at a current density of 1A/g [114]. Subsequently, the synthesized Ni-MOF and reduced

1072   graphene oxide were utilized as the anode and cathode electrode materials, respectively, in a

1073   two-electrode asymmetric supercapacitor device (ASC) setup (**Fig. 6(e)**). This ASC manifested

1074   a specific capacitance of 125 F/g (at 0.2 A/g) and showcased a high energy density of 50.17

1075   Wh/kg at a power density of 335.1 W/kg. Furthermore, the ASC demonstrated excellent

1076   reversibility (97.9% Coulombic efficiency) and cyclic stability (94%) after 5000 constant

1077   charge-discharge cycles. In the investigation by Sahoo et al. [131], a microporous 2D Ni-MOF

1078   was elaborated, demonstrating high scalability and thermodynamic stability across a wide pH

1079   range (2–10). Upon introducing GO with a weight percentage of 3%, a specific capacitance

1080   value of approximately 840 F/g at 2 A/g was achieved, ranking among the highest within the

1081   category of bare MOFs and their composites/derived materials. Subsequently, when used as the

1082   electrode material in an asymmetric supercapacitor (**Fig. 6(f)**), it displayed a specific

1083   capacitance of 111.4 F/g at a current density of 2 A/g and exhibited excellent retention of 84%

1084   cycle life over 7000 cycles [131].

1085

1086   The study by Wechsler et al. [133] reported the fabrication of supercapacitor electrodes using

1087   pristine nickel hexaaminobenzene ($Ni_3(HAB)_2$) metal-organic framework (MOF) via

1088   electrophoretic deposition (EPD). The symmetric supercapacitor employing the MOF

1089   showcases remarkable electrochemical capacitive performance within a potential range of 0–1

1090   V, demonstrating an areal capacitance of 13.64 mF/cm^2 and exceptional ultra-high cycling

1091 stability, maintaining 81% of its capacity over 50,000 cycles. The superior performance of the

1092 supercapacitor is attributed to the binder-free electrophoretic deposition (EPD) process and the

1093 distinctive structure of 2D MOF nanosheets, which promote ion diffusion throughout the

1094 electrodes. Additionally, the literature review explored the utilization of a combination of

1095 MOFs and conducting polymers. Nanocomposites were fabricated by combining a cerium-

1096 based MOF (Ce-MOF-808) with poly(3,4-ethylene dioxythiophene) (PEDOT) through pulse

1097 electrodeposition of PEDOT within thin films of Ce-MOF-808 [132]. he highly porous Ce-MOF-

1098 808 displays reversible electrochemical reactivity, offering pseudocapacitance, while

1099 electronically conducting PEDOT contributes to a notable double-layer capacitance and

1100 enhances electronic conduction between the redox-active cerium sites in the MOF **(Fig. 6(g))**.

1101 As a result, the composite demonstrates superior performance compared to both pristine MOF

1102 and pristine electrodeposited PEDOT as active materials for supercapacitors [132].

1103 ### 3.2.2 Nanocrystalline MOFs

1104 Research has also advanced in the field of nanocrystalline MOFs (nMOFs) and coin-type cell

1105 SCs, this is another example of altering the morphologies of pristine MOFs to enhance their

1106 supercapacitive properties. Gu et al. [119] posit that decreasing the particle size of MOFs into

1107 nanometre dimensions is an effective method for increasing their achievable capacitance.

1108 Particle size reduction improves the material's electrochemical performance significantly by

1109 lowering the electrolyte ion diffusion distance and raising the material's ESA [134]. These nMOFs

1110 were not commonly reported until recently. Only a few well-known MOFs, like MOF-5, ZIF-

1111 8, and ZIF-67, attracted attention because of their composition, which made downscaling

1112 simple. A variety of brand-new nMOFs have been developed and tested as part of recent

1113 research. Gu et al. [119] begin by synthesizing two MOF crystals via the adoption of the redox-

1114 organic linker from 3,30 5,50 -oxybenzobenzenetetracarboxylic acid (H_4L) and metal centres

1115 of Ni2þ/Cu2þ **(Fig. 7(a))**. An in-situ solvothermal procedure was used in a single step to obtain

1116   the appropriate nanomaterials. One significant finding was that, with careful choice of solvent

1117   and surfactant, the different morphologies attained during material production could be

1118   efficiently controlled. When evaluated at current densities of 1 A/g and 5 A/g, respectively, one

1119   sample of the as-synthesised nano-NiMOF electrode produced capacitances of 1024.4 F/g and

1120   648.9 F/g, demonstrating exceptional SC performance [119].

1121

1122   Work by Choi et al. [135] explores the synthesis of a range of nMOF structures including HKUST-

1123   1, Zr-MOF, nMOF-867, and MOF-5. The nMOF-867 sample exhibited very good

1124   supercapacitive behaviour, achieving a capacitance of 5.085 mF/cm^2, almost 6 times higher

1125   than the achievable capacitance from a fabricated electrode using commercially available AC

1126   (**Fig. 7(b))**. After 10,000 charge-discharge cycles, the nMOF-867 electrode continued to show

1127   exceptionally good cyclic stability, with a retention of over 90%. With a capacitance of 5.085

1128   mF/cm2, the Zr-MOF sample under evaluation demonstrated exceptional supercapacitive

1129   qualities. This is nearly a 6-fold increase above the capacitance provided by an AC electrode

1130   made from commercially available AC. Additionally, the Zr-MOF electrode demonstrated

1131   exceptionally high cyclic stability (greater than 90%, which is considered ultrahigh) even after

1132   10,000 cycles [135].
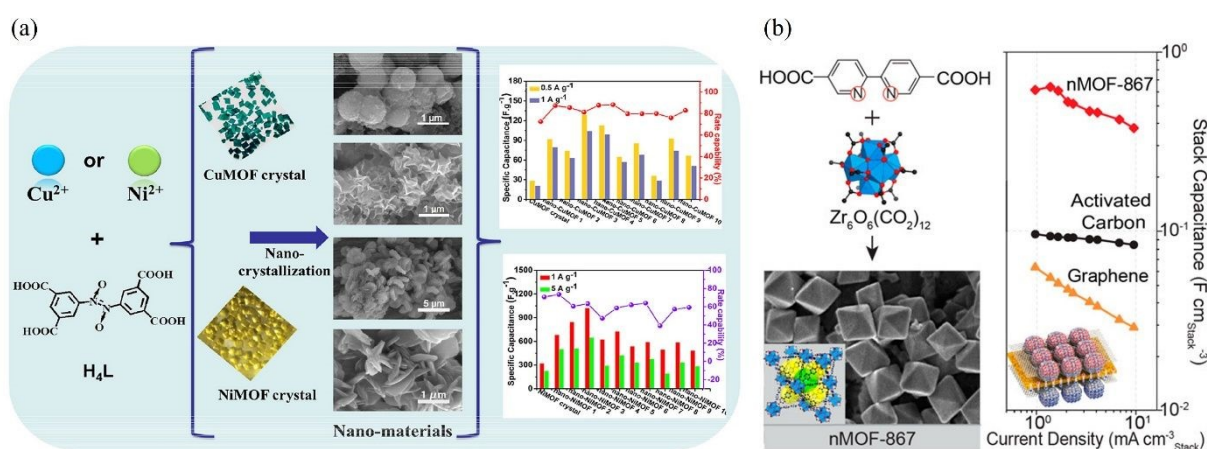
1133

1134   **Fig. 7.** (a) *In-situ* solvothermal synthesis of nanoscale CuMOF and NiMOF crystals and their
1135   specific capacitance (1024.44 F/g and 128.82 F/g for nano-NiMOF and nano-CuMOF
1136   respectively) and rate capacitance. Adopted from Ref. [119] with permission. (b) Nanocrystals

1137 nMOF-867 with exceptionally high capacitance showing a stack and areal capacitance of 0.64

1138 and 5.09 mF cm², respectively, with performance maintained over at least 10,000

1139 charge/discharge cycles. Adopted from Ref. [135] with permission.

1140

1141 Some 2-dimensional (2D) MOFs with a high SSA and tuneable porosity have been discovered

1142 recently. In their pure state, these MOFs can give sufficiently high electrical conductivity for

1143 SC applications [136]. Charge delocalisation inside the material's planes and prolonged pi-

1144 conjugation provide this electrical conductivity [137]. Sheberla et al. [136] observed MOF

1145 $Ni_3(HITP)_2$'s high bulk electrical conductivity (over 5000 S/m), a value that exceeds those

1146 achieved by AC and porous graphite. The first non-carbon-based EDLC symmetric SC was

1147 fabricated using Ni3(HITP)2 electrodes after this discovery. After 10,000 cycles, the

1148 supercapacitor showed an extremely high areal capacitance of 18 mF/cm², and 90% capacity

1149 retention [136]. Another 2D MOF that has been investigated for high-performing SC electrodes is

1150 hexaaminobenzene (HAB)-derived MOF. Feng et al. [138] reported both a high volumetric and

1151 areal capacitance (760 F/cm³ and 20 F/cm² respectively). The cycle life data were similarly

1152 encouraging, demonstrating that capacitance retention could only be increased by a factor of 10

1153 after 12000 charging-discharging cycles. Research indicates that selecting the right electrolyte

1154 is essential for optimal SC performance. In one experiment, a 1 M LiOH aqueous electrolyte

1155 and a Co-based MOF electrode operated at a current density of 0.6 A/g produced a specific

1156 capacitance of 206.76 F/g [123]. Furthermore, retention of this capacitance was good (up to 98.5%)

1157 over 1000 test cycles. Although, when the electrolyte was changed to KCl or KOH, the

1158 performance of the electrode was not satisfactory.

1159 ### 3.2.3 Environmental impacts

1160 Literature focusing on MOF toxicity is limited, and the topic is generally poorly understood [125].

1161 If a MOF is toxic, this is likely the result of the organic ligand metal ions or functional groups

1162 [139]. The metal ions in MOFs are in the form of nanoparticles that are nonbiodegradable [125].

1163   Kumar et al. [125], have suggested that out of the most common metal ions in MOFs, zinc and

1164   iron are likely to be the least toxic as they are used in the human body. While the toxicity of

1165   MOFs may not be fully known, some sources suggest that when MOFs decompose, they may

1166   exhibit the same toxicity levels as constituent raw materials from which they are generated. In

1167   summary, when considering the environmental impact of MOFs, several factors come into play:

1168   (1) Synthesis process: The synthesis of MOFs often involves solvents and energy-intensive

1169   processes. Depending on the specific synthesis route, this could contribute to environmental

1170   impacts such as greenhouse gas emissions and resource depletion. However, efforts are being

1171   made to develop more sustainable synthesis methods, such as using green solvents or employing

1172   energy-efficient techniques. (2) Resource utilization: The materials used in MOF synthesis,

1173   such as metal ions and organic ligands, can have environmental implications depending on their

1174   sources and extraction methods. For example, if the extraction of metal ions involves

1175   environmentally damaging processes or if rare or toxic elements are used, it could pose

1176   environmental concerns. (3) End-of-life disposal: Consideration should be given to the disposal

1177   of MOF-based supercapacitors at the end of their lifespan. While MOFs themselves are

1178   generally stable materials, the electrodes and other components of supercapacitors may contain

1179   metals or other materials that could pose environmental risks if not properly managed through

1180   recycling or safe disposal methods. (4) Performance and durability are key considerations for

1181   MOF-based supercapacitors. These devices have inherent advantages such as high surface area

1182   and customizable pore structures, which can significantly improve their performance. If MOFs

1183   can facilitate the development of supercapacitors with greater energy density and prolonged

1184   cycle life compared to conventional materials, it could have a positive impact on the

1185   environment. By extending the lifespan of electronic devices and minimizing the frequency of

1186   replacements, this advancement has the potential to reduce environmental impacts. (5) Scale of

1187   production: As with any technology, the environmental impact of MOF-based supercapacitors

1188 will depend on the scale of production and deployment. Large-scale production could lead to

1189 increased energy consumption, waste generation, and resource depletion if not managed

1190 properly. The environmental impact and sustainability of Metal-Organic Frameworks (MOFs)

1191 used in supercapacitors necessitate a thorough examination, particularly when compared to

1192 traditional materials. MOFs like nMOF-867 exhibit superior electrochemical properties, with a

1193 stack capacitance of 0.644 F cm³ and an areal capacitance of 5.085 mF cm², far surpassing

1194 commercial activated carbon supercapacitors [140].

1195

1196 However, most of the methods for MOF synthesis incorporate eco-toxic solvents, such as N,N-

1197 dimethylformamide, coupled with high energy requirements, which may pose a serious

1198 environmental impact. Therefore, an in-depth LCA is needed in estimating these materials. For

1199 instance, high carbon footprint and energy use can be associated with the production of MOFs;

1200 for instance, nMOF-867 is associated with high environmental cost despite its high performance

1201 and long lifetime, maintaining activity beyond 10,000 cycles [141]. Moreover, the environmental

1202 advantages of MOFs like UiO-66-NH$_2$, which can be synthesized using aqueous methods

1203 reducing environmental impacts by up to 91%, must be weighed against challenges such as

1204 degradation and scalability. These methods yield a cradle-to-gate carbon footprint of 43 kg CO$_2$

1205 eq/kg and a lower production cost of $15.8/kg compared to solvothermal processes [142]. On the

1206 long-term sustainability front, MOFs still hold much promise because green synthesis methods

1207 using either water or ethanol as solvents have already been developed, and biodegradable MOFs

1208 that can minimize their impact on the environment are under construction. Although this might

1209 be the case, there is a clear lack of long-term data relating to MOF recyclability and degradation,

1210 and their high initial production costs underline the necessity for performing holistic LCA with

1211 respect to end-of-life disposal and possible environmental release to make such next-generation

1212 materials more environmentally and economically feasible against traditional ones [143].

1213 **3.3   Metal-organic frameworks for battery technologies**

1214 MOFs and their derivatives have accommodated much interest and proved rather promising to

1215 improve sodium-ion batteries (SIBs), and lithium-ion batteries (LIBs) performance. The work

1216 by Zhao et al. [144] proved the potential of Prussian blue analogues (PBAs) as SIB cathode

1217 material through effective etching. Specifically, etching $Na_2NiFe(CN)_6$ (NaNiHCF) into a dice

1218 shape increased its specific surface area, enhancing sodium storage sites and accelerating Na^+

1219 diffusion. The etched NaNiHCF-3 showed a large reversible capacity of 83.5 mAh/g that

1220 accounted for about 98.2 % relative to the theoretical capacity, while the unetched counterpart

1221 precursor only delivered 76.8 mAh/g. Moreover, NaNiHCF-3 exhibited 71.2 mAh/g at 10 C

1222 with a rate capability far beyond that of other electrodes and maintained a very stable life with

1223 94% capacity retention over 1,000 cycles at 1 C. These results further underline the role of

1224 morphological control in the electrochemical performance of MOFs with respect to capacity

1225 use and cycling stability. Indeed, the tunable porosity and high surface area of MOFs enable

1226 theoretically improved ion transport and storage capabilities. For example, nitrogen-doped

1227 amorphous Zn-carbon multichannel fibers have exhibited a Coulombic efficiency above 99%

1228 for more than 500 cycles at current densities from 1 to 5 mA cm², demonstrating major

1229 improvements in lithium metal anode performance. Symmetric cells based on these materials

1230 achieve stable cycling for over 2,000 hours, which is the potential for long-term applications

1231 [145]. However, the synthesis process is complex due to electrospinning and MOF coating, and

1232 this complicates large-scale production. The specific capacity of 104 mAh/g during the high

1233 rate of 5 C in the full-cell tests with $LiFePO_4$ cathodes is quite encouraging, but its broader

1234 compatibility with various cathode materials remains to be explored. While these MOF-derived

1235 materials could effectively reduce dendrite formation and issues regarding local current density,

1236 the long-term stability in a range of environmental conditions remains to be evaluated.

1237

1238 Always in the context of LIBs, the study of Du et al. [146] presents an efficient synthesis of 2D

1239 layered Mo-MOF@PPy via reflux heating and coating methods, aimed at improving the

1240 performance of anode materials in LIBs. Serving as a precursor during the electrochemical

1241 reaction, the high-valence Mo within the Mo-MOF effectively binds with Li^+, thereby

1242 contributing to the superior electrochemical performance of the material. Additionally, the

1243 polypyrrole (PPy) coating significantly enhances the electrical conductivity of the composite

1244 by promoting electron transfer. As a result of these synergistic effects, Mo-MOF@ppy achieves

1245 a specific capacity of 930 mAh/g at a current density of 100 mA/g and retains a capacity of 750

1246 mAh/g at 500 mA/g after 200 cycles. In a similar study, Zhao et al. [147] utilized stannous sulfate

1247 ($SnSO_4$) and graphene to synthesize Sn-MOFs/G nanorods, which were evaluated as anode

1248 materials for LIBs. The resulting material exhibited a high specific capacity of 462 mAh/g after

1249 500 cycles at 1 A/g and demonstrated remarkable rate performance, achieving 265 mAh/g at 2

1250 A/g.

1251

1252 In detail, recent progress involving MOFs and MOF-derived materials has unveiled their huge

1253 potential towards enhancing the performance of batteries. For example, the synthesis of copper-

1254 substituted CoS_2@CuxS DSNBs by a multistep MOF-based templating strategy possessed very

1255 impressive electrochemical properties, such as high capacity (535 mAh/g at 0.1 A/g), better rate

1256 capability (333 mAh/g at 5 A/g), and extended cycling stability (76% capacity retention over

1257 300 cycles) [148]. The improvements may be attributed to their complex nanostructure, which

1258 provided enhanced ionic and electronic conductivity, improved electrochemical reactivity, and

1259 mechanical stability. In this respect, this approach can overcome the poor conductivity and fast

1260 capacity fading of sulfur metal through the combination of different active materials with

1261 hierarchical hollow structures, which can reduce ion diffusion paths and strain accommodation

1262 during cycling. Rational design and controlled composition, as emphasized in the present work,

1263 are preliminary steps for the development of high-performance anode materials, and this work

1264   further confirms the bright application of MOF-derived materials in next-generation batteries.

1265   Although these results are very promising, problems like intrinsic instability of MOFs in

1266   electrolyte environments and scalability issues, coupled with generally low electrical

1267   conductivity, have to be resolved before their full potential is tapped. Therefore, future studies

1268   should address the issues of scalability and stability if the full potential of MOFs in battery

1269   applications is to be exploited, ensuring technological advancement with sustainability.

1270

1271   The main advantage of MOFs over activated carbon in energy storage devices lies in their

1272   highly tunable structure and functional versatility. MOFs are composed of metal nodes

1273   connected by organic linkers, allowing precise control over pore size, shape, and surface

1274   chemistry. This tunability enables the design of materials with optimized ion transport and

1275   storage, potentially leading to higher capacitance and energy density. Unlike activated carbon,

1276   which often has a broad and irregular pore size distribution, MOFs can be synthesized with

1277   uniform and well-defined pores, ensuring consistent ion diffusion and reducing resistance

1278   during charge-discharge cycles. Additionally, the organic linkers in MOFs can be chemically

1279   modified to introduce specific functional groups that enhance interactions with electrolyte ions,

1280   while the metal centers can be selected or doped to introduce redox activity, contributing

1281   additional pseudocapacitance. MOFs can also encapsulate or host other functional materials,

1282   further enhancing their electrochemical performance by providing additional active sites or

1283   improving electrical conductivity. This versatility in synthesis and integration with conductive

1284   materials makes MOFs a promising material for next-generation supercapacitors, offering the

1285   potential for higher energy densities, improved ion transport, and customizable electrochemical

1286   properties. However, challenges such as low conductivity, stability, and cost still need to be

1287   addressed for MOFs to become a widely adopted alternative in commercial applications.

1288 **3.4 MOF metal nodes, ligand architecture and synthesis strategies**

1289 In MOFs, the metal nodes, also known as metal clusters or secondary building units (SBUs),

1290 play a pivotal role in determining the structure and properties of these materials. These nodes

1291 form the inorganic backbone of the MOF and are interconnected by organic ligands to create

1292 an extended porous network. The composition of these nodes can vary widely, ranging from

1293 simple single metal ions like Zn^{2+}, Cu^{2+}, or Fe^{3+}, which can coordinate with multiple ligands,

1294 to more complex metal clusters such as $Zr_6O_4(OH)_4$ or Cr_3O, which involve multiple metal ions

1295 linked together, contributing to the stability and diversity of the MOF structure [149]. The

1296 coordination environment of the metal nodes, defined by the number of ligands or atoms bonded

1297 to the metal ion, is crucial in determining the geometry of the node, which in turn influences

1298 the overall topology and dimensionality of the MOF. For example, a metal node with a high

1299 coordination number can lead to the formation of highly connected, three-dimensional

1300 frameworks, whereas lower coordination numbers might result in simpler, two-dimensional or

1301 even one-dimensional structures.

1302

1303 The metal nodes not only shape the structural framework but also impart distinct chemical

1304 properties to the MOF. The choice of metal can significantly influence attributes such as

1305 thermal stability, chemical reactivity, and catalytic activity. Transition metals like chromium

1306 (Cr), zirconium (Zr), or titanium (Ti) are known for imparting higher stability and robustness

1307 to the MOF, making them suitable for applications that require durability. On the other hand,

1308 metals like copper (Cu) or zinc (Zn) offer tunable reactivity, which can be advantageous in

1309 catalytic processes. Metal nodes also play a critical role in the functionality of MOFs. For

1310 instance, they can act as active sites for catalysis, with MOFs containing iron (Fe) or cobalt

1311 (Co) nodes being explored for oxidation reactions [150,151]. Additionally, the type of metal used

1312 in the nodes affects the adsorption characteristics of the MOF, particularly in gas adsorption

1313 applications. MOFs with unsaturated metal sites, such as those with open metal sites, can

1314 strongly adsorb gases like CO_2 or H_2, making them valuable for gas storage and separation

1315 technologies.

1316

1317 Moreover, the electrical properties of MOFs are influenced by the metal nodes, which is

1318 particularly important in applications such as supercapacitors and batteries, where conductivity

1319 is essential. Metal nodes can also be tuned through post-synthetic modifications, allowing for

1320 the enhancement or alteration of the MOF's properties. This can be achieved through metal

1321 exchange or doping, introducing new functionalities or improving stability. For example, in

1322 MOFs like HKUST-1, which utilizes Cu^{2+} ions as the metal node, the resulting structure is a

1323 robust three-dimensional framework that has been widely studied for gas storage [152]. Similarly,

1324 MIL-101, which contains Cr^{3+} ions, is renowned for its exceptional thermal and chemical

1325 stability, making it suitable for various industrial applications [153]. Another notable example is

1326 UiO-66, where Zr^{4+} ions provide high stability, making it a popular choice for gas storage and

1327 separation [154]. Overall, metal nodes are a crucial design element in MOFs, as they not only

1328 determine the structural framework but also significantly influence the functional properties,

1329 making them central to the development of advanced materials for a wide range of applications.

1330

1331 On the other hand, ligand architecture in MOFs is a crucial determinant of their structural

1332 integrity, topology, and functional properties. Organic ligands, or linkers, connect metal nodes

1333 or clusters to form the extended porous networks characteristic of MOFs. The size and shape

1334 of these ligands significantly influence the MOF's pore dimensions and overall framework

1335 [155,156]. For instance, longer ligands typically create larger pores, which can be advantageous for

1336 applications like gas storage or catalysis, while the geometric arrangement of the ligands

1337 whether linear, angular, or branched affects the dimensionality and complexity of the MOF

1338 structure. Functional groups on the ligands, such as carboxylates, phosphonates, imidazolates,

1339 or sulfonates, play a pivotal role in determining the strength and nature of the coordination

1340 bonds with metal nodes, impacting the MOF's stability and reactivity. For example, carboxylate

1341 groups form strong bonds with metal ions, leading to highly stable frameworks like those in

1342 UiO-66, while functional groups such as amines or hydroxyls can enhance adsorption properties

1343 by introducing sites for hydrogen bonding [154]. The connectivity of the ligands how many

1344 coordination sites they offer affects the density of the network and the robustness of the

1345 resulting MOF. Ligands with higher connectivity can create more intricate and stable 3D

1346 frameworks, as seen in HKUST-1, where the bidentate trimesic acid ligand coordinates with

1347 multiple metal ions [157]. Additionally, the coordination mode of the ligand, whether

1348 monodentate, bidentate, or multidentate, influences the rigidity and stability of the framework.

1349 Ligand architecture can also be tuned through post-synthetic modifications, allowing for the

1350 introduction of new functionalities or enhancements, such as improved CO_2 capture capacities

1351 through the addition of amine groups. Examples of MOFs that showcase the importance of

1352 ligand architecture include the IRMOF series, which utilizes terephthalic acid ligands to form

1353 various frameworks with different properties, and ZIFs (Zeolitic Imidazolate Frameworks),

1354 where the imidazolate ligands create highly stable, zeolite-like structures [158,159]

1355

1356 Regarding the synthesis of MOFs, it encompasses a variety of methods, each tailored to achieve

1357 specific structural, compositional, and functional characteristics in the final material [160].

1358 Hydrothermal synthesis involves dissolving metal salts and organic ligands in water, followed

1359 by heating the solution in a sealed container under high temperature and pressure. This method,

1360 widely used for its simplicity, produces high-quality MOF crystals, as seen in the synthesis of

1361 UiO-66, where zirconium chloride reacts with terephthalic acid [161]. Solvothermal synthesis, a

1362 variant that uses organic solvents instead of water, allows for the formation of MOFs that are

1363 sensitive to water or require particular solvents for solubility, such as HKUST-1, which is

1364 synthesized using a solvent system involving alcohols and acetic acid [162]. Ligand-assisted

1365 synthesis leverages pre-formed metal-organic complexes to guide the growth of MOFs,

1366 enhancing uniformity and control over the final product's properties.

1367

1368 Microwave-assisted synthesis of MOFs is grounded in the principle of using electromagnetic

1369 radiation to interact with removable electronic components, such as electrons, ions, or polar

1370 molecules in solids, or ions and electrons in liquids. This method typically operates at

1371 temperatures above 100°C and within reaction times of no more than 60 minutes. Improvements

1372 in reaction conditions can be achieved by optimizing various factors, including the choice of

1373 solvent, duration of radiation exposure, temperature, intensity of microwave radiation, and the

1374 quantities of reactants. Adjusting these variables helps to enhance the efficiency and quality of

1375 the MOF synthesis process [163]. Electrochemical synthesis utilizes an electric current to drive

1376 the formation of MOFs from metal salts and ligands, allowing precise control and the creation

1377 of MOFs with unique properties, including thin films or coatings on conductive substrates.

1378 Moreover, solvothermal-hydrothermal hybrid synthesis combines aspects of both methods,

1379 using a solvent system that interacts with both water and organic components, useful for

1380 synthesizing MOFs with specific property balances. Post-synthetic modification, though not a

1381 primary synthesis method, involves altering the MOF framework after its initial formation

1382 through techniques like ligand exchange or metal ion substitution, tuning the MOF's

1383 functionality and stability for specialized applications. Direct synthesis from metal oxides uses

1384 metal oxides or salts directly to form MOFs in the presence of organic ligands under controlled

1385 conditions, advantageous for creating highly stable frameworks. Each of these methods offers

1386 unique advantages depending on the desired MOF properties, such as crystal size, pore

1387   structure, stability, and functional capabilities, making them crucial for tailoring MOFs to

1388   specific applications [164,165].

4. Photocatalysis

1390   In 1972, Fujishima and Honda's pioneering work saw the creation of the first photocatalytic

1391   system using TiO_2 and ultraviolet light irradiation [166]. Since then, a variety of materials have

1392   been investigated for photocatalysis applications. As noted by Djurišić et al. [167], there have been

1393   few advancements or breakthroughs in photocatalyst concepts and designs. The majority of

1394   current research shows only modest advancements, and if photocatalytic technologies are to

1395   ever be used on an industrial scale, a significant amount of research and development will be

1396   needed. The standards for an effective photocatalyst are generally agreed upon in the literature.

1397   The material's characteristics should, in general, permit well-visible light absorption, sufficient

1398   degree of resistance to photo corrosion and ideally should inhibit the recombination of electron-

1399   hole pairs [168]. Work by Dhakshinamoorthy et al. [169] further stresses the importance of

1400   responsiveness to visible light to ensure the efficient use of solar energy, by emphasizing that

1401   visible light makes up 43% of total solar energy. Shanmugham et al. [168] provide a range of ideal

1402   photocatalyst material properties to help achieve these goals, including a high surface area,

1403   narrow band gap, and thermal stability. In addition, several papers agree on the importance of

1404   photocatalyst morphology and structure for performance as it influence the surface area and the

1405   availability of active sites.

4.1   Conventional photocatalytic materials

1407   Photocatalysis is a transformative technology that leverages light to drive chemical reactions,

1408   offering innovative solutions in various fields including environmental remediation, energy

1409   production, and chemical synthesis. At the heart of this technology are photocatalyst materials,

1410   which absorb photons and use this energy to facilitate or accelerate chemical processes. Among

1411   conventional photocatalyst materials are titanium dioxide (TiO_2), zinc oxide (ZnO), and carbon-

1412   based materials such as graphene oxide (GO), and reduced graphene oxide (rGO). Each of these

1413   materials has its strengths and limitations, so the choice of photocatalyst often depends on the

1414   specific application and the desired properties. Pawar et al. [170] hail titanium dioxide (TiO_2)

1415   nanoparticles as being among the most promising photocatalyst materials for commercial use.

1416   This is due to their superb optical and electronic characteristics, excellent chemical stability,

1417   high photoactivity, low cost, and reusability. Various morphologies of titania photocatalysts,

1418   spanning from nano to macrostructures, have been documented in the literature [171]. These

1419   encompass spherical particles, rod-like structures, tubular forms, fibrous configurations, and

1420   sheet-like arrangements at the nanoscale (**Fig. 8(a)**). These diverse morphologies have been

1421   meticulously designed to achieve distinct photocatalytic capabilities by fine-tuning factors such

1422   as particle size, specific surface area, pore structure and volume [171]. Research by Zhao et al. [172],

1423   however, emphasizes the disadvantages of semiconductor nanoparticles (NPs) such as TiO_2

1424   including a complex separation process from reaction systems, and a high rate of recombination

1425   of photogenerated electron-hole pairs. TiO_2 is also prone to aggregation in reactions which

1426   reduces its effective surface area and therefore performance.

1427

1428   In their work, Moma and Baloyi [173] postulate that the main issue with TiO_2 photocatalysts is the

1429   bandgap (3.2 eV). As a result, only 5% of the solar spectrum of the UV light region can be used

1430   for photocatalysis. TiO_2 has a low photocatalytic efficiency as a result. Research by Zhao et al.

1431   [172] supports this view, by arguing that this disadvantage is the primary hindrance preventing the

1432   use of TiO_2 in isolation for photocatalysis. To increase TiO_2's efficiency, current research also

1433   attempts to enhance its photocatalytic activity under visible light irradiation [174] . One method

1434   investigated is nitrogen-doped TiO_2, results of such studies show enhanced photocatalytic

1435   activity compared to pure TiO_2 [173]. Recent studies suggest also that modifying the defects in

1436 TiO_2 can expand the range of light absorption and enhance the efficiency of charge separation.

1437   Various methods, including hydrogenation, plasma treatment, chemical reduction,

1438   electrochemical reduction, and oxidation (**Fig. 8(b)**) [175], are employed to produce defective

1439 TiO_2 photocatalysts. These catalysts exhibit different types of defects, encompassing bulk and

1440   surface defects, and their relevance in photocatalytic applications is documented [175]. Notably,

1441   oxygen vacancies and Ti^{3+} defects are identified as pivotal factors in augmenting photocatalytic

1442   performance.

1443

1444   Due to the wide band gap of TiO_2, its application in visible photocatalysis is limited. To address

1445   this issue, several studies propose introducing oxygen vacancies and carbon quantum dots

1446   (CQDs) with up-conversion properties to enhance photocatalytic activity. Li et al. [176] prepared

1447   various configurations, including one-dimensional TiO_2 nanotubes (TNs), TNs with oxygen

1448   vacancies (OVTNs), TNs embedded with composite CQDs (CQD-TNs), and OVTNs

1449   embedded with composite CQDs (CQD-OVTNs). The impact of oxygen vacancies and CQDs

1450   on NOx removal through photocatalysis was investigated. Results show that CQD-OVTNs

1451   exhibit a significant synergistic effect between CQDs and oxygen vacancies, enhancing visible

1452   photocatalytic NO removal efficiency by approximately 12, 2, and 2.6 times compared to TNs,

1453   OVTNs, and CQD-TNs, respectively (**Fig. 8(c)**) [176]. Similarly, nitrogen-doped carbon quantum

1454   dots (NCQDs) were utilized to enhance TiO_2 through a simple hydrothermal-calcination

1455   synthesis method [177]. The incorporation of NCQDs enhances visible light absorption and

1456   facilitates electron transfer, thereby improving the separation of photo-generated electron-hole

1457   pairs. Even with a low NCQDs content of 3 wt%, the photodegradation rate for methylene blue

1458   was 2.25 times faster compared to pristine TiO_2.

1459

1460   A plausible mechanism for the photocatalytic degradation of methylene blue (MB) by

1461 NCQDs/TiO$_2$ is depicted in **Fig. 8(d)** [177]. When exposed to sunlight, electrons within the

1462 valence band (VB) of TiO$_2$ absorb photon energy from solar radiation, generating electron (e−)

1463 hole (h+) pairs in the conduction band (CB) and VB, respectively. The e− can readily combine

1464 with dissolved oxygen in water to form •O$_2$-. Furthermore, the h+ can oxidize OH$^-$ and H$_2$O

1465 molecules adsorbed on the TiO$_2$ surface to produce •OH radicals. However, e− and h+ often

1466 recombine with low efficiency, limiting photocatalytic activity. The introduction of nitrogen-

1467 doped carbon quantum dots (NCQDs) serves to enhance visible light absorption and promote

1468 charge transfer. Consequently, more photocarriers are generated, and their recombination is

1469 substantially suppressed, resulting in a notable increase in efficient active radicals.

1470 Consequently, with the combined action of h+, •O$_2$-, and •OH radicals, methylene blue (MB)

1471 molecules undergo mineralization to yield CO$_2$ and H$_2$O [177].

1472

1473 In a comprehensive photocatalytic process employing a TiO$_2$-based photocatalyst, three

1474 primary stages are involved: (1) absorption of light and the generation of photogenerated

1475 electron-hole pairs by TiO$_2$, (2) separation and transfer of these photogenerated electron-hole

1476 pairs, and (3) redox reactions occurring on the surface of TiO$_2$ and cocatalysts (as depicted in

1477 **Fig. 8(e)**). These consecutive steps collectively govern the overall photocatalytic effectiveness

1478 of TiO$_2$-based photocatalysts [178]. On the other hand, to utilize semiconductor photocatalysts for

1479 water treatment, several requirements must be met: the process should be feasible at room

1480 temperature and pressure, ensuring complete mineralization without generating secondary

1481 pollution [179]. In addition, it should enable repetitive cycles and maintain low operational costs.

1482 TiO$_2$ photocatalysis embodies a photo-induced charge separation process occurring on the TiO$_2$

1483 surface, which generates highly reactive oxygen species capable of microbial inactivation and

1484 organic mineralization without producing secondary pollutants.
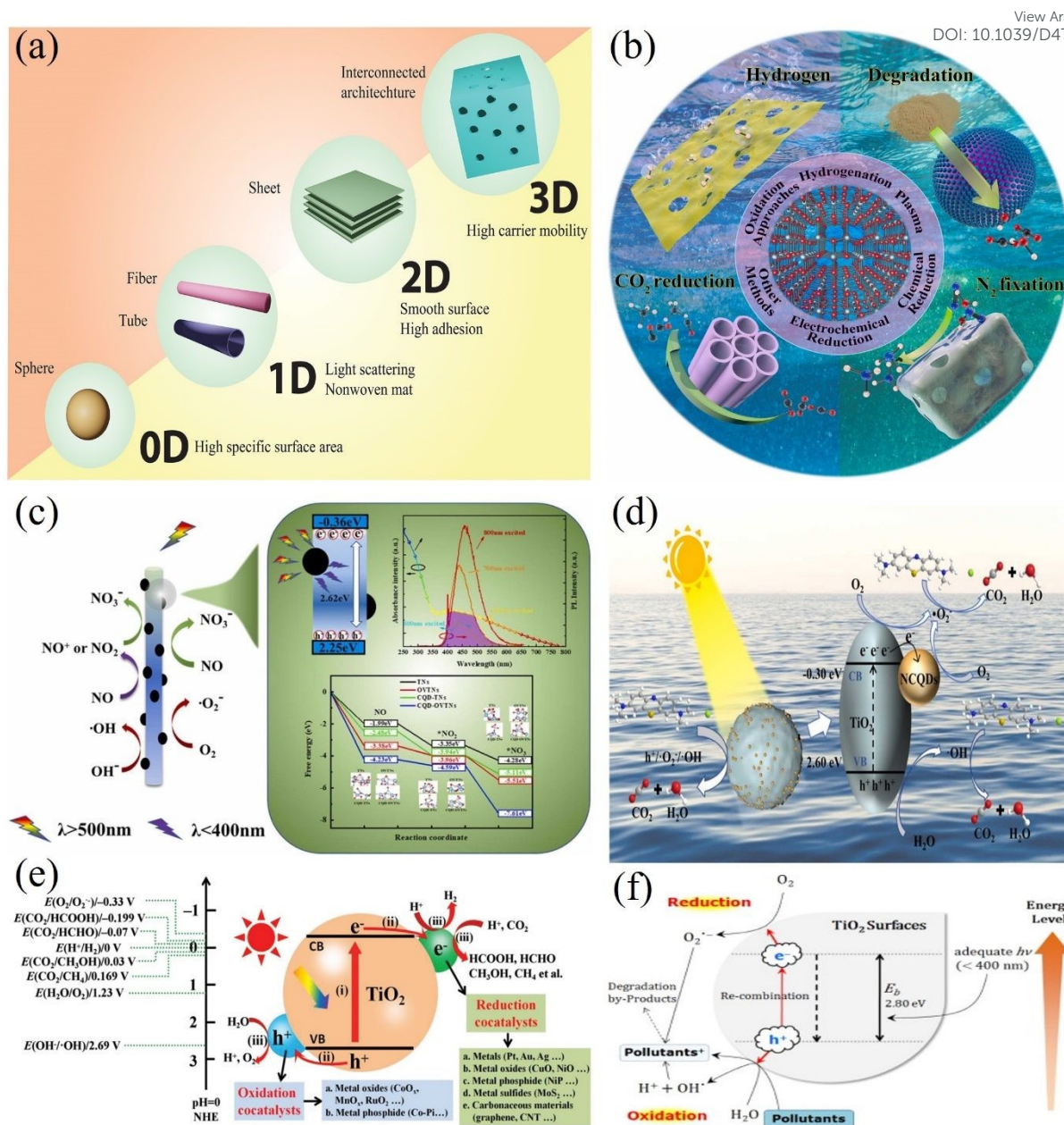
Fig. 8. (a) Various structural configurations of TiO_2 at both the nano and macro scales. Adopted from Ref. [171] with permission. (b) A schematic diagram depicting the utilization of defective TiO_2 materials in photocatalytic applications. TiO_2 photocatalysts are fabricated using various methods such as hydrogenation, plasma treatment, chemical reduction, electrochemical reduction, and oxidation. Adopted from Ref. [175] with permission. (c) Oxygen vacancies and carbon quantum dots (CQDs) with up-conversion properties for enhanced photocatalytic activity of TiO_2 for NO removal under visible light irradiation. Adopted from Ref. [176] with permission. (d) Mechanism for the degradation of methylene blue using $NCQDs/TiO_2$ under solar irradiation. Adopted from Ref. [177] with permission. (e) Illustration of the photocatalytic reactions occurring on TiO_2-based photocatalysts, enhanced with reduction and oxidation cocatalysts. The redox potentials of various species at pH = 0, referenced to the NHE, are also depicted. Adopted from Ref. [178] with permission. (f) Pollutant removal through the generation of photoinduced charge carriers (e−/h+) on the surfaces of semiconductor TiO_2 particles. Adopted from Ref. [179] with permission.

1501   The schematic representation depicted in **Fig. 8(f)**, illustrates the elimination of pollutants

1502   through the generation of photoinduced charge carriers (e−/h+) on the surfaces of

1503   semiconductor TiO_2 particles [179]. Upon exposure to UV light, the surface of TiO_2 catalysts

1504   suspended in water triggers photo-induced electrons in the conduction band to participate

1505   actively in reduction processes. Typically, they interact with dissolved oxygen in the air,

1506   resulting in the generation of superoxide radical anions. Meanwhile, the photo-induced holes in

1507   the valence band migrate to the surface of TiO_2 and react with adsorbed water molecules,

1508   leading to the formation of hydroxyl radicals [179]. It is worth noting that hydroxyl radicals (OH•)

1509   play a crucial role as primary active species in the photocatalytic oxidation reaction.

1510

1511   Regarding the environmental impact, TiO_2 has been described as eco-friendly as not only is it

1512   reusable (for photocatalysis) but it is also non-toxic [170,180], with Chen et al. [181] claiming it's "the

1513   most efficient and environmentally benign photocatalyst". However, there is concern over the

1514   potential effects of TiO_2 nanoparticles on humans and animals [182]. Although the shape and

1515   magnitude of TiO_2 nanoparticle effects are mostly determined by the physical and chemical

1516   properties of the particles, research on the mechanistic toxicology of these particles indicates

1517   that they may induce genotoxicity, inflammation, and cell destruction. TiO_2 nanoparticles have

1518   been identified by the National Institute for Occupational Safety and Health as potentially

1519   carcinogenic to humans as a result [182]. In their life cycle assessment (LCA), Wu et al. [183]

1520   evaluated the impact of nano-TiO_2 based on a range of synthesis routes. They discovered that

1521   physical synthesis approaches produced a greater environmental impact since they needed large

1522   amounts of supporting gas and substantial energy inputs. Chemical routes have a fair amount

1523   of impact, with upstream precursor production accounting for a large share of that impact.

1524   Because of the bacteria culture media utilised, biological channels also posed a significant

1525   environmental impact. Because organic precursors required large amounts of organic solvents,

1526   they performed especially poorly. The LCA model included a freshwater ecotoxicity evaluation

1527   factor to account for the possibility of nano-TiO$_2$ leakage into water sources. It is crucial to

1528   remember that while appropriate modelling assumptions have been made and some TiO$_2$

1529   production pathways are not covered by this LCA, total correctness cannot be guaranteed [183].

1530

1531   On the other hand, TiO$_2$ is generally considered cost-effective for photocatalytic uses [180].

1532   Furthermore, novel cost-effective production methods are still being developed. An example is

1533   the facile sequential calcination and ball milling strategy [184]. It was stated that a post-treatment

1534   procedure was developed for less expensive TiO$_2$ photocatalysts with lower photocatalytic

1535   activity. The straightforward and affordable method seeks to raise the less expensive TiO$_2$

1536   photocatalysts' photocatalytic activity to the same degree as more expensive commercial

1537   counterparts with higher photoactivities. This procedure about ninety-fold improves the

1538   performance of inexpensive KA100 in lab testing. In addition to TiO$_2$, zinc oxide (ZnO) and

1539   carbon-based materials have garnered significant attention as photocatalysts due to their

1540   excellent transport properties, affordability, and versatile morphological structures. In the work

1541   of Sansenya et al. [185], photocatalyst based on ZnO with a specific surface area of about 10.6

1542   m²/g were prepared. The materials have demonstrated high photodegradation capacity of

1543   reactive red 141 (R141), Congo red (CR), and Ofloxacin after 20, 60, and 180 minutes of solar

1544   light irradiation, respectively. The stability of the photocatalyst was confirmed after three

1545   cycles of use, maintaining high performance even after the third cycle, indicating its promising

1546   reusability. In similar context, silver was incorporated into ZnO photocatalysts at varying

1547   concentrations, exhibited a hexagonal phase with notable performance under visible light and

1548   improved anti-photocorrosion properties [186]. Complete removal of reactive red dye and

1549   ofloxacin antibiotic was achieved after 25 and 80 minutes of irradiation, respectively. The

1550   enhanced photocatalytic activity is attributed to the efficient separation of electron-hole pairs

1551   at the photocatalyst interface. The introduction of metallic silver onto the ZnO photocatalyst

1552   creates a Schottky barrier at the silver/ZnO interface, which enhances quantum efficiency and

1553   photocatalytic activity.

1554

1555   Kim et al. [187] introduced a novel, high-efficiency catalyst based on a boron-doped C3N4/ZnO

1556   composite. This composite demonstrated a significantly enhanced photocatalytic hydrogen

1557   evolution rate, approximately 2.9 times greater than that of undoped C3N4/ZnO. This is a

1558   straightforward and effective approach for designing highly efficient heterojunction

1559   photocatalysts by utilizing charge transfer switching via doping. Recently, it has been found

1560   that decorating the Rh co-catalyst of the benchmark GaN–ZnO photocatalyst with Al_2O_3 species

1561   via atomic layer deposition significantly mitigates reverse reactions [188]. This modification

1562   enhances photocatalytic oxygen water splitting (OWS) activity by more than an order of

1563   magnitude, with an apparent quantum efficiency increasing from 0.3 to 7.1% at 420 nm. The

1564   partial coverage of Rh surface sites with inert Al_2O_3 effectively suppresses reverse reactions by

1565   obstructing the reduction/oxidation cycle of Rh atoms during the photocatalytic OWS process.

1566   Moreover, combining ZnO with carbon-based materials, such as graphene oxide, can further

1567   enhance its photocatalytic properties. Indeed, an efficient photocatalyst was successfully

1568   synthesized using GO/ZnO nanocomposites with embedded metal nanoparticles through a

1569   simple one-pot method [189]. A catalytic activity of 84% for the degradation of methylene blue

1570   (MB) dyes was achieved with a nanocomposite containing 3.125% GO after 90 minutes of

1571   sunlight irradiation. Thus, the GO–ZnO–Ag nanocomposite demonstrates significant potential

1572   as an efficient and adaptable photocatalyst for the photodegradation of organic dyes in industrial

1573   wastewater. In another work, the photocatalytic degradation of Rhodamine B (RhB) and MB

1574   by a material comprising sol-gel synthesized ZnO nanochips, GO and RGO was discussed [190].

1575   Results indicated that ZnO nanochips integrated onto graphene sheets exhibited enhanced

1576 photocatalytic activity, achieving approximately 76.5–98.9% degradation of RhB and MB

1577 within 90 minutes of visible light irradiation. Furthermore, ZnO@RGO demonstrated superior

1578 photocatalytic performance compared to ZnO@GO, with approximately 2.4 and 2 times higher

1579 kinetic rates for the removal of RhB and MB, respectively.

1580

1581 Common materials like TiO_2, ZnO, and GO are popular photocatalysts, but they have notable

1582 limitations compared. TiO_2 and ZnO both have wide band gaps (~3.0-3.2 eV and ~3.2 eV,

1583 respectively), restricting their activity to UV light, which limits their effectiveness under visible

1584 light. Both materials also suffer from rapid recombination of electron-hole pairs, reducing their

1585 photocatalytic efficiency. Additionally, TiO_2 and ZnO have lower surface areas, limiting the

1586 number of active sites, and ZnO is further hampered by photo corrosion under UV light. GO,

1587 while possessing a high surface area, offers limited photocatalytic activity on its own and

1588 primarily functions as a support material. Its variable band gap and the complexity of reducing

1589 GO to rGO for enhanced activity also pose challenges. In contrast, MOFs offer greater

1590 flexibility with tunable band gaps, higher surface areas, and versatile functionalization options,

1591 making them superior photocatalysts for a wide range of applications.

4.2 Metal organic frameworks as photocatalysts

1593 Heterogeneous photocatalysis (HP) stands as an advanced oxidation method that has surfaced

1594 as a promising alternative with a broad spectrum of applications. These applications include

1595 treating effluents for decontamination and disinfection, addressing environmental challenges

1596 related to pollutants like CO_2 and NO_x in the atmosphere, and facilitating energy conversion.

1597 These are among the most prevalent and widespread uses of this technology. In this context,

1598 metal-organic frameworks (MOFs) have been developed to enhance the characteristics and

1599 photocatalytic capabilities of conventional semiconductors. MOFs have emerged as innovative

1600 photocatalysts due to their intrinsic structural features, which include vast surface area,

1601   organised porous structure, and structural diversity. This application is especially well-suited

1602   for MOFs since they can combine photosensitiser and catalytic functions into a single structure

1603   [191]. The high porosity of MOFs (macropores larger than 50 nm in some cases) enables rapid

1604   substrate and product transport/diffusion from the catalytic sites [22]. Additionally, organic

1605   ligands have the ability to absorb photons and transfer electrons from the ligand to the metal

1606   centre, thereby generating an excited state in the process. Thus, the utilization of MOFs as

1607   photocatalysts encompasses a diverse and extensive range of applications (**Fig. 9(a)**) [192].
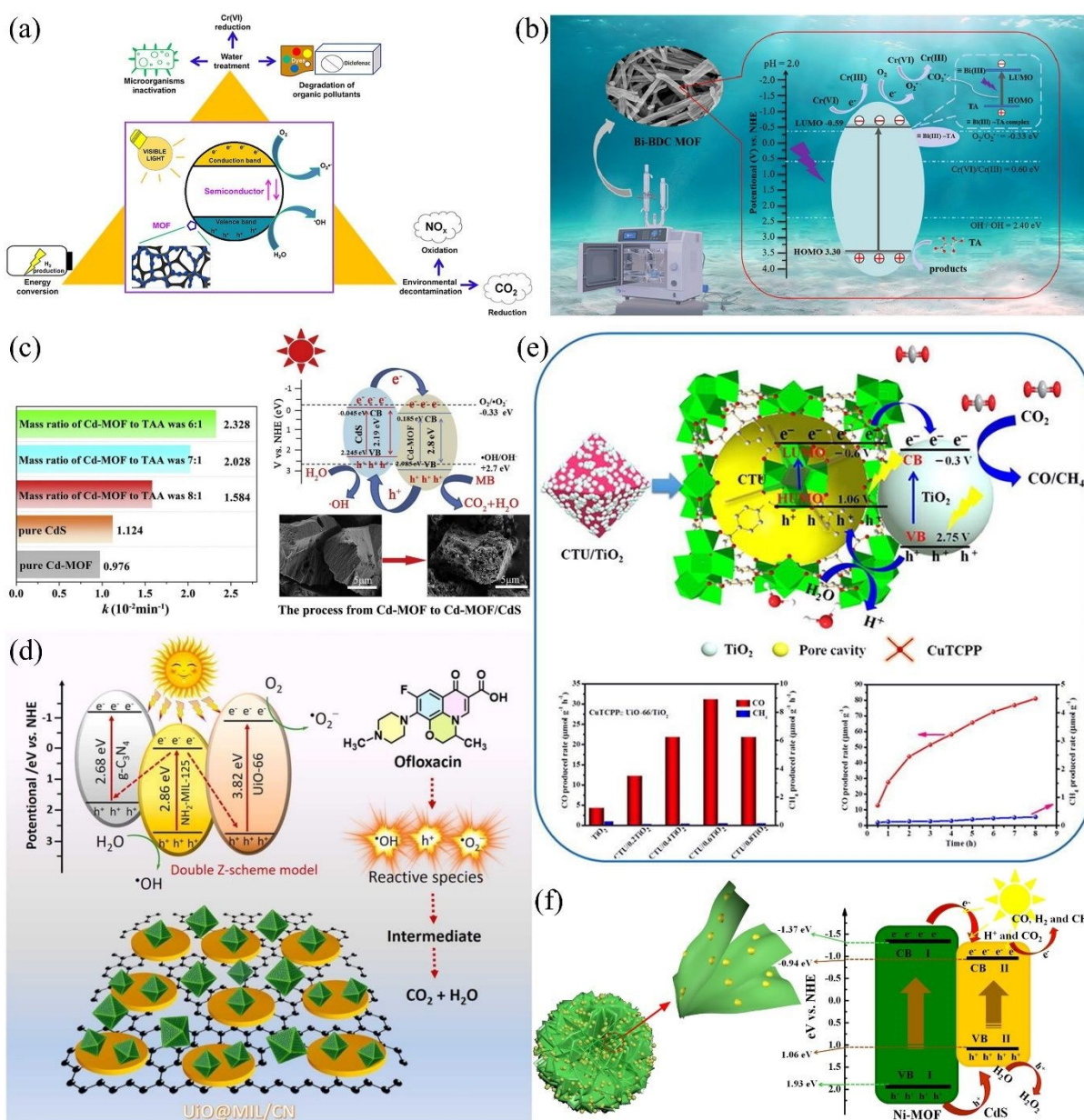
1608

1609   **Fig. 9.** (a) Composite materials featuring metal-organic frameworks for heterogeneous
1610   photocatalysis driven by visible light. MOF-based composites have potential applications in the

degradation of organic compounds, reduction of Cr(VI), inactivation of microorganisms, oxidation of NOx, reduction of CO_2, and production of H_2. Adopted from Ref. [192] with permission. (b) Microwave-assisted synthesis of Bi-BDC MOF photocatalyst and its efficient reduction of Cr(VI) within 6.0 min under low-power LED UV light. Adopted from Ref. [193] with permission. (c) Visible light CdS/Cd-MOF photocatalyst with enhanced photodegradation of methylene blue (91.9% in 100 minutes under simulated sunlight irradiation). Adopted from Ref. [194] with permission. (d) Double Z-scheme heterojunction based on UiO/MIL/CN for the photocatalytic degradation of ofloxacin under visible light irradiation. Adopted from Ref. [195] with permission. (e) CuTCPP-functionalized zirconium MOF and TiO_2 for photocatalytic CO_2 reduction to CO under simulated solar illumination. The figure contains the dependence of total CO/CH_4 evolution on the amount of TiO_2 and various CTU/TiO_2 ratios under Xe lamp irradiation ($\lambda > 300$ nm) within 1 hour, total CO/CH_4 evolution amount produced by $CTU/0.6TiO_2$ under Xe lamp irradiation within 8 hours, and a proposed photocatalytic CO_2 reduction pathway over CTU/TiO_2. Adopted from Ref. [196] with permission. (f) 3D hierarchical structure of CdS/Ni-MOF and schematic diagram illustrating the electron transfer process and photocatalytic mechanism involved in the reduction of CO_2. Adopted from Ref. [197] with permission.

Regarding the elimination of Cr(VI) from water, Gao et al. [193] have synthesized a high-throughput MOF composed of Bi-benzene-1,4-dicarboxylic acid (Bi-BDC) and featuring a consistent rod-like structure using a microwave-assisted technique (**Fig. 9(b)**). This MOF demonstrated the capability to achieve a complete photocatalytic reduction of Cr(VI) in just 6.0 minutes when exposed to low-power LED UV light [193]. Furthermore, the degradation of contaminant was also reported using MOFs photocatalyst. Jing et al. [194] constructed a binary CdS-Cd-MOF nanocomposite by an *in-situ* sulfurization of Cd-MOF. When exposed to simulated sunlight, the degradation rate of methylene blue using 10 mg of the material reached 91.9% within 100 minutes [194]. The mechanism of the photocatalytic degradation is described based on the difference in the band gap between the CdS (2.29 eV) and Cd-MOF (2.8 eV) (**Fig. 9(c)**). In a similar context, a recent study investigates the photocatalytic degradation of ofloxacin using UiO/MIL/CN [195]. In this work, the synthesis involved growing UiO-66 on the surface of NH_2-MIL-125 using the solvothermal method to create MOF-on-MOF architectures. Following that, the authors achieved the successful deposition of g-C_3N_4 nanosheets onto the surface of UiO-66/NH_2-MIL-125, resulting in the development of a novel double Z-scheme heterojunction photocatalyst (**Fig. 9(d)**). When exposed to visible light, this double Z-scheme

1645 heterojunction serves as an exceptionally efficient photocatalyst for the degradation of

1646 ofloxacin, exhibiting a rate constant of 0.07 min^{-1} [195].

1647

1648 Furthermore, the photocatalytic reduction of carbon dioxide into valuable chemicals stands as

1649 an appealing technique, addressing both environmental concerns and energy scarcity

1650 simultaneously. Interestingly, MOFs have garnered significant interest in this field due to their

1651 remarkable chemical and structural diversity. Wang et al. [196] employed an in-situ hydrothermal

1652 process to combine TiO_2 nanoparticles with a mixed ligand-based MOF structure consisting of

1653 CuTCPP and BDC (CTU). This integration resulted in the formation of CTU/TiO_2

1654 nanocomposites, which effectively merge MOFs with inorganic semiconductors (**Fig. 9(e)**).

1655 When employed as photocatalysts for CO_2 conversion under simulated solar light ($\lambda > 300$ nm),

1656 the optimized CTU/TiO_2 heterostructure demonstrated significantly enhanced performance [196].

1657 The rate of CO_2 reduction into CO reached 31.32 μmol/g h, approximately seven times higher

1658 than that achieved with bare TiO_2. In another study conducted by Xu et al. [197], they explored

1659 the development of 3D hierarchical CdS/Ni-MOF photocatalysts. These photocatalysts

1660 exhibited a notably CO yield, surpassing the yields achieved by both Ni-MOF and CdS

1661 individually by 16 and 7 times, respectively. The researchers proposed a preliminary

1662 mechanism for the CO_2 conversion process (**Fig. 9(f)**). Upon exposure to UV-Vis light, both

1663 Ni-MOF and CdS become excited, generating electrons (e-) and holes (h+). Their intimate

1664 interface facilitates the efficient transfer of excited electrons from Ni-MOF to CdS, which

1665 boasts a more positive conduction band [197]. Consequently, CdS, acting as the active site,

1666 proficiently reduces CO_2 to CO. Concurrently, the holes in the valence bands of Ni-MOF and

1667 CdS engage in oxidation reactions, yielding oxygen and hydrogen peroxide, effectively

1668 eliminating the holes. This well-coordinated charge separation and electron-hole pair transfer

1669 contribute to the enhanced photocatalytic activity of the system.

1670

1671 Because the careful selection of linkers/metal clusters or the addition of catalysts can

1672 significantly increase light adsorption, reactant adsorption, charge separation, and reactant

1673 activation, the modification of MOF elements is especially crucial for photocatalyst

1674 applications [23]. As a result, photocatalytic performance will be enhanced. Sensitiser addition is

1675 one example of modulating ligand and metal clusters. MOFs can incorporate sensitisers (metal

1676 complexes or organic dyes) to increase the amount of visible-light-driven photocatalysis [167]. In

1677 their study, Furukawa et al. [24] successfully introduced dyes and encapsulated precious metals

1678 into a series of MOF photocatalysts, producing an enhanced photocatalytic performance for

1679 almost all MOFs tested as well as a slightly increased spectrum region for photoactivity. In a

1680 similar vein, Pt/ NH_2-MIL-125(Ti) was used in visible light for CO_2 reduction [23]. The results

1681 of this were also positive with the material showing an improvement in photocatalytic

1682 performance when compared to the plain NH_2-MIL-125(Ti). Pt/NH_2-MIL-125(Ti) exhibited a

1683 remarkable boost in its photocatalytic efficiency for CO_2 reduction into formate. Over the

1684 course of 8 hours of irradiation, Pt/NH_2-MIL-125(Ti) yielded approximately 12.96 mmol of

1685 formate, representing a notable 21% increase in activity when compared to the performance of

1686 pure NH_2-MIL-125(Ti). These experiments suggest that the use of precious metals in MOFs to

1687 improve photocatalytic behaviour has great potential.

1688

1689 Furthermore, studies indicate that MOFs' thermal and chemical stabilities are a bonus and

1690 contribute to their appeal as catalysts and catalytic hosts. Zhao et al. [22] posit that MOF

1691 photocatalysts should be stable under service conditions, including water. In addition to this,

1692 MOF photocatalysts have shown resistance to moderately acidic and basic solutions [22]. An

1693 example of an aquatically stable MOF can be found in Drache et al. [198] report in which they

1694 investigated a series of Zr-based MOFs and found they exhibited excellent stability in water.

1695 The authors suggest that this is a result of the strong coordination between the organic ligands

1696 and the Zr nodes. Howarth et al. [199] recommend another method to improve the stability of

1697 MOFs in water, involving decorating the MOF organic linkers with sulphonic, fluorinated, or

1698 phosphonate substituents. Metal oxide encapsulation within MOF photocatalysts is an

1699 additional line of inquiry. POMs, or polyoxometalates, have attracted a lot of interest because

1700 of their exceptional redox capacity, highly negative charges, and structural characteristics [22].

1701 When POM $[(PW_9O_{34})_2Co_4(H_2O)_2]$ was encapsulated in MOF-545 the product was able to

1702 endure reversible electron transfer reactions with negligible structural degradation [200]. This

1703 material was also successfully used for water oxidation under visible light. As demonstrated,

1704 recent advancements have introduced numerous new MOFs and MOF-based composites

1705 specifically designed for the photocatalytic reduction of CO_2. MOFs are recognized as state-of-

1706 the-art photocatalysts due to their exceptional coordination between active metal centers and

1707 organic linkers. Their unique structural features such as vast surface areas, well-ordered

1708 frameworks, high porosity, and significant structural tunability contribute to their effectiveness

1709 [201]. Compared to traditional catalysts, MOF-based photocatalysts present several advantages,

1710 including ultra-high specific surface areas, adjustable pore structures that enhance CO_2

1711 adsorption and reduction and unlike homogenous photocatalysts, they are easily separated from

1712 the reaction products and can therefore be reused many times [22]. As such, MOF photocatalysts

1713 will have a longer lifetime, contributing to a decrease in waste, end-of-life process costs, and

1714 pollution. Additionally, the metal nodes and organic ligands in MOFs can be selectively

1715 functionalized, and the abundant pores allow for the accommodation of various functional guest

1716 substances.

1717

1718 Despite these benefits, challenges persist in the use of MOFs composites as photocatalysts.

1719 These include low visible light utilization efficiency, poor stability with rapid loss of activity

1720 and structural integrity after several cycles, and reliance on organic sacrificial reagents and

1721 solvents that pose environmental concerns. Furthermore, not much research has been done on

1722 how MOFs employed in photocatalytic applications affect the environment. An LCA could be

1723 performed to more accurately assess the possible impact of MOF photocatalysts. On the other

1724 hand, as previously noted, the synthesised MOFs continue to be costly because of the intricate

1725 synthesis procedures and the absence of mass production processes, even though the component

1726 linkers and ions are frequently quite affordable [18]. However, MOFs improved efficiency

1727 compared to TiO_2 photocatalysts and their potential for an extended lifetime will likely reduce

1728 their long-term costs.

5. Evaluation and comparison

1729

1730 Investigating potential MOF as sorbents, SCs electrodes or photocatalysts is a difficult

1731 endeavour due to the vast number available, with over 90,000 synthesized MOFs in the public

1732 domain [202]. However, the creation of software with these capabilities is yet to be achieved [35].

1733 To increase the TRL level of MOF sorbents, pilot-scale MOF production needs to be

1734 investigated. Methods of bulk-producing structured MOFs are imperative if they are to be used

1735 for industrial use. **Table 3** shows a summary of the advantages and disadvantages of MOFs,

1736 liquid amine, activated carbon, as well as titanium dioxide for application in various

1737 technologies identified from a review of recent literature.

1738 **Table 3.** Advantages and disadvantages of MOFs, liquid-amine, activated carbon, and TiO_2
1739 technologies for uses in CCS, SCs electrodes and photocatalysis.
1740

Advantages	Disadvantages
• Controllable morphology (pore size). • MOFs are used for CCS at lower temperatures compared to amines [52]. • CO_2 capture capacity ≥ amine scrubber under the same dry working conditions [32]. • Solid sorbents have a much lower heat capacity compared to liquid-amine solutions [32]. • Suitable for DAC processes [33].	• Still in early developmental stages – further research is required [191]. • Poor stability under CCS operational conditions [18]. • Prone to decompose when exposed to moisture [18]. • Poor thermal conductivity (leading to higher regeneration costs and slower regeneration processes) [36].

MOFs	• Some MOFs can provide a greater CO_2 uptake capacity, good SCN, and acceptable regeneration energy requirements [50]. • Reduced effect on power plant efficiencies [203]. • High capacitance compared to ACs. • Some MOFs show exceptional cyclic stability [22]. • High power densities. • Possibility of using waste PET for production [113]. • Light harvesting range can be extended to include visible/NIR light through the inclusion of long-wavelength-light-responsive units within the MOF. • Can reduce recombination of the photogenerated electrons and holes. • Some MOFs have shown improved photocatalytic behaviour. • Reported successful application under mild conditions.	• CO_2 capture capacity can be reduced in the presence of moisture [18]. • Lack of processes to convert MOF powders into devices [18]. • Low CO_2 capacity in the presence of water [27]. • Reports of poor stability over multiple cycles of absorption/desorption [27]. • Can have high production costs [27]. • All the feasible methods to modify MOFs for DAC currently rely on amine doping [62]. • Little known about MOF toxicity. • Suitability for widescale deployment not well established • Comparatively complex synthesis process. • The stability of MOFs under photocatalytic reaction conditions requires more research – some reports of low stability.
Liquid amines	• Proven success in bulk scale CCS [18]. • The most developed method of CCS [25]. • MEA has a high CO_2-carrying capacity [27]. • MEA has a fast absorption rate [27]. • Amines can provide high separation/purification performance [18]. • Some liquid amines like MEA are low-cost [26]. • MEA is readily biodegradable [26].	• Energy intensive - High solvent regeneration energies (>140 °C) [31]. • Requires large equipment [31]. • Prone to equipment corrosion and requires inhibitors to prevent it [31]. • Prone to degradation [25]. • Can reduce the overall efficiency of a powerplant [18]. • Limited potential for performance improvement [19]. • High cost, and levels of sorbent loss [33,35]. • Highly toxic and environmentally harmful, not suitable for DAC [33]. • Insufficient CO_2 capacity for industrial-scale emissions mitigation [25].
Coconut shell activated carbon	• Low cost [80]. • Raw material readily available [80]. • High thermal and electrochemical stability [204]. • Renewable and non-toxic [204]. • Low net GHG emissions over the lifespan [96].	• Low power densities. • Capacitive performance is not as high as that offered by some MOFs • Low specific capacitance [83].
Titanium dioxide	• Showed great promise for commercial use [170]. • Non-toxic [170]. • Environmentally benign [181]. • Suitably efficient photoactivity [205]. • High stability [205]. • Low cost [205].	• Complex separation process [206]. • Prone to aggregation [206]. • Rapid rate recombination of the photogenerated electron-hole pairs [206].

- Photocatalytic activity is restricted to the UV region (low photocatalytic efficiency) [207].

1741

5.1 Carbon capture

1742

1743 Metal-organic frameworks (MOFs) present numerous advantages over non-MOF materials for

1744 applications in carbon capture. MOFs such as MOF-5 and HKUST-1 exhibit exceptional

1745 surface areas and porosity, exceeding 1000 m²/g, which translates to higher CO_2 adsorption

1746 capacities up to 33.5 wt% and 31.0 wt% respectively under standard conditions [208]. This is

1747 significantly better than traditional materials like zeolites and activated carbons, which have

1748 lower surface areas and CO_2 adsorption capacities. The tunability of MOFs allows for precise

1749 control over pore size and functionality, enhancing selectivity towards CO_2, as demonstrated

1750 by ZIF-8's CO_2/N_2 selectivity of 25 at room temperature. However, MOFs generally show high

1751 sensitivity toward moisture and high structural degradation, such as MOF-5, which can lose as

1752 much as 90% of its CO_2 adsorption capacity under humid conditions. Moreover, high synthesis

1753 and processing costs, along with difficulties in the production of defect-free membranes, are of

1754 vital importance against scalability. Carbon capture performance metrics are important.

1755 Although MOFs showed an upper CO_2-carrying capacity compared to liquid amines in the

1756 laboratory tests, both materials showed a suitable level of CO_2 selectivity with excellent

1757 selectivity shown by MOFs doped with amines. MOFs doped with amine dopants also had

1758 lower regeneration energies compared to liquid amines. The possibility of development is

1759 higher for MOFs due to their tunable structure and number of available MOFs. While MOFs

1760 are under development, liquid amines find industrial applications. Both materials have stability

1761 problems under CCS conditions, and as far as reported there was no problem of corrosion

1762 observed with MOF, unlike liquid amines which in addition to being corrosive are volatile. On

1763 performance, MOF scores 128 against liquid amine's 93. The three broad factors were further

1764 allocated relative weightings based on the findings of the literature review and summed up to

1765   100. For C-capture, the weights were distributed as performance 34/100, environmental impact

1766   25/100 and cost implications 41/100. The factors, along with weightings for the evaluation of

1767   carbon capture materials, are shown in **Table 4**, and the comparison matrix showing the scoring

1768   of liquid-amine and MOF-based materials against these factors is presented in **Table 5**.

1769   **Table 4.** C-capture factors and corresponding suggested weighting along with the justifications.
1770

Subject	Factor	Weighting	Justification
Performance	CO$_2$-carrying capacity	3	This affects the efficiency of the material and influences the amount of sorbet required for a CCS application [18].
	CO$_2$ selectivity	3	This affects the purity of adsorbed CO$_2$ and the concentration of CO$_2$ in the emitted flue gases [18].
	Regenerability	3	This affects the energy efficiency of the C-capture process [31].
	Potential for development	1	All current technologies (both liquid amine and MOF sorbents) require further improvement before they can be deployed on an industrial scale. Therefore, the material must offer enough scope/potential for these changes [31].
	Current successful application	2	CCS technology takes a considerable period of time to test and validate, very few materials make it to trials and even fewer are successful in reaching real-world applications [19]. Successful small-scale trials or real-world trials are good indications of the material's suitability.
	Stability under service conditions	3	The material used in CCS applications must be able to withstand the operating conditions and regeneration conditions to perform well.
	Corrosivity and volatility	2	Ideally, materials used should not be volatile as that can lead to high levels of sorbent loss and reduced levels of performance over time [33]. Corrosive materials can also cause performance issues as they may damage equipment, thus reducing its efficiency [33].
	Material recyclability	3	For the technology to be "future-proof" it needs to be sustainable.
	Toxicity	2	A toxic material is detrimental to the environment, it can also result in

Environmental impact			higher costs for disposal at the end of the products life.
	Production methods	2	Energy-intensive production methods may negate some of the benefits of the technology use.
	Functional energy requirements	3	Literature suggests that the application of post-combustion CCS can lead to an overall reduction of a power plant's efficiency [19].
Cost	Raw material cost	2	Influences the overall cost of a material. It is also important to consider the likelihood of a significant change in the price of a material.
	Usage costs (equipment, temperature/pressure requirements)	3	If a technology is excessively expensive then it will likely never be suitable for wide-scale deployment. Furthermore, if the costs of using the technology outweigh the benefits then it is likely the technology will fail or be superseded and become obsolete.
	Synthesis/manufacturing costs	3	High production costs can act as a barrier to wide-scale technology deployment. It is also important to consider if the production costs are likely to reduce when the technology develops further/becomes more mainstream.

1771

1772 **Table 5.** Comparison matrix between liquid amines and MOFs for C-capture applications.

Factor	Weighting	Material score		Justification
		Liquid-amines	MOFs	
CO_2-carrying capacity	6	3	5	MOFs have shown higher CO_2-carrying capacities in laboratory tests [52].
CO_2 selectivity	5	3	3	Both materials have shown suitable levels of CO_2 selectivity [52]. While pristine MOF sorbents have shown SCN values below those of liquid-amine sorbents, amine-doped MOF sorbents have shown excellent SCN values exceeding those of liquid-amine sorbents [18].
Regenerability	5	3	4	While both materials have shown acceptable (albeit high) results for required regenerability energy, some amine-doped MOF sorbents have exhibited lower regeneration energies [18,31].

Journal of Materials Chemistry A

Potential for development	4	1	5	Liquid amine technology provides little potential for further development whereas MOF sorbents provide vast potential due to their customisable structure and the number of available MOFs [19,25]. Furthermore, MOFs have shown potential for DAC [62].
Current successful application	5	4	2	Liquid amines are already used in industry but are yet to be rolled out on a wide scale [25]. MOFs for CCS are still in their developmental stages and are a long way from real-world trials [52].
Stability under service conditions	6	3	3	Both pristine MOF sorbents and liquid-amine sorbents have issues with stability under CCS conditions [18,25]. Whilst, amine-doped MOFs have shown improved stability under regeneration and service conditions, they are still mildly affected by the presence of moisture [18].
Corrosivity and volatility	3	1	5	Liquid amines are shown to be very corrosive and can cause damage to equipment if it has not been given a protective coating [25]. Liquid amines are also very volatile and therefore the process can be subject to high levels of sorbent loss [33]. There are currently no reported issues with MOF sorbents and corrosion.
Performance score:		93	128	
Recyclability	4	3	3	Recycling prospects for both materials are reasonably poor [18,26].
Toxicity	8	1	4	Liquid amines are toxic [33]. There is limited research into the toxicity of MOFs however, the literature suggests that some may be toxic when they start to decompose [125].
Production methods	7	3	3	The production of both materials is both complex and reasonably energy-intensive.
Functional Energy requirements	6	3	4	MOFs have shown potential for CCS at a lower temperature than those used for liquid-amine CCS [52]. Furthermore, amine-doped MOF sorbents have a lower regeneration energy requirement compared to liquid-amine sorbents [18].
Environmental impact score:		59	89	
Raw material cost	14	3	2	The cost of the MOFs constituent linkers and metal clusters is relatively cheap [18]. However, pre-synthesised MOFs are expensive due to complex production processes [18]. Some liquid-

				amines like MEA are relatively low-cost [26].
Usage costs (equipment, temperature/pressure requirements)	15	3	4	MOFs have demonstrated the potential for CCS at lower temperatures [52]. Liquid-amine scrubbers have also been shown to reduce the overall efficiency of a power plant to a greater degree than the predicted effects of MOF sorbents [18,203].
Production costs	12	3	2	As previously discussed, MOFs are expensive due to complex production processes. Liquid-amine technology is comparatively well-developed, and processing costs are cheaper [26].
Cost score:		123	112	
Overall scores:		275	329	

Note: All materials were evaluated for each factor using a scale ranging from 1 to 5 (where 1 corresponds to "very bad," 2 to "bad," 3 to "suitable," 4 to "good," and 5 to "very good").

Carbon capture technology stands as one of the most important strategies for mitigating climate change through the reduction of CO_2 emissions from industrial sources. There are three major parameters used that express a comparison among the different carbon capture methods: their cost, efficiency, and environmental impact. Cost means the financial expenditure incurred to capture, transport, and store CO_2, including capital, operational, and maintenance costs. Advanced carbon capture methods using MOFs reduce this cost to a large extent. For example, conventional amine-based capture processes may range between \$40–\$100 per ton of CO_2 captured while advanced materials, such as MOFs, are expected to drop these costs down to \$20–\$50 per ton by the increase in efficiency and reduction in energy requirements [209]. Efficiency is the percentage of CO_2 that can be captured from the sources of emission relative to the total amount of emissions produced. Traditional methods have efficiencies of 85–90%, while MOFs and other advanced materials could theoretically be as high as 95–99% according to the study on 2D MOFs for the reduction of CO_2, where $Cu_3(C_{12}N_6S_6)_2$ demonstrated very high activity with small overpotentials, which reflects high efficiency in the processes of capture and conversion of CO_2 [210]. Environmental impact looks at the bigger picture of how carbon capture affects the environment in general, such as the probable risks associated with

1792 the leakage of CO_2 during storage, the energy used by capture and sequestration, and the net

1793 reduction of GHG emissions. While traditional methods may leave room for a capture process

1794 that is 10–20% more energy-intensive, advanced MOF-based methods can reduce this extra

1795 energy requirement to under 10%, making the process more sustainable. Moreover, according

1796 to the researchers in this study, 2D MOFs showed improved selectivity toward CO_2 reduction

1797 relative to competing reactions, such as hydrogen evolution, which further minimizes unwanted

1798 environmental impacts. The utilization of 2D MOF as an advanced material in carbon capture

1799 technology shows a very promising avenue toward cost-effective, efficient, and

1800 environmentally sustainable processes.

1801 ## 5.2 Photocatalysis

1802 Given the very high porosity of the MOFs, the surface area can reach more than 3000 m^2/g.

1803 Such high values raise the adsorption and reduction rates of CO_2 in photocatalysis. Furthermore,

1804 their tunable structure provides conditions for the introduction of different metals, increasing

1805 active sites, and enhancing photocatalytic properties. Also, the MOFs exhibit enhanced light

1806 harvesting and photostability, which is very critical in efficient photocatalysis [211]. However,

1807 these materials have low stability in an aqueous/high-temperature environment and poor light

1808 absorption, thereby mostly limiting their application to only the ultraviolet regime, with the

1809 added need for sophisticated and expensive synthesis methods. MOFs demonstrated lower

1810 recombination rates and higher resistance to aggregation compared to titanium dioxide, which,

1811 although highly stable, is prone to aggregation. While titanium dioxide is restricted to UV light,

1812 MOFs can be active in a broader spectrum that includes visible light. Moreover, the MOFs

1813 provide larger surface areas with increased resistance to photo-corrosion. MOFs score 176

1814 while titanium dioxide scores 116, hence superior efficiency for performance evaluation. The

1815 evaluation parameters are weighted as performance, which is efficiency, at 45/100,

1816 environmental impact at 18/100 and cost implications at 37/100. Performance factors include

1817   photostability, the extent of light absorption and recombination rates 180. Environmental

1818   impact factors include stability of materials in various environments and resistance to photo-

1819   corrosion. These are, among others, the complexity and cost of the synthesis methods. **Table 6**

1820   presents the evaluation criteria in the case of photocatalysis, and **Table 7** presents a detailed

1821   comparison between titanium dioxide and MOFs in photocatalytic applications.

1822
1823   **Table 6.** Photocatalysis factors and the corresponding suggested weighting along with the justifications.

Subject	Factor	Weighting	Justification
Performance	Recombination rate	3	Low recombination rates are desirable as it directly effects the efficiency of the photocatalyst.
	Stability under photocatalytic conditions	3	The photocatalytic material must be able to withstand the operating conditions to perform well.
	Level of current development	2	Successful small-scale trials or real-world trials are good indications of the material's suitability.
	Resistance to Aggregation	2	Material aggregation can block the active sites of a material and therefore reduce the effective surface area of the material and consequently reduce its efficiency.
	Photocatalytic activity under Visible light	3	In order to maximise the efficiency of a photocatalyst, ideally it should be photoactive in a wide region of the light spectrum as possible. Most current photocatalysts are only active in the UV region of the spectrum.
	Material morphology	3	This has been shown to greatly influence the efficiency of photocatalysts [206].
	Resistance to photo corrosion	2	High resistance to photo corrosion is desirable as photo corrosion can lead to a reduction in performance over time.
Environmental impact	Toxicity	3	A toxic material is detrimental to the environment, it can also result in higher costs for disposal at the end of the product's life.
	Energy requirements for processing raw materials	2	Energy-intensive processing methods can be detrimental to the environment. This is an important consideration for technologies with a wide-scale deployment aim.
	End of life outlook	2	For the technology to be "future-proof" it needs to be sustainable.

	Raw material cost	3	This greatly influences the overall cost of a material. It is also important to consider the likelihood of a significant change in the price of a material.
Cost			
	Production costs	3	High production costs can act as a barrier to wide-scale technology deployment. It is also important to consider if the production costs are likely to reduce when the technology develops further or becomes more mainstream.

At the top of the Justification column (continuing from previous row): "Consequently, the option for recycling or safe disposal is very important."

1824

1825 **Table 7.** Comparison matrix for titanium dioxide and MOFs for photocatalytic applications.

Factor	Weighting	Material Score		Justification
		TiO$_2$	MOFs	
Recombination rate	7	2	4	MOFs have shown reduced recombination rates.
Stability under photocatalytic conditions	8	4	3	Titanium dioxide has shown high stability under photocatalytic conditions [205]. MOFs however, have shown some degradation under these conditions [23].
Level of current development	4	5	4	Titanium dioxide has shown issues with aggregation [206] unlike MOFs.
Resistance to Aggregation	5	1	3	ACs are prone to aggregation and therefore often have to be used as a gel suspension, this often limits the reduction of the device size.
Photocatalytic activity under Visible light	9	1	5	Titanium dioxide's photoactivity is restricted to the UV region of the light spectrum (only 5% of available light) [206]. However, some MOFs have shown photoactivity in an extended region of the spectrum.
Material morphology	7	3	4	MOFs can provide a significantly larger surface area [121]. Furthermore, titanium dioxide is prone to aggregation which reduces its effective surface area [206].
Resistance to photo corrosion	5	3	4	MOFs have shown increased resistance to photo corrosion [206]. Titanium dioxide has mild difficulty with photo corrosion [170].
Performance score:		116	176	
Toxicity	6	5	4	Some MOFs used for this application (such as MILMIL-100(Fe)) are non-toxic [121]. Titanium dioxide is non-toxic [170].
Processing raw materials	6	3	4	The production of both materials is both complex and reasonably energy-intensive. However, due to the novelty of MOFs,

				their production costs remain prohibitively high [206].
End of life outlook	6	2	2	Methods for recycling both materials remain largely unsearched.
Environmental impact score:		60	54	
Raw material costs	17	5	2	Titanium Dioxide is a low-cost material whereas MOFs for this application are high-cost [205].
Processing costs	20	3	3	MOFs have a significantly higher processing cost [191].
Cost score:		145	94	
Overall scores:		341	304	

Note: All materials were evaluated for each factor using a scale ranging from 1 to 5 (where 1 corresponds to "very bad," 2 to "bad," 3 to "suitable," 4 to "good," and 5 to "very good").

5.3   Supercapacitors

Supercapacitors, being next-generation energy storage devices, are assessed based on the metrics of specific capacitance, energy density, power density, and cycling stability. The presence of high specific surface areas and porosity contributes to really good electrochemical performance in metal-organic framework materials such as Cu-MOF, Zr-MOF, and Ti-MOF. For example, Cu-MOF showed a specific capacitance of 104.8 F/g with an energy density of 18.2 Wh/kg, greatly outperforming all other materials because of increased ionic transport and charge storage capabilities [212]. Moreover, Ni-DMOF-ADC gave a specific capacitance of 552 F/g and over 98% retention after 16,000 cycles, indicating its excellent cycling stability. Similarly, $Ni_3(HITP)_2$ tends to be 117 F/g and 90% after 10,000 cycles. For instance, MnOx-MHCF has reached as high as 1200 F/g with 94.7% retention after 10,000 cycles in composite materials, whereas rGO/ZIF-8 has reached 336 F/g with 96% retention [213]. While these methods could enhance the capacity, the poor intrinsic conductivity of pristine MOFs remains a large problem and needs conductive additives or hybridization with conductive materials like graphene and conductive polymers. Although this composite approach has improved the conductivity and overall performance, it adds complexities in synthesis and possible trade-offs in mechanical stability [214]. Therefore, innovation in design and optimization of electrode

1846 materials remains the key to unlocking the full potential of supercapacitors so that high power

1847 and long-life energy storage applications are fully satisfied.

1848

1849 However, the complex and rather pricey synthesis processes of MOFs, combined with the fact

1850 that long-term stability and durability under real conditions is still a topic of research, representt

1851 major handicaps. On the other hand, non-MOF materials are normally much more stable and

1852 less expensive but do not offer such high tunability and selectivity as MOFs do. For overall

1853 performance, MOFs score 173, while activated carbon scores 126. The supercapacitors could

1854 therefore have evaluation parameters that are weighted at 40/100 for performance, 15/100 for

1855 environmental impact, and 45/100 for cost implications. Parameters for performance include

1856 those for cyclic stability, capacitance, energy and power densities; parameters in environmental

1857 impact include the stability of the materials and their impact on the environment; those in cost

1858 implication involve the complexity of the methods of synthesis and expenses incurred. The

1859 evaluation criteria for supercapacitors are summarized in **Table 8**, while **Table 9** presents the

1860 comparison matrix between AC and MOFs as electrodes of supercapacitors.

1861
1862 **Table 8.** Supercapacitor factors and corresponding suggested weighting along with
1863 justifications.

Subject	Factor	Weighting	Justification
	Cycle life	3	The electrode's lifespan is very important as it affects which applications the electrode can be used for as well as the level of performance over its lifespan [74].
	Capacitance	3	A poor capacitance can limit an SC's potential applications. A high capacitance is desirable.
	Current successful application	2	Successful laboratory results or real-world trials are good indications of the material's suitability.
	Size and weight	2	Literature suggests that for most applications, weight and size are not a key consideration, as the systems
Performance			they would be used in are already

			very large and packaging space will likely not be an issue [80].
	Integrity under service conditions (e.g. thermal stability)	3	This is important as it affects the lifespan of the electrode as well as its performance (including issues with charge leakage) and overall suitability for this application [119].
	Energy and power densities	3	High energy and power densities are desirable for SCs. High power density would optimise their charging speeds and therefore make the SC an attractive option for electric vehicle charging equipment. A high energy density would increase the number of potential applications of the SC (as it would be able to hold more energy).
Environmental impact	Raw material renewability	3	For the technology to be "future-proof" it needs to be environmentally sustainable. A renewable raw material is desirable as it means the raw material cost is less likely to increase in the future (unlike non-renewable finite resources)
	Toxicity	3	A toxic material is detrimental to the environment, it can also result in higher costs for disposal at the end of the product's life.
	Recyclability	2	For the technology to be "future-proof" it needs to be sustainable.
	Production impacts (e.g. energy use)	2	Energy-intensive processing methods can be detrimental to the environment. This is an important consideration for technologies with a wide-scale deployment aim.
Cost	Material cost	3	Manufacturers want to keep costs low even at the expense of performance. Literature suggests that price is one of the key factors for the material choice of SC electrodes [80].
	Ease of production/ production cost	2	Simple, low-energy production processes are often cheaper. If the production method can be used for bulk production, it also means the cost of the product is likely going to be lower.

1864

1865 **Table 9.** Comparison matrix for AC and MOFs as SC electrodes.

| Factor	Weighting	Material Score		Justification
		Activated carbon	MOFs	
Cycle life	8	3	4	MOFs have exhibited higher cyclic stabilities in both beakers and constructed SC laboratory tests [75]. ACs have shown suitable performances for this application [80].
Capacitance	9	3	5	Secondary data suggests that MOFs are able to achieve higher values for capacitance compared to ACs [106].
Current successful application	6	4	3	ACs have proven to be successful and are currently used by electrode manufacturers [80]. While MOFs have shown success in laboratory tests, there have been not extensive real-life application trials.
Size and weight	7	3	4	ACs are prone to aggregation and therefore often have to be used as a gel suspension, this often limits the reduction of the device size.
Energy and power densities	10	3	5	AC electrodes have shown limited power output due to the device's charge delivery rate [84]. Laboratory testing of MOFs has shown improved power densities [119].
Performance score:		126	173	
Raw material renewability	3	4	3	While ACs can be produced from renewable sources, the majority of commercially available ACs are produced from non-renewable precursors [79]. Many MOFs used for this application involved non-renewable materials for their synthesis [75].
Non-toxicity	4	5	3	ACs are environmentally benign [204]. The toxicity of MOFs is not well understood and there is some suggestion that some may be toxic, especially when they begin to degrade [125].
Recyclability	5	4	3	AC electrodes show great recycling potential, with research suggesting processes and promising results from laboratory tests [97]. While there is little research available on the recycling of MOF SC electrodes, there is research focused on the synthesis of MOFs using waste PET plastics [113].
Production impacts (e.g. energy use)	3	3	4	AC Production is simple and chemical activation requires relatively little energy [80]. It is important to note that bulk production of MOFs is largely unresearched and consequently an accurate assessment of this factor is difficult.
Environmental impact score:		61	48	
Material cost	35	4	2	AC is very cheap [80]. MOFs are prohibitively expensive [74].

Ease of production/ production cost	10	5	4	ACs production process is well-developed and relatively inexpensive [80]. Bulk production of MOFs requires further research as the process is often complex and expensive [74].
Cost score:		190	110	
Overall scores:		383	350	

1866 **Note:** All materials were evaluated for each factor using a scale ranging from 1 to 5 (where 1
1867 corresponds to "very bad," 2 to "bad," 3 to "suitable," 4 to "good," and 5 to "very good").

1868

1869 Overall, MOFs score higher than liquid amines for CCS applications despite their poor cost

1870 score (52 compared to 60 for liquid amines) and the high weighting assigned to cost factors. As

1871 the radar graph (**Fig. 10(a)**) shows, the MOFs score considerably better for environmental

1872 impact due to liquid-amines toxicity and environmental harmfulness. Notwithstanding their

1873 relatively modest stage of development, MOFs have a high-performance grade because they

1874 also have the potential to provide considerable performance improvements over liquid amines.

1875 According to the graph, MOFs' performance score gives them the greatest advantage over liquid

1876 amines. In contrast, ACs receive a slightly better rating for SC electrode applications than

1877 MOFs. However, the radar graph (**Fig. 10(b)**) shows that MOFs score considerably better for

1878 performance and their score for environmental impact is only slightly less than that of AC. It is

1879 apparent from **Fig. 10** that this evaluation suggests that the factor preventing the wide-scale use

1880 of MOF electrodes is cost. Literature suggests that the incredibly low price of AC is acting as

1881 a barrier to the entrance of any other material to the SC electrode market [80], despite the potential

1882 for improved performance. Consequently, further research into the cost-effective synthesis of

1883 MOF electrodes may be beneficial. Regarding photocatalytic application, titanium dioxide

1884 achieved the highest overall score, suggesting that, based on these factors, it provides the most

1885 benefits despite MOFs achieving a considerably higher performance score of 70 (as seen in **Fig.**

1886 **10(c)**). Because of the high weighting of the cost elements, MOFs' cost score was significantly

1887 lower than titanium dioxide's, which is probably what prevents MOFs from being used in this

1888 application. In summary, the cost of MOFs can vary considerably, influenced by factors such

1889 as the specific MOF material, the synthesis method, the production scale, and the purity of the

1890 final product. It's important to note that while some MOFs may be relatively expensive to

1891 produce, they can offer unique properties and advantages in various applications, which can

1892 justify their cost in certain contexts. As research and development in MOFs continue to advance,

1893 there may be efforts to optimize synthesis methods and reduce production costs, making MOFs

1894 more accessible for a broader range of applications.

1895
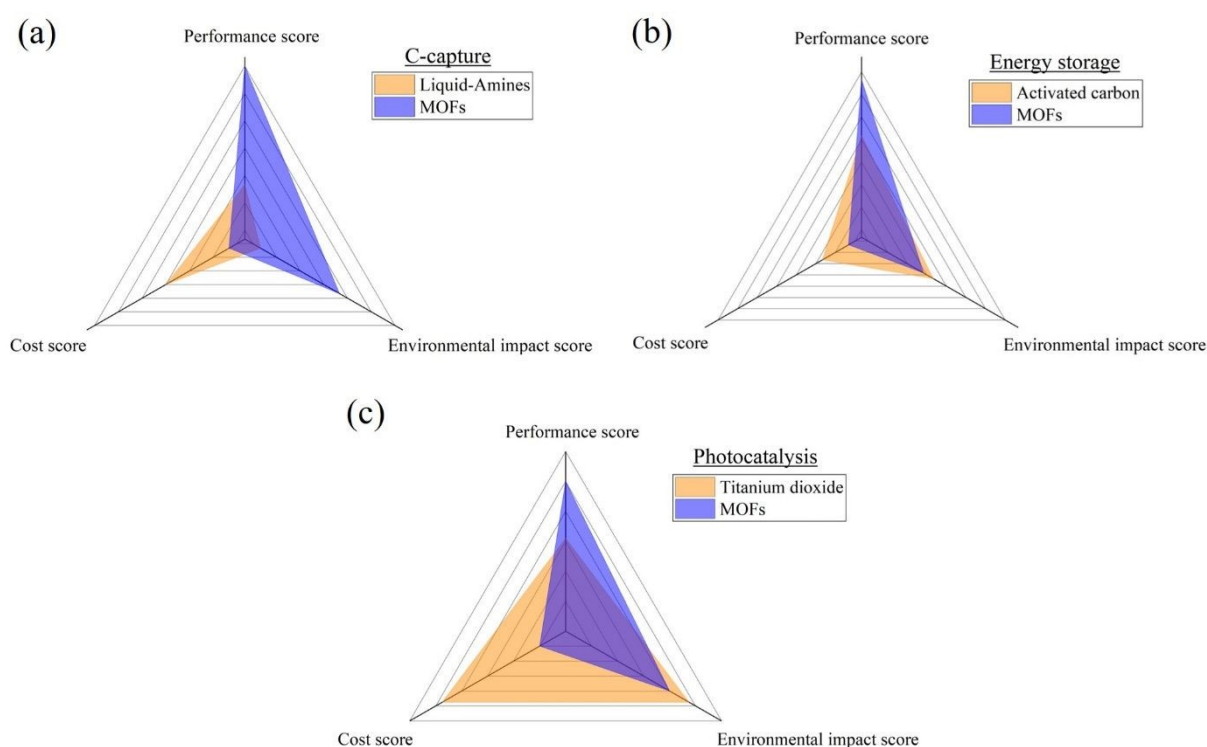
1896
1897 **Fig. 10.** Radar graph showing 3 factor comparison between MOFs and other conventional
1898 materials for; (a) C-capture, (b) Energy storage, and (c) Photocatalysis applications.
1899

1900 ## 6. Limitations and future research directions

1901 ### 6.1 Current MOF technologies

1902 Probably the most stressed limitation of the existing technologies behind MOFs is their poor

1903 thermal stability. The span in the thermal decomposition temperatures (Td) of MOFs is very

1904 large, which is the result of inconsistencies in the experimental conditions that include the

1905 heating rates and atmospheres. As an example, the reported Td values for MOF-5 range from

1906 400 to 500 °C, whereas normally UiO-66 decomposes within the temperature range of 425–

1907 500°C, and HKUST-1 shows Td values between 250–300°C. These are some of the factors that

1908 influence the nature and location of functional groups, the hardness of metal ions, and

1909 coordinated solvent molecules [215]. MOFs with harder metal ions, such as lithium-based UL-

1910 MOF-1, showed the highest stability with Td values as high as about 600 °C due to an increased

1911 ionic character of the metal-oxygen bonds compared to Zn or Zr-based MOFs. For example,

1912 Mg-MOF-74 has extremely high thermal stability with a Td of ca. 400°C under nitrogen

1913 atmosphere [215].

1914

1915 Another large problem is their chemical stability, which is easily influenced by moisture and,

1916 therefore, significantly limits their usability for industrial processes. Many MOFs have been

1917 reported to decompose above 300 °C or under humid conditions, which thus bounds their

1918 practical applications. Their syntheses are often complicated, requiring pricey reagents; large-

1919 scale production is economically challenging. For instance, the price for the production of

1920 MOFs can be as high as $50 per gram, which is very expensive compared with conventional

1921 porous materials like activated carbon with a price of around $1 per kilogram [216]. Moreover,

1922 while some MOFs have very high methane storage capacities, for example, HKUST-1,

1923 impurities can reduce their actual performance by a large extent, significantly diminishing real

1924 application.

1925

1926 Another challenge is that it is somehow difficult to scale up the production of MOFs

1927 sustainably. Traditional methods of synthesis typically utilize highly toxic solvents under harsh

1928 conditions, therefore posing associated environmental and health risks, but usually at high

1929 production costs. With more than 99,075 synthetic variants, the enormous number of possible

1930 MOF structures makes it challenging and cumbersome to identify and optimize MOFs for a

1931 given application with certain desired properties. This leads to long experimental cycles and a

1932 high R&D cost [217]. Even for very promising materials like CALF-20 and MIL-100(Fe), multi-

1933 ton scale syntheses were achieved only recently, which clearly shows the slow transformation

1934 from lab scale to industrial scale production [218]. This is further frustrated by raw material costs

1935 and synthesis processes, which themselves are costly, often using highly toxic solvents like

1936 DMF that add to the cost and energy requirement of purification methods necessary to maintain

1937 the quality of the MOF product.

6.2 Future research directions

1938

1939 Future research in MOF technologies has to be directed toward the enhancement of stability,

1940 precise characterization of catalytic sites, effective regeneration techniques, and controlled

1941 defect engineering. Current MOFs typically show stability up to 300 °C, but future

1942 developments must take it further beyond 500°C through the incorporation of more thermally

1943 stable inorganic components and improvement of the node-linker bonds [219]. Improvement in

1944 chemical stability to less than 10% degradation in catalytic activity over 100 hours in an

1945 aqueous environment must also be attained. Advanced spectroscopic techniques and

1946 computational modelling shall quantify active catalytic sites with an error margin of less than

1947 5% and predict reaction rates to within 10% accuracy of the experimental values. Effective

1948 regeneration protocols restore at least 90% of the original catalytic activity upon deactivation

1949 cycles; long-term studies. This type of controlled defect synthesis thus should give a standard

1950 deviation of less than 10% in defect concentration from batch to batch, while for defect-free

1951 MOFs it has to be below 1% of total sites [219].

1952

1953 One major challenge lies in the naturally very low ionic conductivity of most MOFs, typically

1954 much below the level of 10^{-10} S/cm. Nearly liquid electrolyte conductivities are hard to attain

1955 with solid electrolytes because of the limited carrier mobility and lack of low-energy pathways

1956   for ionic conduction [220]. Future efforts, therefore, need to build on these limitations and focus

1957   on strategies that involve improved density of mobile ions and uninterrupted ionic conduction

1958   pathways. Additionally, it requires the development of MOFs with stable and high ionic

1959   conductivities toward changes in both temperature and humidity. Advancement in synthesis

1960   and functionalization approaches with the design of corresponding theoretical models is highly

1961   imperative for bringing solutions to the above challenges. The inclusion of flexible frameworks

1962   and phase transition mechanisms may yield MOFs with conductivities above 10^{-2} S/cm and

1963   may thus render them applicable in the new class of the next-generation energy storage and

1964   conversion devices [220].

1965

1966   Critical is the reduction in the number of steps involved in the synthesis process to reduce

1967   production costs to less than $10 per gram. This can be realized by developing more efficient

1968   and up-scaled synthesis methods where applicability is maximally enhanced, such as solvent-

1969   free synthesis or the adoption of cheaper and more abundant raw materials [221]. In the future,

1970   research should also focus on green synthesis methods with non-toxic, biocompatible linking

1971   agents and eco-friendly solvents, along with techniques that apply either no use of solvents at

1972   all or solid-state synthesis. High-throughput computation screening and data mining will greatly

1973   accelerate the assessment of MOF properties to find promising candidates more efficiently [222].

1974   Separation and recovery processes relating to vacuum filtration and continuous centrifugation,

1975   for example, need to be optimized in the scale-up of production. It may potentially also provide

1976   more sustainable and cost-effective solutions with respect to reduced energy use and

1977   improvement in scalability [223]. This could provide more sustainable and cost-effective solutions

1978   due to less energy consumption and efficient scaling of microwave-assisted and

1979   mechanochemical synthesis methods.

1980

1981 It is with strategies in creative structural modification and composite material preparation that

1982 finally, such MOF materials could be fabricated with enhanced stability and durability to real-

1983 world working conditions. Comprehensive techno-economic analyses and life cycle assessment

1984 (LCA) are required concerning an evaluation of the feasibility and environmental impact of

1985 large-scale production of MOFs [224]. These assessments will set targets for the development of

1986 green and sustainable economically viable MOF technologies whose industrial applications

1987 would not contradict their environmental benefits. By taking into consideration these points,

1988 there will be a chance for the synthesization of MOFs with improved thermal and chemical

1989 stability, reduced production cost, increased scalability, and finally making them practical in

1990 much more extended temperature range applications and industrial uses [225].

7. Conclusion

1992 In conclusion, this study provides a comprehensive comparative assessment of Metal-Organic

1993 Frameworks (MOFs) and conventional materials across the domains of energy storage,

1994 environmental remediation, and photocatalysis. The results underscore the remarkable potential

1995 of MOFs as versatile and innovative materials in these critical areas, backed by empirical data.

1996 In energy storage, MOFs consistently outperform conventional activated carbons (ACs) with a

1997 performance score of 128, significantly surpassing them. Their exceptional specific surface

1998 areas, often exceeding 3,000 m²/g, enable efficient charge adsorption, rapid charge transfer, and

1999 easy ion diffusion within their porous structures. These characteristics, along with their

2000 chemical, thermal, and mechanical stability, and the ability to be hybridized with conductive

2001 materials, position MOFs as promising contenders for advanced energy storage devices like

2002 supercapacitors. Regarding environmental concerns, MOFs excel as effective carbon capture

2003 agents, scoring 329 compared to 275 for liquid amines. Exposed surface areas and high pore

2004 volumes further increase their potential for the adsorption capacity toward pollutants.

2005 Additionally, besides the presence of functional groups that act specifically toward interactions

2006 with the contaminants, the stability under environmental conditions and recyclability underline

2007 their effectiveness for environmental clean-up and, therefore, in the promotion of

2008 environmental sustainability. In the field of photocatalysis, MOFs exhibit substantial potential

2009 with a total score of 304. They showcase extended light harvesting capabilities into the visible

2010 and near-infrared regions due to their tunable bandgap, allowing for effective utilization of

2011 visible light. They have high surface areas that offer high active sites, while the mechanisms of

2012 charge separation do provide a platform for the prevention of recombination of electron-hole

2013 pairs, therefore enhancing the catalytic activity. Moreover, their photochemical stability and

2014 surface functionalization further enhance their applicability as efficient photocatalysts.

2015 However, it's crucial to acknowledge the cost challenges faced by MOFs, with an overall cost

2016 score of 110 for supercapacitors and 94 for photocatalysis. High production costs due to

2017 complex synthesis processes can act as barriers to widespread technology deployment in these

2018 domains. Some challenges, however, remain, such as stability issues, conductivity, and very

2019 high production costs. It is a problem of stability and poor electrical conductivity that hampers

2020 their potency in energy storage and photocatalysis. Future research should focus on the

2021 development of MOF structures with improved stability and conductivity, integration of MOFs

2022 with other materials to enhance their performance, and expansion of their applications in

2023 environmental remediation. This would have to be supplemented by enhanced environmental

2024 adaptability, low-toxicity development of variants to avoid secondary pollution and a deeper

2025 study of the pathways and kinetics of charge transfer. Computation design of more effective

2026 photocatalysts is probably going to provide the answer. Hence, these issues will be resolved

2027 through focused research and innovative solutions for MOFs to achieve their full potential. This

2028 empirical data underscores MOFs' promising future in energy storage, environmental

2029 remediation, and photocatalysis, showcasing their adaptability and high performance. As the

2030   world seeks sustainable technologies, MOFs emerge as pivotal materials, paving the way for a

2031   more eco-conscious future.

2032   ## Acknowledgement

2038

Reference

1 A. Maghfirah, M. M. Ilmi, A. T. N. Fajar and G. T. M. Kadja, *Mater Today Chem*, 2020, **17**, 100348.

2 A. El Guerraf, W. Zeng, A. Mantel, E. Benhsina, J. M. Chin and H. Shiozawa, *Adv Electron Mater*, 2024, 2300854.

3 M. Ding, X. Cai and H.-L. Jiang, *Chem Sci*, 2019, **10**, 10209–10230.

4 H. C. J. Zhou and S. Kitagawa, *Chem Soc Rev*, 2014, 43, 5415–5418.

5 S. Akhtar, P. Singha, A. De, K. S. Das, S. Saha, S. Bala and R. Mondal, *New Journal of Chemistry*, 2021, **45**, 6438–6449.

6 L. R. Redfern and O. K. Farha, *Chem Sci*, 2019, **10**, 10666–10679.

7 C. Yue, L. Wu, Y. Lin, Y. Lu, C. Shang, R. Ma, X. Zhang, X. Wang, W. D. Wu and X. D. Chen, *ACS Appl Mater Interfaces*, 2021, **13**, 26264–26277.

8 R. Shah, S. Ali, F. Raziq, S. Ali, P. M. Ismail, S. Shah, R. Iqbal, X. Wu, W. He and X. Zu, *Coord Chem Rev*, 2023, **477**, 214968.

9 G. Song, Y. Shi, S. Jiang and H. Pang, *Adv Funct Mater*, 2023, **33**, 2303121.

10 N. F. Suremann, B. D. McCarthy, W. Gschwind, A. Kumar, B. A. Johnson, L. Hammarström and S. Ott, *Chem Rev*, 2023, **123**, 6545–6611.

11 J. Chen and Y. Li, *The Chemical Record*, 2016, **16**, 1456–1476.

12 M. U. Shahid, T. Najam, M. H. Helal, I. Hossain, S. M. El-Bahy, Z. M. El-Bahy, A. ur Rehman, S. S. A. Shah and M. A. Nazir, *Int J Hydrogen Energy*, 2024, **62**, 1113–1138.

13 T. Wu, X. Liu, Y. Liu, M. Cheng, Z. Liu, G. Zeng, B. Shao, Q. Liang, W. Zhang, Q. He and W. Zhang, *Coord Chem Rev*, 2020, **403**, 213097.

14 N. C. Burtch, J. Heinen, T. D. Bennett, D. Dubbeldam and M. D. Allendorf, *Advanced materials*, 2018, **30**, 1704124.

15 D. Senthil Raja and D.-H. Tsai, *Chemical Communications*, 2024.

16 C. Lamiel, I. Hussain, H. Rabiee, O. R. Ogunsakin and K. Zhang, *Coord Chem Rev*, 2023, **480**, 215030.

17 L. Zhang and Y. Hou, *Adv Energy Mater*, 2023, **13**, 2204378.

18 A. Mukherjee, J. A. Okolie, A. Abdelrasoul, C. Niu and A. K. Dalai, *Journal of Environmental Sciences*, 2019, **83**, 46–63.

19 S. Ghosh, *Metal-organic frameworks (MOFs) for environmental applications*, 2019.

20 S. Horike, S. Shimomura and S. Kitagawa, *Nat Chem*, 2009, **1**, 695–704.

2071 21   T. Ghanbari, F. Abnisa and W. M. A. Wan Daud, *Science of The Total Environment*,

2072   2020, **707**, 135090.

2073 22   Y. Zhao, Z. Song, X. Li, Q. Sun, N. Cheng, S. Lawes and X. Sun, *Energy Storage Mater*,

2074   2016, **2**, 35–62.

2075 23   Y. Li, H. Xu, S. Ouyang and J. Ye, *Physical Chemistry Chemical Physics*, 2016, **18**,

2076   7563–7572.

2077 24   H. Furukawa, K. E. Cordova, M. O'Keeffe and O. M. Yaghi, *Science (1979)*, ,

2078   DOI:10.1126/science.1230444.

2079 25   F. Vega, M. Cano, S. Camino, L. M. G. Fernández, E. Portillo and B. Navarrete, *Carbon*

2080   *Dioxide Chemistry, Capture and Oil Recovery*, , DOI:10.5772/INTECHOPEN.71443.

2081 26   M. Bui, C. S. Adjiman, A. Bardow, E. J. Anthony, A. Boston, S. Brown, P. S. Fennell,

2082   S. Fuss, A. Galindo, L. A. Hackett, J. P. Hallett, H. J. Herzog, G. Jackson, J. Kemper, S.

2083   Krevor, G. C. Maitland, M. Matuszewski, I. S. Metcalfe, C. Petit, G. Puxty, J. Reimer,

2084   D. M. Reiner, E. S. Rubin, S. A. Scott, N. Shah, B. Smit, J. P. M. Trusler, P. Webley, J.

2085   Wilcox and N. Mac Dowell, *Energy Environ Sci*, 2018, **11**, 1062–1176.

2086 27   J. J. Vericella, S. E. Baker, J. K. Stolaroff, E. B. Duoss, J. O. Hardin, J. Lewicki, E.

2087   Glogowski, W. C. Floyd, C. A. Valdez, W. L. Smith, J. H. Satcher, W. L. Bourcier, C.

2088   M. Spadaccini, J. A. Lewis and R. D. Aines, *Nat Commun*, 2015, **6**, 6124.

2089 28   A. I. Osman, M. Hefny, M. I. A. Abdel Maksoud, A. M. Elgarahy and D. W. Rooney,

2090   *Environ Chem Lett*, 2021, **19**, 797–849.

2091 29   X. Li, X. Zhou, J. Wei, Y. Fan, L. Liao and H. Wang, *Sep Purif Technol*, 2021, **265**,

2092   118481.

2093 30   M. Stec, A. Tatarczuk, L. Więcław-Solny, A. Krótki, T. Spietz, A. Wilk and D. Śpiewak,

2094   *Clean Technol Environ Policy*, 2016, **18**, 151–160.

2095 31   C. A. Grande, R. Blom, A. Spjelkavik, V. Moreau and J. Payet, *Sustainable Materials*

2096   *and Technologies*, 2017, **14**, 11–18.

2097 32   Z. Zhang, Z.-Z. Yao, S. Xiang and B. Chen, *Energy Environ Sci*, 2014, **7**, 2868.

2098 33   N. Williams, R. C.-C. C. Journal and undefined 2019, *osti.govNJ Williams, R*

2099   *CustelceanCarbon Capture Journal, 2019•osti.gov*.

2100 34   Energy technologies Institute, *Reducing the cost of CCS developments in capture plant*

2101   *technology*, 2016.

2102 35   S. Budinis, S. Krevor, N. Mac Dowell, N. Brandon and A. Hawkes, *Energy Strategy*

2103   *Reviews*, 2018, **22**, 61–81.

Journal of Materials Chemistry A Accepted Manuscript

2104   36   A. Andersen, S. Divekar, S. Dasgupta, J. H. Cavka, Aarti, A. Nanoti, A. Spjelkavik,
2105   N. Goswami, M. O. Garg and R. Blom, *Energy Procedia*, 2013, **37**, 33–39.

2106   37   B. L. Huang, Z. Ni, A. Millward, A. J. H. McGaughey, C. Uher, M. Kaviany and O.
2107   Yaghi, *Int J Heat Mass Transf*, 2007, **50**, 405–411.

2108   38   N. Iqbal, X. Wang, J. Yu and B. Ding, *Adv Sustain Syst*, 2017, **1**, 1600028.

2109   39   Y. Lin, C. Kong, Q. Zhang and L. Chen, *Adv Energy Mater*, 2017, **7**, 1601296.

2110   40   H. R. Khan, Z. Jahan, M. B. Khan Niazi, T. Noor, H. Hou and S. Rafiq, *Carbon Capture*
2111   *Science & Technology*, 2022, **3**, 100048.

2112   41   P. M. Bhatt, Y. Belmabkhout, A. Cadiau, K. Adil, O. Shekhah, A. Shkurenko, L. J.
2113   Barbour and M. Eddaoudi, *J Am Chem Soc*, 2016, **138**, 9301–9307.

2114   42   L. Hu, W. Wu, L. Jiang, M. Hu, H. Zhu, L. Gong, J. Yang, D. Lin and K. Yang, *ACS*
2115   *Appl Mater Interfaces*, 2023, **15**, 43925–43932.

2116   43   G. Greene-Diniz, D. Z. Manrique, W. Sennane, Y. Magnin, E. Shishenina, P. Cordier, P.
2117   Llewellyn, M. Krompiec, M. J. Rančić and D. Muñoz Ramo, *EPJ Quantum Technol*,
2118   2022, **9**, 37.

2119   44   T. Zurrer, K. Wong, J. Horlyck, E. C. Lovell, J. Wright, N. M. Bedford, Z. Han, K. Liang,
2120   J. Scott and R. Amal, *Adv Funct Mater*, , DOI:10.1002/adfm.202007624.

2121   45   A. S. Palakkal and R. S. Pillai, *Sep Purif Technol*, 2022, **295**, 121298.

2122   46   L. Lei, Y. Cheng, C. Chen, M. Kosari, Z. Jiang and C. He, *J Colloid Interface Sci*, 2022,
2123   **612**, 132–145.

2124   47   H. An, W. Tian, X. Lu, H. Yuan, L. Yang, H. Zhang, H. Shen and H. Bai, *Chemical*
2125   *Engineering Journal*, 2023, **469**, 144052.

2126   48   T.-H. Bae, M. R. Hudson, J. A. Mason, W. L. Queen, J. J. Dutton, K. Sumida, K. J.
2127   Micklash, S. S. Kaye, C. M. Brown and J. R. Long, *Energy Environ. Sci.*, 2013, **6**, 128–
2128   138.

2129   49   D. Bahamon and L. F. Vega, *Chemical Engineering Journal*, 2016, **284**, 438–447.

2130   50   H. Li, K. Wang, Y. Sun, C. T. Lollar, J. Li and H.-C. Zhou, *Materials Today*, 2018, **21**,
2131   108–121.

2132   51   Y. He, W. Zhou, G. Qian and B. Chen, *Chem. Soc. Rev.*, 2014, **43**, 5657–5678.

2133   52   E. J. Kim, R. L. Siegelman, H. Z. H. Jiang, A. C. Forse, J.-H. Lee, J. D. Martell, P. J.
2134   Milner, J. M. Falkowski, J. B. Neaton, J. A. Reimer, S. C. Weston and J. R. Long, *Science*
2135   *(1979)*, 2020, **369**, 392–396.

2136   53   T. M. McDonald, J. A. Mason, X. Kong, E. D. Bloch, D. Gygi, A. Dani, V. Crocellà, F.
2137   Giordanino, S. O. Odoh, W. S. Drisdell, B. Vlaisavljevich, A. L. Dzubak, R. Poloni, S.

K. Schnell, N. Planas, K. Lee, T. Pascal, L. F. Wan, D. Prendergast, J. B. Neaton, B. Smit, J. B. Kortright, L. Gagliardi, S. Bordiga, J. A. Reimer and J. R. Long, *Nature*, 2015, **519**, 303–308.

54 Y. Huang, W. Qin, Z. Li and Y. Li, *Dalton Transactions*, 2012, **41**, 9283.

55 T. M. McDonald, W. R. Lee, J. A. Mason, B. M. Wiers, C. S. Hong and J. R. Long, *J Am Chem Soc*, 2012, **134**, 7056–7065.

56 P.-Q. Liao, X.-W. Chen, S.-Y. Liu, X.-Y. Li, Y.-T. Xu, M. Tang, Z. Rui, H. Ji, J.-P. Zhang and X.-M. Chen, *Chem Sci*, 2016, **7**, 6528–6533.

57 D. Saha, Z. Bao, F. Jia and S. Deng, *Environ Sci Technol*, 2010, **44**, 1820–1826.

58 M. Mazaj, N. Z. Logar, E. Žagar and S. Kovačič, *J Mater Chem A Mater*, 2017, **5**, 1967–1971.

59 J. Liu, Y. Wang, A. I. Benin, P. Jakubczak, R. R. Willis and M. D. LeVan, *Langmuir*, 2010, **26**, 14301–14307.

60 G. W. Peterson, J. B. DeCoste, T. G. Glover, Y. Huang, H. Jasuja and K. S. Walton, *Microporous and Mesoporous Materials*, 2013, **179**, 48–53.

61 T. Asadi, M. R. Ehsani, A. M. Ribeiro, J. M. Loureiro and A. E. Rodrigues, *Chem Eng Technol*, 2013, **36**, 1231–1239.

62 Z. Hu, Y. Wang, B. B. Shah and D. Zhao, *Adv Sustain Syst*, , DOI:10.1002/adsu.201800080.

63 P. J. Milner, R. L. Siegelman, A. C. Forse, M. I. Gonzalez, T. Runčevski, J. D. Martell, J. A. Reimer and J. R. Long, *J Am Chem Soc*, 2017, **139**, 13541–13553.

64 V. H. Dalvi and P. J. Rossky, *Proceedings of the National Academy of Sciences*, 2010, **107**, 13603–13607.

65 A. H. Valekar, K.-H. Cho, U.-H. Lee, J. S. Lee, J. W. Yoon, Y. K. Hwang, S. G. Lee, S. J. Cho and J.-S. Chang, *RSC Adv*, 2017, **7**, 55767–55777.

66 R. Das, D. Muthukumar, R. S. Pillai and C. M. Nagaraja, *Chemistry – A European Journal*, 2020, **26**, 17445–17454.

67 J. Yan, Y. Sun, T. Ji, Y. Liu, N. Zhang, B. Sun, S. Meng, B. H. Yin, M. Wu, H. Hu and Y. Liu, *Ind Eng Chem Res*, 2023, **62**, 5973–5983.

68 M. R. Abdul Hamid, Y. Qian, R. Wei, Z. Li, Y. Pan, Z. Lai and H.-K. Jeong, *J Memb Sci*, 2021, **640**, 119802.

69 F. Yang, T. Ge, X. Zhu, J. Wu and R. Wang, *Sep Purif Technol*, 2022, **287**, 120535.

70 J. M. Park, D. K. Yoo and S. H. Jhung, *Chemical Engineering Journal*, 2020, **402**, 126254.

2172   71   Y. Liu, Z. Ng, E. A. Khan, H.-K. Jeong, C. Ching and Z. Lai, *Microporous and*

2173   *Mesoporous Materials*, 2009, **118**, 296–301.

2174   72   C. R. Groom, I. J. Bruno, M. P. Lightfoot and S. C. Ward, *Acta Crystallogr B Struct Sci*

2175   *Cryst Eng Mater*, 2016, **72**, 171–179.

2176   73   S. Huang, X.-R. Shi, C. Sun, Z. Duan, P. Ma and S. Xu, *Nanomaterials*, 2020, **10**, 2268.

2177   74   S. Sundriyal, H. Kaur, S. K. Bhardwaj, S. Mishra, K.-H. Kim and A. Deep, *Coord Chem*

2178   *Rev*, 2018, **369**, 15–38.

2179   75   P. Forouzandeh, V. Kumaravel and S. C. Pillai, *Catalysts*, 2020, **10**, 969.

2180   76   A. C. Forse, C. Merlet, J. M. Griffin and C. P. Grey, *J Am Chem Soc*, 2016, **138**, 5731–

2181   5744.

2182   77   Y. Wu and C. Cao, *Sci China Mater*, 2018, **61**, 1517–1526.

2183   78   S. Kumar, G. Saeed, L. Zhu, K. N. Hui, N. H. Kim and J. H. Lee, *Chemical Engineering*

2184   *Journal*, 2021, **403**, 126352.

2185   79   J. Phiri, J. Dou, T. Vuorinen, P. A. C. Gane and T. C. Maloney, *ACS Omega*, 2019, **4**,

2186   18108–18117.

2187   80   L. Weinstein and R. Dash, *Materials Today*, 2013, **16**, 356–357.

2188   81   P. Pongprayoon and A. Chaimanatsakun, *Acta Mechanica Solida Sinica*, 2019, **32**, 81–

2189   92.

2190   82   A. Gitipour, A. El Badawy, M. Arambewela, B. Miller, K. Scheckel, M. Elk, H. Ryu, V.

2191   Gomez-Alvarez, J. Santo Domingo, S. Thiel and T. Tolaymat, *Environ Sci Technol*,

2192   2013, **47**, 14385–14393.

2193   83   L. Li, X. Wang, S. Wang, Z. Cao, Z. Wu, H. Wang, Y. Gao and J. Liu, *Electroanalysis*,

2194   2016, **28**, 243–248.

2195   84   M. Cossutta, V. Vretenar, T. A. Centeno, P. Kotrusz, J. McKechnie and S. J. Pickering,

2196   *J Clean Prod*, 2020, **242**, 118468.

2197   85   K. M. Ajay and M. N. Dinesh, *IOP Conf Ser Mater Sci Eng*, 2018, **310**, 012083.

2198   86   M. Karnan, A. G. K. Raj, K. Subramani, S. Santhoshkumar and M. Sathish, *Sustain*

2199   *Energy Fuels*, 2020, **4**, 3029–3041.

2200   87   S. Breitenbach, A. Lumetzberger, M. A. Hobisch, C. Unterweger, S. Spirk, D. Stifter, C.

2201   Fürst and A. W. Hassel, *C — Journal of Carbon Research*, 2020, **6**, 17.

2202   88   A. Arenillas, J. A. Menéndez, G. Reichenauer, A. Celzard, V. Fierro, F. J. Maldonado

2203   Hodar, E. Bailón-Garcia and N. Job, 2019, pp. 1–26.

2204   89   Z. S. Iro, C. Subramani and S. S. Dash, *Int J Electrochem Sci*, 2016, **11**, 10628–10643.

View Article Online
DOI:10.1039/D4TA03877K

2205 90 I. I. G. Inal, S. M. Holmes, E. Yagmur, N. Ermumcu, A. Banford and Z. Aktas, *Journal*
2206 *of industrial and engineering chemistry*, 2018, **61**, 124–132.

2207 91 J. Chen, J. Xie, C. Q. Jia, C. Song, J. Hu and H. Li, *Chemical Engineering Journal*, 2022,
2208 **450**, 137938.

2209 92 X. Li, Y. Tang, J. Song, W. Yang, M. Wang, C. Zhu, W. Zhao, J. Zheng and Y. Lin,
2210 *Carbon N Y*, 2018, **129**, 236–244.

2211 93 F. Ma, S. Ding, H. Ren and Y. Liu, *RSC Adv*, 2019, **9**, 2474–2483.

2212 94 R. Mehdi, S. R. Naqvi, A. H. Khoja and R. Hussain, *Fuel*, 2023, **348**, 128529.

2213 95 S. Bhat, U. T. Uthappa, T. Sadhasivam, T. Altalhi, S. Soo Han and M. D. Kurkuri,
2214 *Chemical Engineering Journal*, 2023, **459**, 141577.

2215 96 Y.-P. Gao, Z.-B. Zhai, K.-J. Huang and Y.-Y. Zhang, *New Journal of Chemistry*, 2017,
2216 **41**, 11456–11470.

2217 97 G. Jiang and S. J. Pickering, *Waste Management*, 2016, **48**, 465–470.

2218 98 Q. Ke and J. Wang, *Journal of Materiomics*, 2016, **2**, 37–54.

2219 99 V. Ntuli, I. H.-S. A. J. of Science and undefined 2013, *journals.co.zaV Ntuli, I*
2220 *HapazariSouth African Journal of Science, 2013•journals.co.za*, ,
2221 DOI:10.1590/sajs.2013/1077.

2222 100 E. Glogic, A. K. Kamali, N. M. Keppetipola, B. Alonge, G. R. A. Kumara, G.
2223 Sonnemann, T. Toupance and L. Cojocaru, *ACS Sustain Chem Eng*, 2022, **10**, 15025–
2224 15034.

2225 101 Z. Jiang, Y. Zou, Y. Li, F. Kong and D. Yang, *Biochar*, 2021, **3**, 701–714.

2226 102 V. Ruiz, C. Blanco, M. Granda and R. Santamaría, *Electrochim Acta*, 2008, **54**, 305–
2227 310.

2228 103 C. Li, W. Wu, P. Wang, W. Zhou, J. Wang, Y. Chen, L. Fu, Y. Zhu, Y. Wu and W.
2229 Huang, *Advanced Science*, 2019, **6**, 1801665.

2230 104 D. Dong and Y. Xiao, *Chemical Engineering Journal*, 2023, 144441.

2231 105 L. M. Grishchenko, G. G. Tsapyuk, M. Ricco, V. E. Diyuk, O. Yu. Boldyrieva, R.
2232 Mariychuk, I. P. Matushko, D. Pontiroli, V. V. Lisnyak and S. Scaravonati, in *2020 IEEE*
2233 *40th International Conference on Electronics and Nanotechnology (ELNANO)*, IEEE,
2234 2020, pp. 173–177.

2235 106 F. Cheng, X. Yang, S. Zhang and W. Lu, *J Power Sources*, 2020, **450**, 227678.

2236 107 L.-H. Tseng, W.-C. Li and T.-C. Wen, *J Taiwan Inst Chem Eng*, 2023, **143**, 104684.

2237 108 G. Dhakal, D. R. Kumar, S. Sahoo and J.-J. Shim, *Carbon N Y*, 2023, **208**, 277–289.

2238 109 I. Bordun, V. Pohrebennyk, M. Sadowa, V. Ptashnyk, A. Klos-Witkowska and V.
2239   Martsenyuk, in *2017 9th IEEE International Conference on Intelligent Data Acquisition*
2240   *and Advanced Computing Systems: Technology and Applications (IDAACS)*, IEEE,
2241   2017, pp. 86–90.

2242 110 F. R. Maria Sundar Raj, N. V. Jaya, G. Boopathi, D. Kalpana and A. Pandurangan, *Mater*
2243   *Chem Phys*, 2020, **240**, 122151.

2244 111 I. I. G. Inal, Y. Gokce and Z. Aktas, in *2016 IEEE International Conference on*
2245   *Renewable Energy Research and Applications (ICRERA)*, IEEE, 2016, pp. 458–462.

2246 112 M. A. Yahya, Z. Al-Qodah and C. W. Z. Ngah, *Renewable and Sustainable Energy*
2247   *Reviews*, 2015, **46**, 218–235.

2248 113 A. M. Al-Enizi, M. Ubaidullah, J. Ahmed, T. Ahamad, T. Ahmad, S. F. Shaikh and Mu.
2249   Naushad, *Compos B Eng*, 2020, **183**, 107655.

2250 114 M. K. Sahoo, P. Mane, B. Chakraborty and J. N. Behera, *Inorg Chem*, 2024, **63**, 6383–
2251   6395.

2252 115 B. Ramasubramanian, C. Chinglenthoiba, X. Huiqing, N. Xiping, H. K. Hui, S.
2253   Valiyaveettil, S. Ramakrishna and V. Chellappan, *Surfaces and Interfaces*, 2022, **34**,
2254   102397.

2255 116 S. Xiong, S. Jiang, J. Wang, H. Lin, M. Lin, S. Weng, S. Liu, Y. Jiao, Y. Xu and J. Chen,
2256   *Electrochim Acta*, 2020, **340**, 135956.

2257 117 M. Shaheen, M. Z. Iqbal, M. W. Khan, S. Siddique, S. Aftab and S. M. Wabaidur, *Energy*
2258   *& Fuels*, 2023, **37**, 4000–4009.

2259 118 F. Yi, R. Zhang, H. Wang, L. Chen, L. Han, H. Jiang and Q. Xu, *Small Methods*, ,
2260   DOI:10.1002/smtd.201700187.

2261 119 M. Gu, M. Wu, S.-C. Wang, C. Chen, D. Xiong and F.-Y. Yi, *Electrochim Acta*, 2020,
2262   **343**, 135617.

2263 120 N. Campagnol, R. Romero-Vara, W. Deleu, L. Stappers, K. Binnemans, D. E. De Vos
2264   and J. Fransaer, *ChemElectroChem*, 2014, **1**, 1182–1188.

2265 121 L. Wang, Y. Han, X. Feng, J. Zhou, P. Qi and B. Wang, *Coord Chem Rev*, 2016, **307**,
2266   361–381.

2267 122 R. Ramachandran, W. Xuan, C. Zhao, X. Leng, D. Sun, D. Luo and F. Wang, *RSC Adv*,
2268   2018, **8**, 3462–3469.

2269 123 D. Y. Lee, S. J. Yoon, N. K. Shrestha, S.-H. Lee, H. Ahn and S.-H. Han, *Microporous*
2270   *and Mesoporous Materials*, 2012, **153**, 163–165.

2271 124 Y. Tan, W. Zhang, Y. Gao, J. Wu and B. Tang, *RSC Adv*, 2015, **5**, 17601–17605.

View Article Online
DOI: 10.1039/D4TA03877K

2272 125   P. Kumar, B. Anand, Y. F. Tsang, K.-H. Kim, S. Khullar and B. Wang, *Environ Res*,

2273   2019, **176**, 108488.

2274 126   Y. Yan, P. Gu, S. Zheng, M. Zheng, H. Pang and H. Xue, *J Mater Chem A Mater*, 2016,

2275   **4**, 19078–19085.

2276 127   J. Yang, P. Xiong, C. Zheng, H. Qiu and M. Wei, *J. Mater. Chem. A*, 2014, **2**, 16640–

2277   16644.

2278 128   M. S. Rahmanifar, H. Hesari, A. Noori, M. Y. Masoomi, A. Morsali and M. F. Mousavi,

2279   *Electrochim Acta*, 2018, **275**, 76–86.

2280 129   G. Li, H. Cai, X. Li, J. Zhang, D. Zhang, Y. Yang and J. Xiong, *ACS Appl Mater

2281   Interfaces*, 2019, **11**, 37675–37684.

2282 130   Q. Yang, R. Song, Y. Wang, X. Hu, Z. Chen, Z. Li and W. Tan, *Colloids Surf A

2283   Physicochem Eng Asp*, 2021, **631**, 127665.

2284 131   R. Sahoo, S. Ghosh, S. Chand, S. Chand Pal, T. Kuila and M. C. Das, *Compos B Eng*,

2285   2022, **245**, 110174.

2286 132   Y.-L. Chang, M.-D. Tsai, C.-H. Shen, C.-W. Huang, Y.-C. Wang and C.-W. Kung,

2287   *Materials Today Sustainability*, 2023, **23**, 100449.

2288 133   S. C. Wechsler and F. Z. Amir, *ChemSusChem*, 2020, **13**, 1491–1495.

2289 134   H. S. Kim, M. S. Kang and W. C. Yoo, *J Mater Chem A Mater*, 2019, **7**, 5561–5574.

2290 135   K. M. Choi, H. M. Jeong, J. H. Park, Y.-B. Zhang, J. K. Kang and O. M. Yaghi, *ACS

2291   Nano*, 2014, **8**, 7451–7457.

2292 136   D. Sheberla, L. Sun, M. A. Blood-Forsythe, S. Er, C. R. Wade, C. K. Brozek, A. Aspuru-

2293   Guzik and M. Dincă, *J Am Chem Soc*, 2014, **136**, 8859–8862.

2294 137   M. G. Campbell, D. Sheberla, S. F. Liu, T. M. Swager and M. Dincă, *Angewandte

2295   Chemie International Edition*, 2015, **54**, 4349–4352.

2296 138   D. Feng, W. Sun and W. Hu, *Optical Switching and Networking*, 2018, **29**, 1–14.

2297 139   M. Sajid, *Environmental Science and Pollution Research*, 2016, **23**, 14805–14807.

2298 140   K. M. Choi, H. M. Jeong, J. H. Park, Y.-B. Zhang, J. K. Kang and O. M. Yaghi, *ACS

2299   Nano*, 2014, **8**, 7451–7457.

2300 141   T. N. Tu, M. V Nguyen, H. L. Nguyen, B. Yuliarto, K. E. Cordova and S. Demir, *Coord

2301   Chem Rev*, 2018, **364**, 33–50.

2302 142   H. Luo, F. Cheng, L. Huelsenbeck and N. Smith, *J Environ Chem Eng*, 2021, **9**, 105159.

2303 143   M. Mon, R. Bruno, J. Ferrando-Soria, D. Armentano and E. Pardo, *J Mater Chem A

2304   Mater*, 2018, **6**, 4912–4947.

2305   144   Y. Zhao, J. Peng, K. Chen, L. Luo, H. Chen, H. Zhang, S. Chou, X. Feng, W. Chen and
2306   R. Cao, *Sci China Chem*, 2023, **66**, 3154–3160.

2307   145   Y. Fang, Y. Zeng, Q. Jin, X. F. Lu, D. Luan, X. Zhang and X. W. Lou, *Angewandte
2308   Chemie International Edition*, 2021, **60**, 8515–8520.

2309   146   J. Du, J. Chai, Q. Li, W. Zhang and B. Tang, *Colloids Surf A Physicochem Eng Asp*,
2310   2022, **632**, 127810.

2311   147   J.-G. Zhao, H.-Y. Zhou, Z. Hu, Y.-W. Wu, H. Jia and X.-M. Liu, *Rare Metals*, 2022, **41**,
2312   1504–1511.

2313   148   Y. Fang, D. Luan, Y. Chen, S. Gao and X. W. Lou, *Angewandte Chemie International
2314   Edition*, 2020, **59**, 2644–2648.

2315   149   S. Bibi, S. S. A. Shah, M. A. Nazir, M. H. Helal, S. M. El-Bahy, Z. M. El-Bahy, S. Ullah,
2316   M. A. Wattoo and A. ur Rehman, *Adv Sustain Syst*, 2024, 2400011.

2317   150   X.-Y. Dao, J.-H. Guo, Y.-P. Wei, F. Guo, Y. Liu and W.-Y. Sun, *Inorg Chem*, 2019, **58**,
2318   8517–8524.

2319   151   Y. Wang, Y. Pan, L. Zhu, H. Yu, B. Duan, R. Wang, Z. Zhang and S. Qiu, *Carbon N Y*,
2320   2019, **146**, 671–679.

2321   152   K.-S. Lin, A. K. Adhikari, C.-N. Ku, C.-L. Chiang and H. Kuo, *Int J Hydrogen Energy*,
2322   2012, **37**, 13865–13871.

2323   153   M. Y. Zorainy, M. G. Alalm, S. Kaliaguine and D. C. Boffito, *J Mater Chem A Mater*,
2324   2021, **9**, 22159–22217.

2325   154   Q. Zhao, W. Yuan, J. Liang and J. Li, *Int J Hydrogen Energy*, 2013, **38**, 13104–13109.

2326   155   Z. Yin, Y.-L. Zhou, M.-H. Zeng and M. Kurmoo, *Dalton Transactions*, 2015, **44**, 5258–
2327   5275.

2328   156   T.-H. Chen, I. Popov, W. Kaveevivitchai and O. Š. Miljanić, *Chemistry of Materials*,
2329   2014, **26**, 4322–4325.

2330   157   K.-S. Lin, A. K. Adhikari, C.-N. Ku, C.-L. Chiang and H. Kuo, *Int J Hydrogen Energy*,
2331   2012, **37**, 13865–13871.

2332   158   Z. Mai and D. Liu, *Cryst Growth Des*, 2019, **19**, 7439–7462.

2333   159   M. A. Mohamud and A. B. Yurtcan, *Int J Hydrogen Energy*, 2021, **46**, 33782–33800.

2334   160   S. Bibi, S. S. A. Shah, M. A. Nazir, M. H. Helal, S. M. El-Bahy, Z. M. El-Bahy, S. Ullah,
2335   M. A. Wattoo and A. ur Rehman, *Adv Sustain Syst*, 2024, 2400011.

2336   161   Z. Hu, Y. Peng, Z. Kang, Y. Qian and D. Zhao, *Inorg Chem*, 2015, **54**, 4862–4868.

2337   162   E. M. C. Morales, M. A. Méndez-Rojas, L. M. Torres-Martínez, L. F. Garay-Rodríguez,
2338   I. López, I. E. Uflyand and B. I. Kharisov, *Polyhedron*, 2021, **210**, 115517.

2339 163 S. Bibi, S. S. A. Shah, M. A. Nazir, M. H. Helal, S. M. El-Bahy, Z. M. El-Bahy, S. Ullah,

2340   M. A. Wattoo and A. ur Rehman, *Adv Sustain Syst*, 2024, 2400011.

2341 164 A. Al Obeidli, H. Ben Salah, M. Al Murisi and R. Sabouni, *Int J Hydrogen Energy*, 2022,

2342   **47**, 2561–2593.

2343 165 M. Safaei, M. M. Foroughi, N. Ebrahimpoor, S. Jahani, A. Omidi and M. Khatami, *TrAC*

2344   *Trends in Analytical Chemistry*, 2019, **118**, 401–425.

2345 166 A. FUJISHIMA and K. HONDA, *Nature*, 1972, **238**, 37–38.

2346 167 A. B. Djurišić, Y. He and A. M. C. Ng, *APL Mater*, , DOI:10.1063/1.5140497.

2347 168 S. R. Shanmugham, G. B. Jegadeesan and V. Ponnusami, in *Nanotechnology in the*

2348   *Beverage Industry*, Elsevier, 2020, pp. 25–49.

2349 169 A. Dhakshinamoorthy, Z. Li and H. Garcia, *Chem Soc Rev*, 2018, **47**, 8134–8172.

2350 170 M. Pawar, S. Topcu Sendoğdular and P. Gouma, *J Nanomater*, 2018, **2018**, 1–13.

2351 171 S. Peiris, H. B. de Silva, K. N. Ranasinghe, S. V. Bandara and I. R. Perera, *Journal of*

2352   *the Chinese Chemical Society*, 2021, **68**, 738–769.

2353 172 S.-N. Zhao, G. Wang, D. Poelman and P. Van Der Voort, *Molecules*, 2018, **23**, 2947.

2354 173 J. Moma and J. Baloyi, *Photocatalysts-Applications and Attributes*.

2355 174 S. Higashimoto, *Catalysts*, 2019, **9**, 201.

2356 175 Z. Li, S. Wang, J. Wu and W. Zhou, *Renewable and Sustainable Energy Reviews*, 2022,

2357   **156**, 111980.

2358 176 F. Li, G. Liu, F. Liu, J. Wu and S. Yang, *J Hazard Mater*, 2023, **452**, 131237.

2359 177 Y. Jin, W. Tang, J. Wang, F. Ren, Z. Chen, Z. Sun and P.-G. Ren, *J Alloys Compd*, 2023,

2360   **932**, 167627.

2361 178 A. Meng, L. Zhang, B. Cheng and J. Yu, *Advanced Materials*, ,

2362   DOI:10.1002/adma.201807660.

2363 179 S.-Y. Lee and S.-J. Park, *Journal of Industrial and Engineering Chemistry*, 2013, **19**,

2364   1761–1769.

2365 180 S. Higashimoto, *Catalysts*, 2019, **9**, 201.

2366 181 X. Chen, S. Shen, L. Guo and S. S. Mao, *Chem Rev*, 2010, **110**, 6503–6570.

2367 182 M. Skocaj, M. Filipic, J. Petkovic and S. Novak, *Radiol Oncol*, , DOI:10.2478/v10019-

2368   011-0037-0.

2369 183 F. Wu, Z. Zhou and A. L. Hicks, *Environ Sci Technol*, 2019, **53**, 4078–4087.

2370 184 A.-I. Gopalan, J.-C. Lee, G. Saianand, K.-P. Lee, W.-Y. Chun, Y. Hou, V. Kannan, S.-

2371   S. Park and W.-J. Kim, *Materials*, 2020, **13**, 5072.

2372   185   T. Sansenya, N. Masri, T. Chankhanittha, T. Senasu, J. Piriyanon, S. Mukdasai and S.
2373   Nanan, *Journal of Physics and Chemistry of Solids*, 2022, **160**, 110353.

2374   186   T. Chankhanittha, N. Komchoo, T. Senasu, J. Piriyanon, S. Youngme, K. Hemavibool
2375   and S. Nanan, *Colloids Surf A Physicochem Eng Asp*, 2021, **626**, 127034.

2376   187   D. Kim and K. Yong, *Appl Catal B*, 2021, **282**, 119538.

2377   188   Z. Li, R. Li, H. Jing, J. Xiao, H. Xie, F. Hong, N. Ta, X. Zhang, J. Zhu and C. Li, *Nat
2378   Catal*, 2023, **6**, 80–88.

2379   189   N. A. F. Al-Rawashdeh, O. Allabadi and M. T. Aljarrah, *ACS Omega*, 2020, **5**, 28046–
2380   28055.

2381   190   K. Chaudhary, M. Aadil, S. Zulfiqar, S. Ullah, S. Haider, P. O. Agboola, M. F. Warsi
2382   and I. Shakir, *Fullerenes, Nanotubes and Carbon Nanostructures*, 2021, **29**, 915–928.

2383   191   A. Alshammari, Z. Jiang and K. E. Cordova, in *Semiconductor Photocatalysis -
2384   Materials, Mechanisms and Applications*, InTech, 2016.

2385   192   V. García-Salcido, P. Mercado-Oliva, J. L. Guzmán-Mar, B. I. Kharisov and L.
2386   Hinojosa-Reyes, *J Solid State Chem*, 2022, **307**, 122801.

2387   193   Y. Gao, X.-H. Yi, C.-C. Wang, F. Wang and P. Wang, *Mater Res Bull*, 2023, **158**,
2388   112072.

2389   194   C. Jing, Y. Zhang, J. Zheng, S. Ge, J. Lin, D. Pan, N. Naik and Z. Guo, *Particuology*,
2390   2022, **69**, 111–122.

2391   195   H. Sepehrmansourie, H. Alamgholiloo, N. Noroozi Pesyan and M. A. Zolfigol, *Appl
2392   Catal B*, 2023, **321**, 122082.

2393   196   L. Wang, P. Jin, S. Duan, H. She, J. Huang and Q. Wang, *Sci Bull (Beijing)*, 2019, **64**,
2394   926–933.

2395   197   M. Xu, C. Sun, X. Zhao, H. Jiang, H. Wang and P. Huo, *Appl Surf Sci*, 2022, **576**,
2396   151792.

2397   198   F. Drache, V. Bon, I. Senkovska, C. Marschelke, A. Synytska and S. Kaskel, *Inorg
2398   Chem*, 2016, **55**, 7206–7213.

2399   199   A. J. Howarth, Y. Liu, P. Li, Z. Li, T. C. Wang, J. T. Hupp and O. K. Farha, *Nat Rev
2400   Mater*, 2016, **1**, 15018.

2401   200   G. Paille, M. Gomez-Mingot, C. Roch-Marchal, B. Lassalle-Kaiser, P. Mialane, M.
2402   Fontecave, C. Mellot-Draznieks and A. Dolbecq, *J Am Chem Soc*, 2018, **140**, 3613–
2403   3618.

2404   201   S. S. A. Shah, M. A. Nazir, K. Khan, I. Hussain, M. Tayyab, S. S. Alarfaji, A. M. Hassan,
2405   M. Sohail, M. S. Javed and T. Najam, *J Energy Storage*, 2024, **75**, 109725.

Journal of Materials Chemistry A Accepted Manuscript

View Article Online
DOI: 10.1039/D4TA03877K

2406 202 D. Crawford, J. Casaban, R. Haydon, N. Giri, T. McNally and S. L. James, *Chem Sci*,
2407 2015, **6**, 1645–1649.

2408 203 J. C. Glier and E. S. Rubin, *Energy Procedia*, 2013, **37**, 65–72.

2409 204 M. Karnan, A. G. K. Raj, K. Subramani, S. Santhoshkumar and M. Sathish, *Sustain*
2410 *Energy Fuels*, 2020, **4**, 3029–3041.

2411 205 J. Moma and J. Baloyi, in *Photocatalysts - Applications and Attributes*, IntechOpen,
2412 2019.

2413 206 S.-N. Zhao, G. Wang, D. Poelman and P. Van Der Voort, *Molecules*, 2018, **23**, 2947.

2414 207 R. Asahi, T. Morikawa, T. Ohwaki, K. Aoki and Y. Taga, *Science (1979)*, 2001, **293**,
2415 269–271.

2416 208 H. Demir, G. O. Aksu, H. C. Gulbalkan and S. Keskin, *Carbon Capture Science and*
2417 *Technology*, , DOI:10.1016/j.ccst.2021.100026.

2418 209 S. Ali, P. M. Ismail, F. Wahid, A. Kumar, M. Haneef, F. Raziq, S. Ali, M. Javed, R. U.
2419 Khan and X. Wu, *Fuel Processing Technology*, 2022, **236**, 107427.

2420 210 S. Ali, P. M. Ismail, M. Humayun, M. Bououdina and L. Qiao, *Fuel Processing*
2421 *Technology*, 2024, **255**, 108049.

2422 211 M. Khan, Z. Akmal, M. Tayyab, S. Mansoor, A. Zeb, Z. Ye, J. Zhang, S. Wu and L.
2423 Wang, *Carbon Capture Science and Technology*, , DOI:10.1016/j.ccst.2024.100191.

2424 212 P. Dubey, V. Shrivastav, P. H. Maheshwari, M. Hołdyński, A. Krawczyńska and S.
2425 Sundriyal, *J Energy Storage*, , DOI:10.1016/j.est.2023.107828.

2426 213 Y. Cao, W. Yang, M. Wang, N. Wu, L. Zhang, Q. Guan and H. Guo, *Int J Hydrogen*
2427 *Energy*, 2021, **46**, 18179–18206.

2428 214 J. Khan, A. Khan, B. Rubab, F. Jamshaid, A. A. Al-Kahtani and A. Dahshan, *Appl Mater*
2429 *Today*, 2023, **34**, 101906.

2430 215 C. Healy, K. M. Patil, B. H. Wilson, L. Hermanspahn, N. C. Harvey-Reid, B. I. Howard,
2431 C. Kleinjan, J. Kolien, F. Payet and S. G. Telfer, *Coord Chem Rev*, 2020, **419**, 213388.

2432 216 S. Bhattacharyya and T. K. Maji, *Coord Chem Rev*, 2022, **469**, 214645.

2433 217 Q. He, F. Zhan, H. Wang, W. Xu, H. Wang and L. Chen, *Materials Today Sustainability*,
2434 2022, **17**, 100104.

2435 218 D. Chakraborty, A. Yurdusen, G. Mouchaham, F. Nouar and C. Serre, *Adv Funct Mater*,
2436 2023, 2309089.

2437 219 D. Yang and B. C. Gates, *ACS Catal*, 2019, **9**, 1779–1798.

2438 220 W. Xue, C. D. Sewell, Q. Zhou and Z. Lin, *Angewandte Chemie International Edition*,
2439 2022, **61**, e202206512.

2440   221   R. Freund, O. Zaremba, G. Arnauts, R. Ameloot, G. Skorupskii, M. Dincă, A. Bavykina,

2441   J. Gascon, A. Ejsmont and J. Goscianska, *Angewandte Chemie International Edition*,

2442   2021, **60**, 23975–24001.

2443   222   A. Bavykina, N. Kolobov, I. S. Khan, J. A. Bau, A. Ramirez and J. Gascon, *Chem Rev*,

2444   2020, **120**, 8468–8535.

2445   223   P. Falcaro, R. Ricco, C. M. Doherty, K. Liang, A. J. Hill and M. J. Styles, *Chem Soc Rev*,

2446   2014, **43**, 5513–5560.

2447   224   E.-S. M. El-Sayed and D. Yuan, *Green Chemistry*, 2020, **22**, 4082–4104.

2448   225   X. Song, Y. Wang, C. Wang, D. Wang, G. Zhuang, K. O. Kirlikovali, P. Li and O. K.

2449   Farha, *J Am Chem Soc*, 2022, **144**, 10663–10687.

2450

2451

Journal of Materials Chemistry A Accepted Manuscript

Data availability statement

The data that support the findings of this study are available from the corresponding author, upon reasonable request.

Journal of Materials Chemistry A Accepted Manuscript